Mechanisms of Discharge Product Evolution and Solvent Stability in Lithium-Oxygen Batteries

by

Thomas Peter Batcho

B.S. Materials Science and Engineering
The Johns Hopkins University, 2011

SUBMITTED TO THE DEPARTMENT OF MATERIALS SCIENCE AND ENGINEERING IN PARTIAL FULFILLMENT OF THE REQUIREMENTS FOR THE DEGREE OF

DOCTOR OF PHILOSOPHY IN MATERIALS SCIENCE AND ENGINEERING
AT THE
MASSACHUSETTS INSTITUTE OF TECHNOLOGY

JUNE, 2018

Signature of the Author: _____
Department of Materials Science and Engineering
May 23, 2018

Certified by: _____
Carl V. Thompson
Stavros Salapatas Professor of
Materials Science and Engineering
Thesis Supervisor

Certified by: _____
Yang Shao-Horn
W.M. Keck Professor of Energy
Thesis Supervisor

Accepted by: _____
Donald R. Sadoway
John F. Elliott Professor of Materials Chemistry
Chair, Departmental Committee on Graduate Students

Mechanisms of Discharge Product Evolution and Solvent Stability in Lithium-Oxygen Batteries

by

Thomas Peter Batcho

Submitted to the Department of Materials Science and Engineering on May 23, 2018
in Partial Fulfillment of the Requirements for the
Degree of Doctor of Philosophy in Materials Science and Engineering

ABSTRACT

Lithium-oxygen batteries offer the possibility of achieving twice the gravimetric energy density of lithium-ion batteries. However, several challenges remain to achieve commercially-available lithium-oxygen batteries. Capacity must be optimized by maximizing the formation of Li_2O_2 discharge product. Side reactions with the solvent and electrode must be suppressed. This study seeks to improve understanding of the mechanisms of Li_2O_2 evolution and Li-O_2 decomposition reactions in order to design strategies to optimize capacity and stability.

Decomposition reactions in the solvent dimethyl sulfoxide were studied due to conflicting reports about its stability. Discharged electrodes in dimethyl sulfoxide were aged for varying amounts of time then characterized. Li_2O_2 reacted with dimethyl sulfoxide to form LiOH and dimethyl sulfone. This demonstrated that dimethyl sulfoxide is unsuitable for commercial application. The study also illustrated the importance of performing aging studies in the discharged condition to determine the stability of Li-O_2 battery components.

Adding small amounts of water to Li-O_2 solvents has been demonstrated to enhance capacity but the effect on stability was not well understood. Discharges were performed in dimethoxyethane and acetonitrile with and without added water. Water caused an unwanted side reaction to form LiOH in acetonitrile but not in dimethoxyethane, due to a higher favorability of deprotonation in acetonitrile. Interactions between capacity enhancing additives and solvent molecules must be carefully studied to avoid side reactions.

A model of the two competing mechanistic pathways of Li-O_2 discharge was developed to understand how these pathways depend on discharge conditions and solvent properties. The model was fitted to experimental results from rotating ring-disk electrode discharges in order to check that model assumptions were physical. The model demonstrates that Li_2O_2 film evolution is heavily dependent on solvent properties and that promotion of toroidal Li_2O_2 primarily depends on slower surface passivation rather than faster solvation of lithium superoxide.

Thesis Supervisor: Carl V. Thompson
Title: Stavros Salapatas Professor of Materials Science and Engineering

Thesis Supervisor: Yang Shao-Horn
Title: W.M. Keck Professor of Energy

Acknowledgements

Many people have provided invaluable help and support to me over the course of researching and writing this thesis. I would like to sincerely thank my advisors Prof. Carl V. Thompson and Prof. Yang Shao-Horn for their mentorship. Prof. Harry Tuller and Prof. Yet-Ming Chiang provided important feedback throughout my graduate research as members of my thesis committee. I would like to thank all of the peers I had the pleasure of working with in the Electrochemical Energy Laboratory and the Materials for Micro and Nano Systems Laboratory. In particular, I would like to thank Dr. Robert Mitchell, Prof. Betar Gallant, and Dr. David Kwabi for teaching me so much about science and research. I would like to thank all of the members of my first-year class, whose friendship and support were crucial as we struggled through classes, qualifying exams, and research. I would like to thank all the friends and family members who have provided so many different types of support, especially Patricia Peiffer, William Peiffer, James Peiffer, and Jane Polanka. Thank you Nan and Tom Batcho for creating so many opportunities for me and being by my side my whole life. Thank you John Batcho for being my friend and my brother. Thank you Don Trisler and Catherine Davis for being like a second family. And thank you Molly for your love and partnership.

Table of Contents

Chapter One: Introduction to Lithium-Oxygen Batteries

1.1 Possibilities for Li-O_2 Batteries

Climate change poses a unique and urgent problem, requiring radical restructuring of the global energy economy to reduce carbon dioxide emissions[1]. Some of the largest contributions to carbon dioxide emissions are electricity generation and transportation[2]. Reducing carbon dioxide emissions will require the large scale adoption of technologies such as solar panels and wind turbines to produce electricity and the replacement of gasoline powered vehicles with electric vehicles. Both of these changes will require improved battery technology. Wind and solar energy are intermittent; peaks in supply do not correspond with peaks in energy use. Batteries for grid storage can store energy produced by renewable energies like wind and solar energy and then supply electricity to consumers when it is needed. Battery-powered electric vehicles enable energy generated by wind or solar sources to be used in transportation. Improvements in battery technology that reduce the cost of energy storage and expand the driving range between battery recharges will contribute to the wide-scale adoption of electric vehicles.

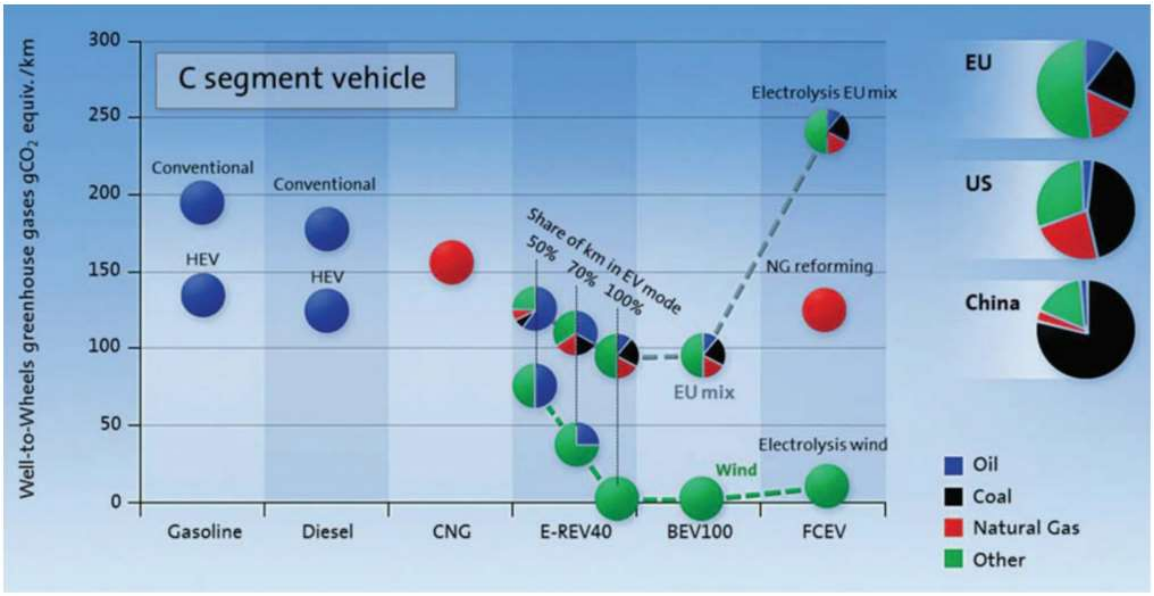

Figure 1.1.1: Potential for Large Scale CO_2 Emissions Reduction through Renewable Energy and Battery Powered Electric Vehicles Figure by Eberle et al.[3] on possible reductions in CO_2 emissions gained by switching from gasoline-powered vehicles to electric vehicles for compact cars (CNG = compressed natural gas, E-REV40 = extended range electric vehicle with 40 miles all electric, BEV100 = 100% battery electric vehicle, FCEV = fuel cell electric vehicle). Reproduced from Ref. 3 with the permission of The Royal Society of Chemistry.

The possible CO_2 emissions reductions that can be achieved by converting from gasoline-powered vehicles to electric vehicles are significant. For example, in the United States transportation represents about 25% of energy use[2]. Almost all of this energy derives from the combustion of carbon dioxide emitting petroleum gasoline. Switching from gasoline powered vehicles to battery electric vehicles in regions such as the European Union with low levels of coal-generated electricity would cause a roughly 50% reduction in vehicle carbon dioxide emissions, even without any improvements in the share of renewable-generated electricity (Figure 1.1.1)[3]. As the share of electricity generation for wind and solar energy approaches 100%, carbon emissions are almost entirely eliminated. It is notable that

battery electric vehicles possess a near-term advantage in terms of CO_2 emissions compared to the competing technology of fuel cell electric vehicles. Fuel cells actually represent greater CO_2 emissions with the current mixture of electrical generation sources, due to the energy costs associated with H_2 fuel production[3,4].

Because of these large possible reductions in world CO_2 emissions, the challenge of designing new battery chemistries for electric vehicles and grid storage with greater capacity than currently available lithium-ion batteries is critical. Lithium-ion batteries operate by intercalating Li^+ ions into a metal oxide compound such as $LiCoO_2$ as a cathode and graphite as an anode[5,6]. These batteries have a capacity determined by the amount of Li^+ that can be inserted into a given compound. This limit corresponds to about 100 Wh/kg in usable energy for an electric vehicle[7]. This translates to a driving range of about 310 miles for the 2018 Tesla Model 3 Long Range, 238 miles for the 2018 Chevrolet Bolt, and 151 miles for the 2018 Nissan Leaf[8]. Opinion surveys suggest that while the average driver drives for less than 100 miles a day, the minimum acceptable range for a consumer is between 200 to 300 miles[9]. Li-ion capacity limitations have motivated the search for "next generation" batteries with higher theoretical capacity limitations that can affordably deliver longer driving ranges in electric vehicles.

Li-O_2 batteries are a promising candidate for achieving enhanced capacity. The Li-O_2 battery was first demonstrated in 1996 by K.M. Abraham[10]. Li-O_2 batteries operate by reacting Li^+ with O_2 to form Li_2O_2, following the overall equation:

$$2Li^+ + 2e^- + O_2 \rightarrow Li_2O_2$$

On discharge, the anode provides Li^+ ions which diffuse through an oxygen saturated non-aqueous electrolyte solvent to the cathode (Figure 1.1.2). Oxygen is reduced to Li_2O_2 by electron transfers at the surface of the cathode material. Li_2O_2 is an electrically insulating solid which deposits on the surface of

the cathode and fills up void space[11]. The discharge will continue until the insulating Li_2O_2 discharge product passivates the electrode surface and blocks further electron transfers.

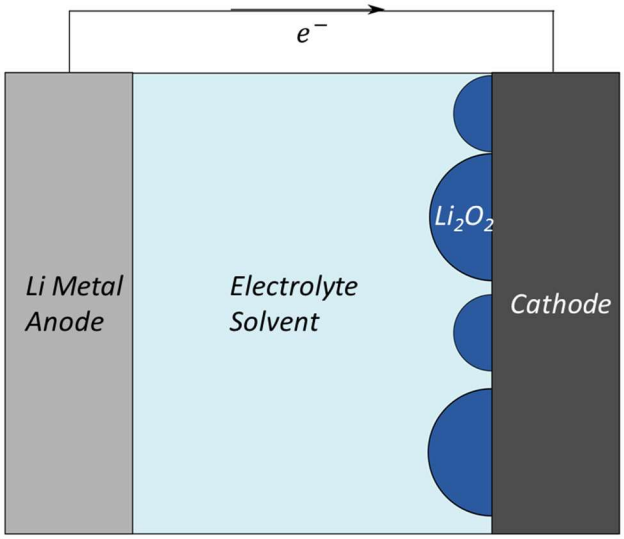

$$2Li^+ + 2e^- + O_2 \rightarrow Li_2O_2$$

Figure 1.1.2: Schematic of Li-O_2 Discharge Lithium peroxide (dark blue) forms on the cathode (black) from the reduction of oxygen during discharge and then reversibly decomposes on charge.

The theoretical capacity of Li-O_2 batteries is favorable compared to the capacity of $LiCoO_2$ Li-ion batteries. Lu et al. calculate that the possible gravimetric energy density is about twice that of Li-ion batteries, while possessing a comparable volumetric energy density[12].

a)

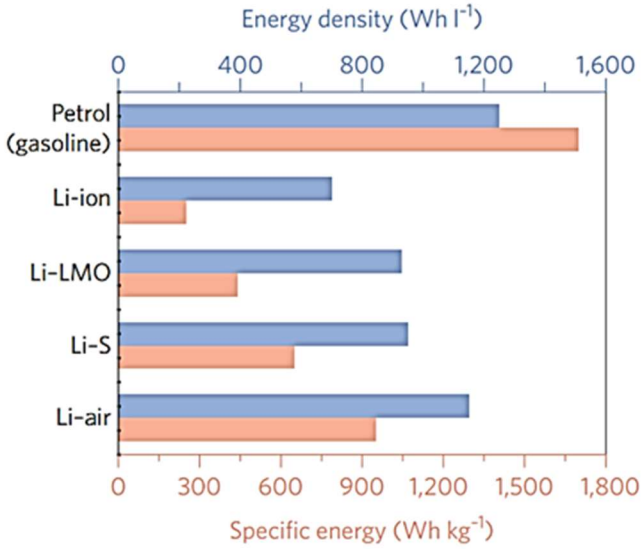

b)

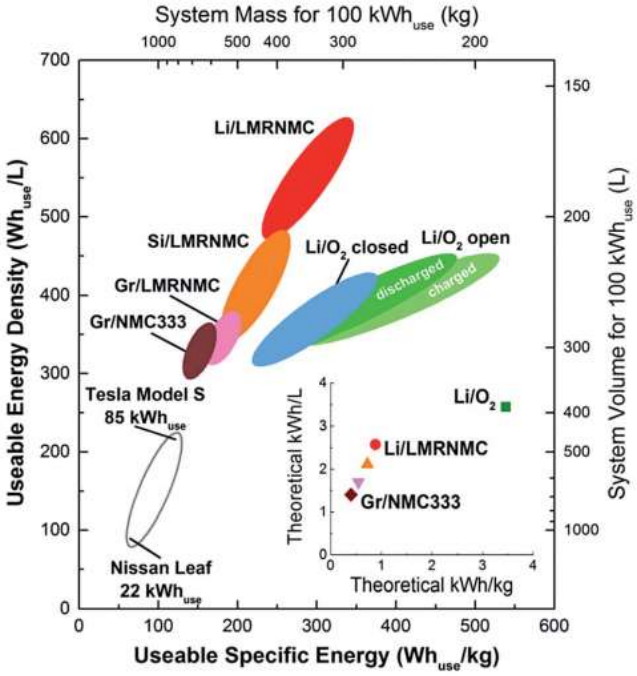

Figure 1.1.3 Comparing Next-Generation Batteries a) Figure reproduced from Lin et al[13]. Comparison of estimates of Li-O_2 battery energy normalized to weight (blue) and volume (pink) to gasoline, existing Li-ion batteries, and possible next generation batteries lithium-sulfur (Li-S) and lithium-layered metal oxide batteries (Li-LMO). Reprinted by permission from Springer Nature, Nature Nanotechnology, Ref. 13, Lin

et al., “Reviving the lithium metal anode for high-energy batteries,” 2017. b) Figure reproduced from Gallagher et al[7]. Comparison of estimates of Li-O_2 system (blue and green) energy storage to Li-ion and lithium layered metal oxide (Li/LiMRNMC) (red) system energy storage. Inset is a comparison of theoretical energy densities for electrodes ignoring weights and volumes of non-electrode system components. Reproduced from Ref. 7 with the permission of The Royal Chemistry Society.

Considerations of the theoretical energy density of next-generation battery electrodes are a reasonable first-pass metric for comparison. Estimates of energy gain once system components are considered yield a better practical sense of the possible improvements in commercial settings such as electric vehicles (Figure 1.1.3). Lin et al. provide estimates of energy storage for three next-generation batteries, including Li-O_2, which include the weight and size of battery separators, electrolytes, and casings. By these estimates, Li-O_2 batteries provide roughly three times the specific energy (energy normalized by mass) and two times the energy density (energy normalized by volume) of existing Li-ion batteries[13]. Even compared to other next-generation batteries such as lithium layered metal oxide batteries (Li-LMO) and lithium sulfur-batteries (Li-S), Li-O_2 provides comparable energy density and ~1.5 to 2x the specific energy of these other technologies. Gallagher et al. yield more conservative estimates of Li-O_2 battery specific energy and energy density by considering the impact of components to regulate oxygen pressure and cell temperature[7]. With these considerations, both lithium layered metal oxide batteries and lithium oxygen batteries significantly outperform existing commercial Li-ion batteries. Li-O_2 batteries offer a roughly 50% gain in specific energy but a weaker energy density relative to lithium layered metal oxide batteries. What is clear from these various estimates is that Li-O_2, Li-S, and Li-LMO chemistries all offer the possibility of significantly higher energy storage than commercially available Li-ion batteries. This motivates extensive research into all three coupled with research into lithium anode stabilization. What is also clear from these various estimates is that Li-O_2 batteries possess the largest upper-bound in terms of possible energy storage that could be realized in a practical cell.

A critical component of how close a Li-O_2 cell comes to this estimated upper-bound on energy storage depends on how efficiently the Li_2O_2 discharge product fills the void space in the cathode. Since discharge ends when the surface of the electrode is covered by Li_2O_2, forming Li_2O_2 away from the electrode surface is critical to optimizing the capacity of Li-O_2 batteries. A precise understanding of the discharge sizes and morphologies of Li_2O_2 is required.

1.2 Li_2O_2 Discharge Morphology and Evolution

Li_2O_2 forms in one of two morphological regimes. In one case, the Li_2O_2 forms as nanometer scale particles on the surface of the cathode. These particles grow and coalesce to form a thin film of no more ~10 nm by the end of discharge (Figure 1.2.1)[14]. This morphology is referred to as the thin film morphology. The creation of small deposits of Li_2O_2 at the beginning of discharge is observed in a carbon nanotube electrode in Figure 1.2.1a. The deposits become more copious and begin to converge at roughly four times the discharge depth in Figure 1.2.1b and the film is nearly uniform at roughly ten times the discharge depth in Figure 1.2.1c. Thin film Li_2O_2 is more likely to occur when the discharge is at high overpotential or high discharge rate.

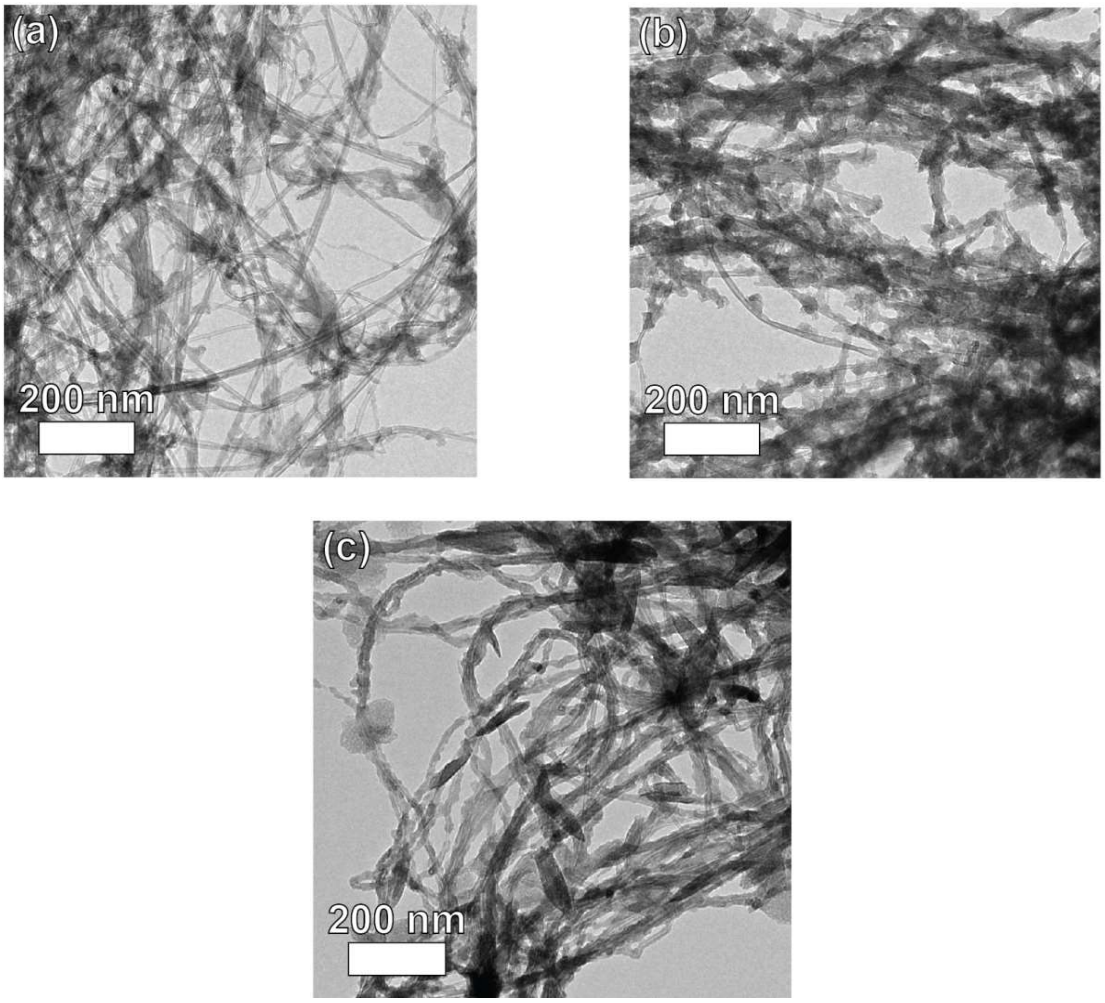

Figure 1.2.1: Transmission electron microscopy of Li_2O_2 thin film morphology Figure reproduced from Mitchell et al[14]. Small particles and thin film are observed on the surface of the carbon nanotube electrode after a discharge at 250 mA/g_{CNT} to a) 1000 mAh/g_{CNT} b) 4200 mAh/g_{CNT} and c) 9800 mAh/g_{CNT} in 0.1 M $LiClO_4$ DME (dimethoxyethane). Reprinted with permission from Mitchell et al., Mechanisms of Morphological Evolution of Li_2O_2 Particles during Electrochemical Growth, *J. Phys. Chem. Lett.* **4,** 1060–1064 (2013). Copyright 2013 American Chemical Society.

The other possible Li_2O_2 discharge morphology are large toroidal deposits. These Li_2O_2 toroids can form with diameters from ~10-1000 nm (Figure 1.2.2a)[14,15]. Toroids do not appear to form on the electrode surface but rather in solution. They can be chemically formed by mixing KO_2 and Li salt,

indicating that toroid formation involves a chemical step in solution[16]. Toroids are likely the result of agglomeration of smaller platelets of Li_2O_2 that form in solution. Stacked platelets have been observed in the microstructure of toroids (Figure 1.2.2b)[14]. Toroids have been shown to have a crystalline structure with six fold symmetry (Figure 1.2.2c,d)[14]. The Li_2O_2 toroid morphology is more likely to form at low overpotential and low discharge rate[14,17].

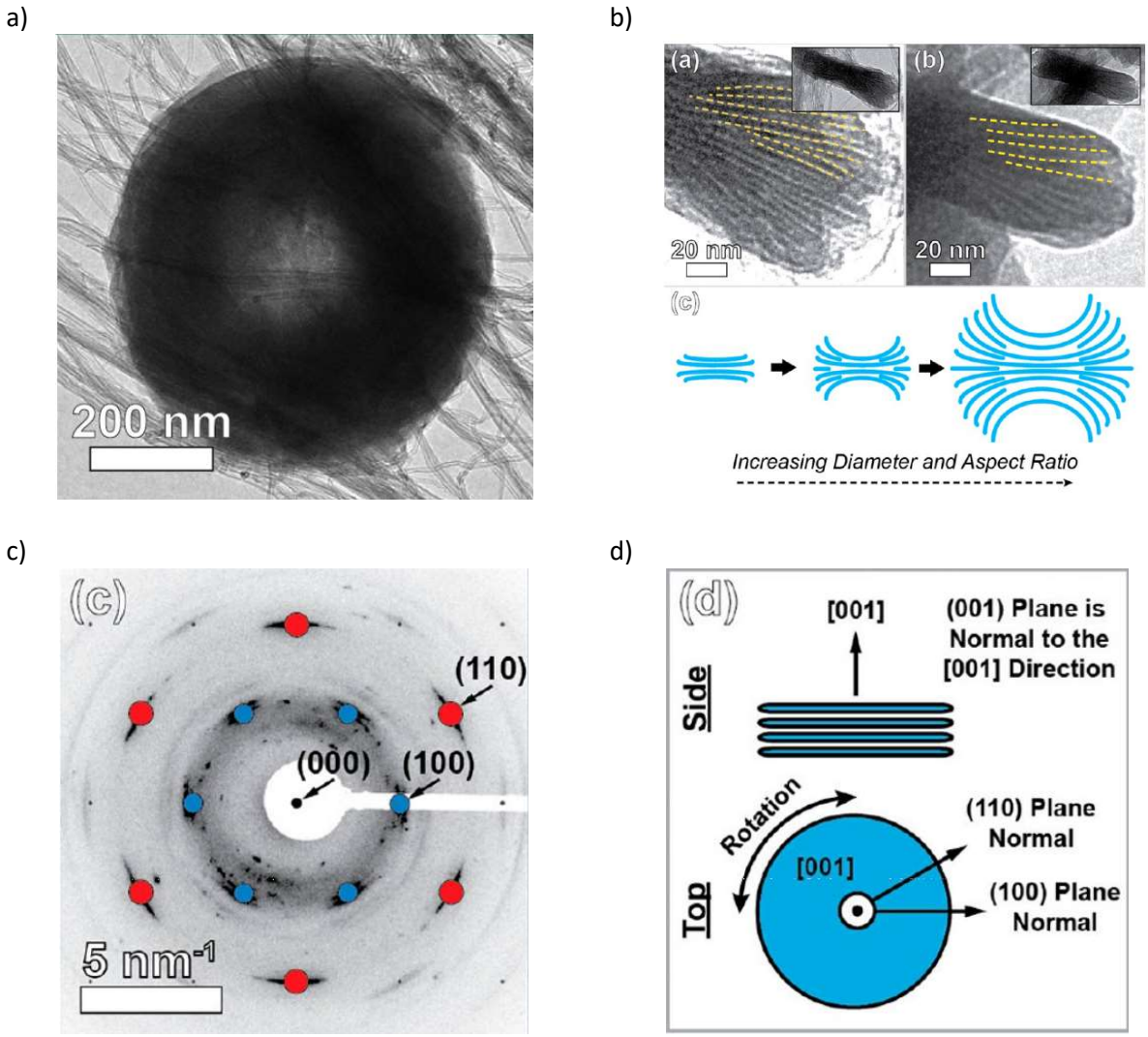

Figure 1.2.2: Transmission electron microscopy images of Li_2O_2 toroids Reproduced from Mitchell et al.[14] All discharges occurred with carbon nanotube electrodes in 0.1 M $LiClO_4$ DME. a) Li_2O_2 imaged by

transmission electron microscopy (TEM) from a discharge at 10 mA/g_{CNT} to 1400 mAh/g_{CNT} b) TEM micrographs of Li_2O_2 from discharges at 50 mA/g_{CNT} to 1000 mAh/g_{CNT} (top left) and 90 mA/g_{CNT} to 13,000 mAh/g_{CNT} (top right) and a schematic of platelet microstructure (bottom) c) TEM diffraction pattern for the toroid in 1.2.2a. d) Schematic of crystal structure orientation. Reprinted with permission from Mitchell et al., Mechanisms of Morphological Evolution of Li_2O_2 Particles during Electrochemical Growth. *J. Phys. Chem. Lett.* **4,** 1060–1064 (2013). Copyright 2013 American Chemical Society.

Li-O_2 discharge is defined by a competition between these two morphological regimes. In addition to potential/current density, other factors that have been shown to affect Li_2O_2 discharge morphology include the type of solvent[18], water content of the solvent[19,20], lithium salt concentration[21], and lithium salt anion[22]. Since the toroid morphology is more favorable for achieving close to ideal capacities by efficient void filling of the cathode, it is important to understand the underlying mechanisms behind these trends.

1.3 Li-O_2 Discharge Mechanistic Pathways

The origin of the two distinct morphological regimes of Li_2O_2 are two competing pathways for Li-O_2 discharge[18]. One pathway involves only electron transfers at the surface of the electrode while the other involves a solvent-mediated process. The first will be referred to as the surface pathway and the latter as the solvent pathway. The surface pathway forms Li_2O_2 thin films and the solvent pathway forms Li_2O_2 toroids.

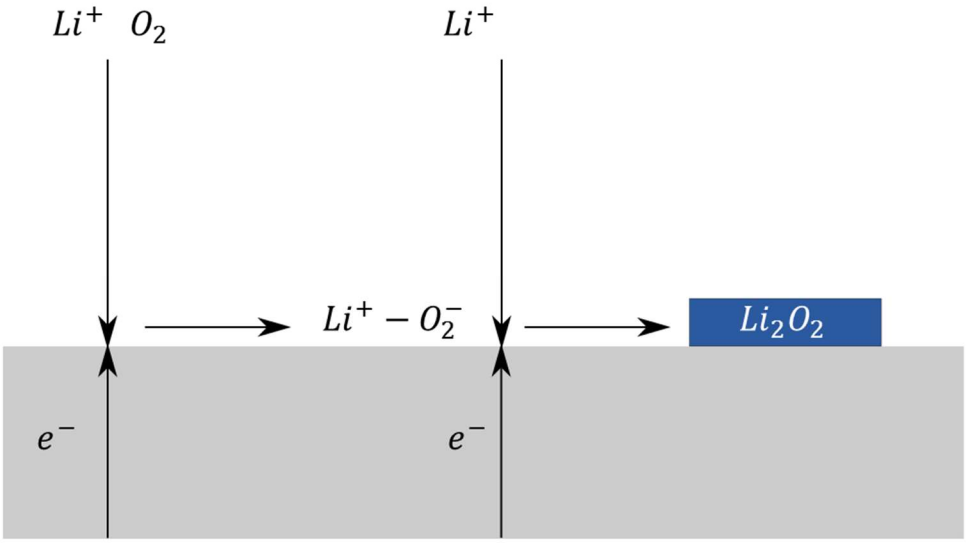

Figure 1.3.1: Schematic of the Surface Pathway Two electron transfers occurring at the electrode (gray) to form lithium peroxide (blue). Vertical arrows indicate transport of the reactants; horizontal arrows indicate a reaction forming a product.

The surface pathway involves an initial electron transfer to oxygen at the surface of the electrode to form Li^+-O_2^- intermediate (Figure 1.3.1).

$$Li^+ + e^- + O_2 \rightarrow (Li^+ - O_2^-)_{surface}$$

Lithium superoxide intermediate is then further reduced by a second electron transfer at the surface of the electrode to form Li_2O_2.

$$Li^+ + e^- + (Li^+ - O_2^-)_{surface} \rightarrow Li_2O_2$$

As the surface pathway requires an electron transfer at the surface of the electrode for both steps, reactions are limited by the conductivity of electrons through lithium peroxide. As the limit of electron

tunneling through Li_2O_2 has been shown to be about ~10 nm, the surface pathway produces a thin film of Li_2O_2[11].

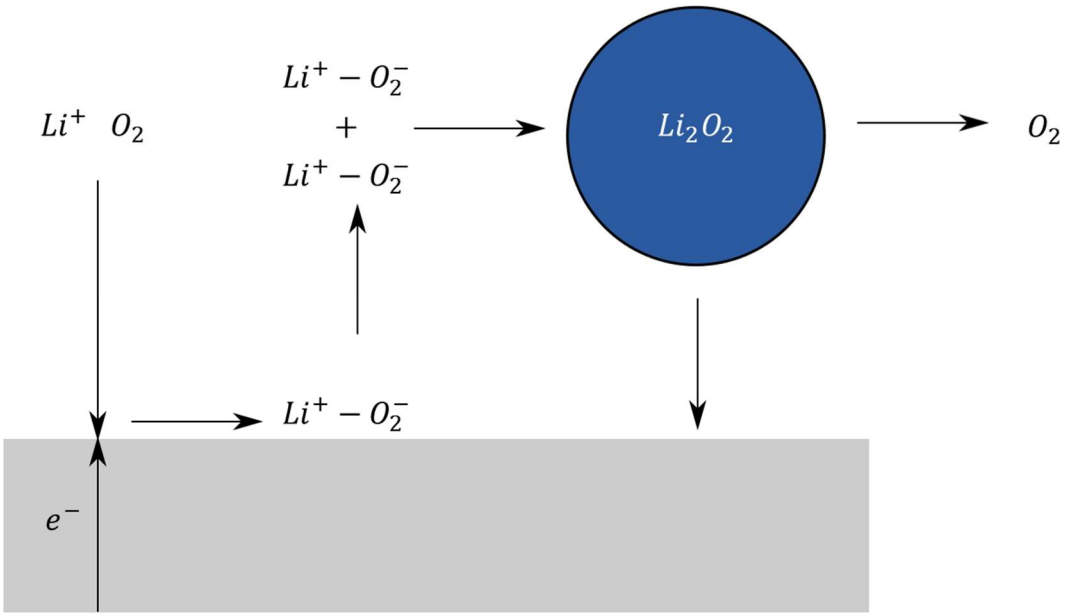

Figure 1.3.2: Schematic of the Solvent Pathway An initial electron transfer at the electrode (gray) forms a lithium superoxide ion pair which solvates. Two lithium superoxide molecules chemically react by disproportionation to form aggregates of lithium peroxide (blue) in solution, which precipitate onto the electrode surface.

The solvent pathway involves the same initial step as the surface pathway: an electron transfer to reduce oxygen at the electrode surface (Figure 1.3.2).

$$Li^+ + e^- + O_2 \rightarrow (Li^+ - O_2^-)_{surface}$$

However, lithium superoxide intermediate is then solvated into the electrolyte solution. Two solvated lithium superoxide complexes can participate in a disproportionation reaction to form Li_2O_2. No electron transfer is required so the reaction can occur away from the electrode surface.

$$(Li^+ - O_2^-)_{surface} \rightarrow (Li^+ - O_2^-)_{solvent}$$

$$2(Li^+ - O_2^-)_{solvent} \rightarrow Li_2O_2 + O_2$$

As the second step in the solvent pathway does not require contact with the electrode surface, large length scales of Li_2O_2 are possible.

While it is generally accepted that Li-O_2 discharge occurs by these two competing mechanisms, it is not yet fully understood how to control each pathway to optimize capacity and maintain stability of the solvent and discharge product.

1.4 Challenges for Li-O_2 Batteries

There are a number of challenges that remain to be resolved in order to produce a commercially viable Li-O_2 secondary battery. The primary issues to be resolved are achieving high capacity, improving rate capability, and avoiding parasitic side reactions with either the solvent, discharge intermediate and product, and the electrode (Figure 1.4.1).

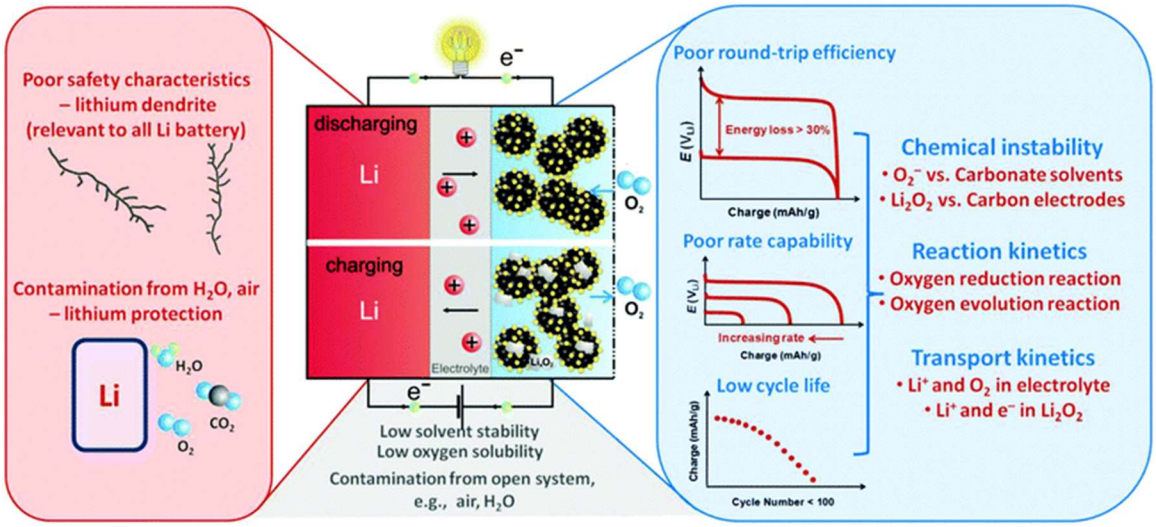

Figure 1.4.1: Schematic Summarizing Needed Improvements in Li-O_2 Performance Figure reproduced from Lu et al[12]. Red box contains challenges related to the anode reaction; blue box contains challenges related to the cathode reaction. Reproduced from Ref. 12 with the permission of The Royal Chemistry Society.

Stabilization of the lithium anode is a critical problem in advancing battery technology. Significant gains in energy are possible with Li-O_2 batteries when a lithium anode is used as opposed to a graphite anode with inserted lithium[12]. Lithium anodes were first used in the 1970s in commercial batteries but were discontinued due to safety issues caused by dendritic growth on cycling leading to shorts and fires[23]. Lithium anode stabilization has received renewed attention in order to allow for next-generation batteries and numerous promising strategies such as polymer coatings and solvent additives have been reported[13,24]. While the lithium anode is important, these studies are beyond the scope of this thesis, which will focus on optimizing stability and discharge capacity in the Li-O_2 cathode.

Issues of solvent stability have received a large amount of attention due to the need for stable discharging and charging of the cell over many cycles. McCloskey et al. highlighted the instability in Li-O_2

batteries of traditional Li-ion battery solvents based on carbonates[25]. Some degree of parasitic side reactions have been observed in all solvents tested including ethers and sulfoxides[25–29]. Commonly used carbon electrode materials have also been observed to react with either lithium superoxide or lithium peroxide[26,30,31]. Many types of catalysts that had been seeded on electrode materials were found to promote parasitic side reactions rather than the reversible formation and decomposition of Li_2O_2[32]. More recently, significant progress in improving rate capability and solvent stability has been demonstrated by the use of redox mediators for both discharge[33] and charge[34–36]. Issues of solvent stability will be further discussed in Chapters Two and Three of this thesis.

The problem of improving electrolyte solvent stability is tied to the problem of enhancing capacity by toroid promotion. Certain solvents are more likely to have high capacity due to high solubility for the Li^+-O_2^- reaction intermediate[18,37]. However, Khetan et al. demonstrated that as a general trend solvents more likely to produce toroidal Li_2O_2 are also more likely to decompose through nucleophilic attack by superoxide intermediates[38]. Overcoming these design limitations requires a precise knowledge of the solvent and surface pathway, how they interact, and how they contribute to stability issues.

1.5 Outline of the Thesis

This thesis will focus on the intimately intertwined issues of increasing the capacity of a Li-O_2 battery during a single discharge and improving the stability of all cell components to allow for many cycles of discharge and charge. Resolving these issues requires a careful study of the two mechanistic pathways that have been identified: the solvent pathway and the surface pathway.

The solvent pathway produces solvated lithium superoxide, which is necessary for capacity enhancing large Li_2O_2 toroids, but also prolongs the exposure of this highly reactive intermediate with

solvent molecules. The surface pathway, in contrast, should involve less interactions between lithium superoxide and solvent molecules but has a very limited possible capacity due to its passivation of the electrode by a Li_2O_2 film. Both pathways will ultimately form Li_2O_2 and a practical solvent must be stable with Li_2O_2.

Chapter Two will focus on stability by examining a common battery solvent, dimethyl sulfoxide (DMSO), used in fundamental study of Li-O_2 batteries and attempting to determine if this solvent could be applicable for commercial use. Time series of morphological and chemical characterization provided insight into how lithium superoxide and lithium peroxide interact with the solvent chemically over prolonged periods of time. The chapter concludes that while DMSO might be suitable for laboratory-scale studies, it is not stable in the presence of Li_2O_2 over long time scales and not suitable for commercial use.

Chapter Three will focus on efforts to improve Li-O_2 discharge capacity by increasing water content and resulting effects on solvent and Li_2O_2 stability. Cells were discharged in different solvents with different water contents and characterized. These studies show that the effect of water content on both capacity and stability is heavily dependent on solvent properties such as the solvation and deprotonation energies of water in the solvent.

Chapter Four will focus on the issue of capacity optimization through control of each pathway. Rotating ring disk electrode experiments were performed to determine the trend of the rate of each pathway with various solvent parameters. A model of Li-O_2 discharge was then built to interpret these trends. The model shows that inhibition of the surface pathway rate, rather than promotion of the solvent pathway rate, is what determines the resulting increase in capacity. This conclusion points towards certain strategies that could inhibit the surface pathway rate without affecting the stability of

the solvent, such as oxygen reduction reaction redox mediators, as promising approaches for achieving commercial Li-O_2 batteries.

Chapter Five will summarize the results of all chapters and provide closing insights. It will also suggest possible strategies for achieving highly reversible high capacity Li-O_2 batteries.

Li-O_2 batteries are a promising candidate for achieving higher discharge capacities than existing Li-ion batteries. Optimizing capacity while improving stability are key challenges that need to be addressed. This study helps to advance this goal by providing insight into parasitic reactions that can occur between the solvent and discharge product and between solvent additives and discharge product. Effects on mechanistic pathways are modeled in order to show which modifications are the most likely to promote or decrease capacity. Modifications that inhibit the surface pathway are desirable and focusing on this aspect could avoid the stability issues present in highly solvating battery solvents. The study provides a guide between the desire to maximize capacity and minimize side reactions.

References

1. International Panel on Climate Change. *Climate Change 2014: Mitigation of Climate Change*. (Cambridge University Press, 2014).
2. Lawrence Livermore National Laboratory & U.S. Department of Energy. Estimated U.S. Energy Consumption in 2016. Available at: https://flowcharts.llnl.gov/content/assets/images/charts/Energy/Energy_2016_United-States.png. (Accessed: 8th March 2018)
3. Eberle, U., Müller, B. & von Helmolt, R. Fuel cell electric vehicles and hydrogen infrastructure: status 2012. *Energy Environ. Sci.* **5,** 8780 (2012).
4. Gröger, O., Gasteiger, H. A. & Suchsland, J.-P. Review—Electromobility: Batteries or Fuel Cells? *J. Electrochem. Soc.* **162,** A2605–A2622 (2015).
5. Mizushima, K., Jones, P. C., Wiseman, P. J. & Goodenough, J. B. LixCoO2 (0<x<-1): A new cathode material for batteries of high energy density. *Mater. Res. Bull.* **15,** 783–789 (1980).
6. Reynier, Y. F., Yazami, R. & Fultz, B. Thermodynamics of Lithium Intercalation into Graphites and Disordered Carbons. *J. Electrochem. Soc.* **151,** A422 (2004).

7. Gallagher, K. G. *et al.* Quantifying the promise of lithium–air batteries for electric vehicles. *Energy Environ. Sci.* **7,** 1555–1563 (2014).

8. fueleconomy.gov, U.S. Environmental Protection Agency & U.S. Department of Energy. Fuel Economy of New All-Electric Vehicles. (2018). Available at: https://www.fueleconomy.gov/feg/PowerSearch.do?action=alts&path=3&year1=2018&year2=2019&vtype=Electric&srchtyp=newAfv. (Accessed: 16th March 2018)

9. Franke, T. & Krems, J. F. What drives range preferences in electric vehicle users? *Transp. Policy* **30,** 56–62 (2013).

10. Abraham, K. M. A Polymer Electrolyte-Based Rechargeable Lithium/Oxygen Battery. *J. Electrochem. Soc.* **143,** 1 (1996).

11. Viswanathan, V. *et al.* Electrical conductivity in Li2O2 and its role in determining capacity limitations in non-aqueous Li-O 2 batteries. *J. Chem. Phys.* **135,** (2011).

12. Lu, Y.-C. *et al.* Lithium–oxygen batteries: bridging mechanistic understanding and battery performance. *Energy Environ. Sci.* **6,** 750 (2013).

13. Lin, D., Liu, Y. & Cui, Y. Reviving the lithium metal anode for high-energy batteries. *Nat. Nanotechnol.* **12,** 194–206 (2017).

14. Mitchell, R. R., Gallant, B. M., Shao-Horn, Y. & Thompson, C. V. Mechanisms of Morphological Evolution of Li2O2 Particles during Electrochemical Growth. *J. Phys. Chem. Lett.* **4,** 1060–1064 (2013).

15. Black, R., Adams, B. & Nazar, L. F. Non-aqueous and hybrid Li-O2 batteries. *Adv. Energy Mater.* **2,** 801–815 (2012).

16. Zakharchenko, T. K., Kozmenkova, A. Y., Itkis, D. M. & Goodilin, E. A. Lithium peroxide crystal clusters as a natural growth feature of discharge products in Li-O2 cells. *Beilstein J. Nanotechnol.* **4,** 758–762 (2013).

17. Nazar, L. *et al.* Current Density Dependence of Peroxide Formation in the Li-O2 Battery and its Effect on Charge. *Energy Environ. Sci.* **6,** 1772–1778 (2013).

18. Johnson, L. *et al.* The role of LiO2 solubility in O2 reduction in aprotic solvents and its consequences for Li-O2 batteries. *Nat. Chem.* **6,** 1091–1099 (2014).

19. Schwenke, K. U., Metzger, M., Restle, T., Piana, M. & Gasteiger, H. A. The Influence of Water and Protons on Li2O2 Crystal Growth in Aprotic Li-O2 Cells. *J. Electrochem. Soc.* **162,** A573–A584 (2015).

20. Aetukuri, N. B. *et al.* Solvating additives drive solution-mediated electrochemistry and enhance toroid growth in non-aqueous Li-O2 batteries. *Nat. Chem.* **7,** 50–56 (2015).

21. Tatara, R. *et al.* Oxygen Reduction Reaction in Highly Concentrated Electrolyte Solutions of Lithium Bis(trifluoromethanesulfonyl)amide/Dimethyl Sulfoxide. *J. Phys. Chem. C* **121,** 9162–9172 (2017).

22. Kwon, H.-M. *et al.* Effect of Anion in Glyme-based Electrolyte for Li-O2 Batteries: Stability/Solubility of Discharge Intermediate. *Chem. Lett.* **46,** 573–576 (2017).

23. Thackeray, M. M., Wolverton, C. & Isaacs, E. D. Electrical energy storage for transportation—approaching the limits of, and going beyond, lithium-ion batteries. *Energy Environ. Sci.* **5,** 7854 (2012).

24. Tikekar, M. D., Choudhury, S., Tu, Z. & Archer, L. A. Design principles for electrolytes and interfaces for stable lithium-metal batteries. *Nat. Energy* **1,** 1–7 (2016).

25. McCloskey, B. D., Bethune, D. S., Shelby, R. M., Girishkumar, G. & Luntz, A. C. Solvents' Critical Role in Nonaqueous Lithium–Oxygen Battery Electrochemistry. *J. Phys. Chem. Lett.* **2,** 1161–1166 (2011).

26. Gallant, B. M. *et al.* Chemical and Morphological Changes of Li–O2 Battery Electrodes upon Cycling. *J. Phys. Chem. C* **116,** 20800–20805 (2012).

27. Sharon, D. *et al.* Oxidation of Dimethyl Sulfoxide Solutions by Electrochemical Reduction of Oxygen. *J. Phys. Chem. Lett.* **4,** 3115–3119 (2013).

28. Kwabi, D. G. *et al.* Chemical Instability of Dimethyl Sulfoxide in Lithium–Air Batteries. *J. Phys. Chem. Lett.* **5,** 2850–2856 (2014).

29. Mozhzhukhina, N. *et al.* Insights into dimethyl sulfoxide decomposition in Li-O2 battery: Understanding carbon dioxide evolution. *Electrochem. commun.* **80,** 16–19 (2017).

30. McCloskey, B. D. *et al.* Twin Problems of Interfacial Carbonate Formation in Nonaqueous Li–O2 Batteries. *J. Phys. Chem. Lett.* **3,** 997–1001 (2012).

31. Ottakam Thotiyl, M. M., Freunberger, S. A., Peng, Z. & Bruce, P. G. The Carbon Electrode in Non-aqueous Li-O2 Cells. *J. Am. Chem. Soc.* **135,** 494–500 (2012).

32. McCloskey, B. D. *et al.* On the efficacy of electrocatalysis in nonaqueous Li-O2 batteries. *J. Am. Chem. Soc.* **133,** 18038–41 (2011).

33. Gao, X., Chen, Y., Johnson, L. & Bruce, P. G. Promoting solution phase discharge in Li-O2 batteries containing weakly solvating electrolyte solutions. *Nat. Mater.* **15,** 882–888 (2016).

34. Liang, Z. & Lu, Y. C. Critical Role of Redox Mediator in Suppressing Charging Instabilities of Lithium-Oxygen Batteries. *J. Am. Chem. Soc.* **138,** 7574–7583 (2016).

35. Chen, Y., Freunberger, S. A., Peng, Z., Fontaine, O. & Bruce, P. G. Charging a Li-O_2 battery using a redox mediator. *Nat. Chem.* **5,** 489–94 (2013).

36. Liu, T. *et al.* Cycling Li-O2 batteries via LiOH formation and decomposition. *Science (80-.).* **350,** 530–533 (2015).

37. Laoire, C. O., Mukerjee, S., Abraham, K. M., Plichta, E. J. & Hendrickson, M. A. Influence of nonaqueous solvents on the electrochemistry of oxygen in the rechargeable lithium-air battery. *J. Phys. Chem. C* **114,** 9178–9186 (2010).

38. Khetan, A., Luntz, A. & Viswanathan, V. Trade-offs in capacity and rechargeability in nonaqueous Li-O2 batteries: Solution-driven growth versus nucleophilic stability. *J. Phys. Chem. Lett.* **6,** 1254–1259 (2015).

Chapter Two: Long Term Chemical Stability of Li-O_2 Solvents

2.1 The Search for a Stable Solvent with High Capacity

One of the primary limitations in the development of Li-O_2 batteries is the need for better electrolyte solvents. An ideal Li-O_2 battery solvent would allow for large formations of Li_2O_2 while being completely stable to parasitic side reactions during both discharge and charge. The search for a solvent that meets these ideal characteristics has resulted in studies of many different types of candidates. Liquid non-aqueous solvents studied include ethers[1], sulfoxides[2], amides[3], nitriles[4], and carbonates[5]. Other types of electrolytes studied have included ionic liquids[6], polymers[7], and ceramic solid-state electrolytes[8]. While liquid organic solvents are the most promising from the stand-point of maximizing capacity due to their high ionic conductivity, flexibility, and low weight, they also appear to be the most susceptible to various side reactions. Carbonate electrolytes typically used in Li-ion batteries such as ethylene carbonate and dimethyl carbonate were found to produce Li_2CO_3 instead of Li_2O_2 due to the dominance of side reactions[1]. Ethers such as dimethoxyethane were found to produce some side product but stably form and decompose Li_2O_2 for tens of cycles[9].

One solvent of interest from the standpoint of optimizing stability and capacity is dimethyl sulfoxide (DMSO). Dimethyl sulfoxide has a high solubility for lithium superoxide, Li^+-O_2^-, which could translate to high capacity by enabling copious toroid formation[10]. Dimethyl sulfoxide supports the formation of Li_2O_2 upon discharge[11,12]. Prior to this study, conflicting reports concerning the stability of DMSO had been published. Mozhzhukhina et al. reported no decomposition of DMSO with Li_2O_2 over long times but noted superoxide nucleophilic attack of DMSO could cause solvent decomposition to dimethyl sufone[13]. Sharon et al. observed the conversion of Li_2O_2 to LiOH in the presence of DMSO during discharge[14]. However, Peng et al. and Ottakam Thotiyl et al. had shown very promising cycling results for DMSO on gold and TiC electrodes[15,16]. Cycling was performed on the order of hundreds of

cycles and differential electrochemical mass spectroscopy measured evolved gases to check for parasitic side reactions. They reported only the consumption and evolution of oxygen, consistent with negligible side reactions. Efforts to reproduce the results of Peng et al. by McCloskey et al. were unsuccessful[17].

In order to determine whether DMSO was stable for commercial Li-O_2 application, we performed a time series of microscopy and spectroscopy measurements of electrochemically-formed and commercial ball-milled Li_2O_2 in the presence of DMSO. This helped determine that DMSO is initially stable in the presence of lithium superoxide and lithium peroxide, but decomposes to dimethyl sulfone over sufficiently long time scales.

2.2 Electrochemically Formed Li_2O_2 in Dimethyl Sulfoxide

In order to study the possible chemical interactions between Li_2O_2 and DMSO, Li-O_2 cells were constructed with 0.1 M $LiClO_4$ DMSO and discharged to high capacity at a constant discharge rate. The electrodes were free-standing carpets of carbon nanotubes (~1 cm x 1cm x ~1 μm). Carbon nanotubes have high surface area, allowing for the copious formation of Li_2O_2 and providing better signal for spectroscopic measurements. Additionally, as the diameter of the carbon nanotubes is on the order of nanometers, imaging of the discharge product by scanning electron microscopy (SEM) and transmission electron microscopy (TEM) is readily performed[18].

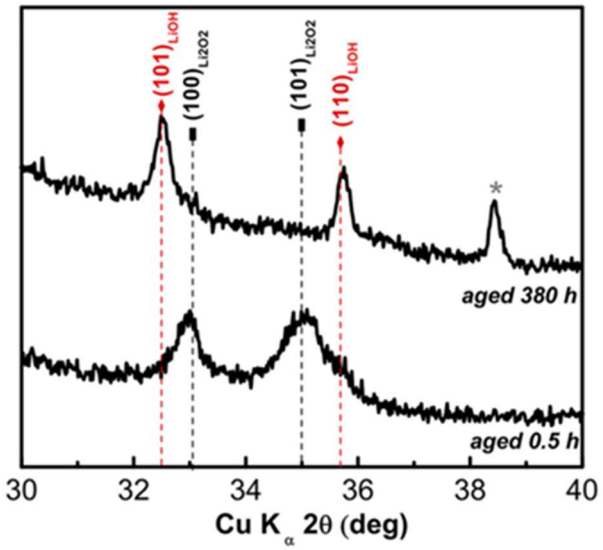

Figure 2.2.1: X-Ray Diffraction of Discharged Li-O_2 Electrodes in DMSO X-ray diffraction pattern of a discharged electrode in 0.1 M $LiClO_4$ DMSO at 100 mA/g_{CNT} to a capacity of ~3000 mAh/g_{CNT}. The bottom spectrum was taken ~30 minutes subsequent to discharge and the top spectrum was taken of the same sample after ~380 hours of aging[19].

Performing X-ray diffraction at various times subsequent to discharge in CNT electrodes with 0.1 M $LiClO_4$ DMSO offered some immediate insight into why conflicting reports of DMSO stability existed. X-ray diffraction is a technique which involves the measurement of the angle of diffraction of incident X-rays on a material to characterize its crystalline structure. Both Li_2O_2 and LiOH have crystalline phases with characteristic peaks in the regime of 30-40 degrees (2θ). The characteristic peaks of Li_2O_2 occur at ~33 and ~35 degrees (2θ) while LiOH has characteristic peaks closer to ~32 and ~36 degrees (2θ). Measurements were taken using a sealed sample holder with an argon atmosphere to prevent reactions with ambient air. A sample discharge at 100 mA/g_{CNT} only produced the characteristic peaks for Li_2O_2 when measured after a half hour subsequent to discharge. However, the same sample produced the characteristic peaks for LiOH after ~380 hours (Figure 2.2.1). This suggests the chemical conversion of

Li_2O_2 to LiOH. It also rationalizes the mixed reports in the literature. Optimistic studies concerning the stability of Li_2O_2 in DMSO were likely based on measurements during or immediately after discharge.

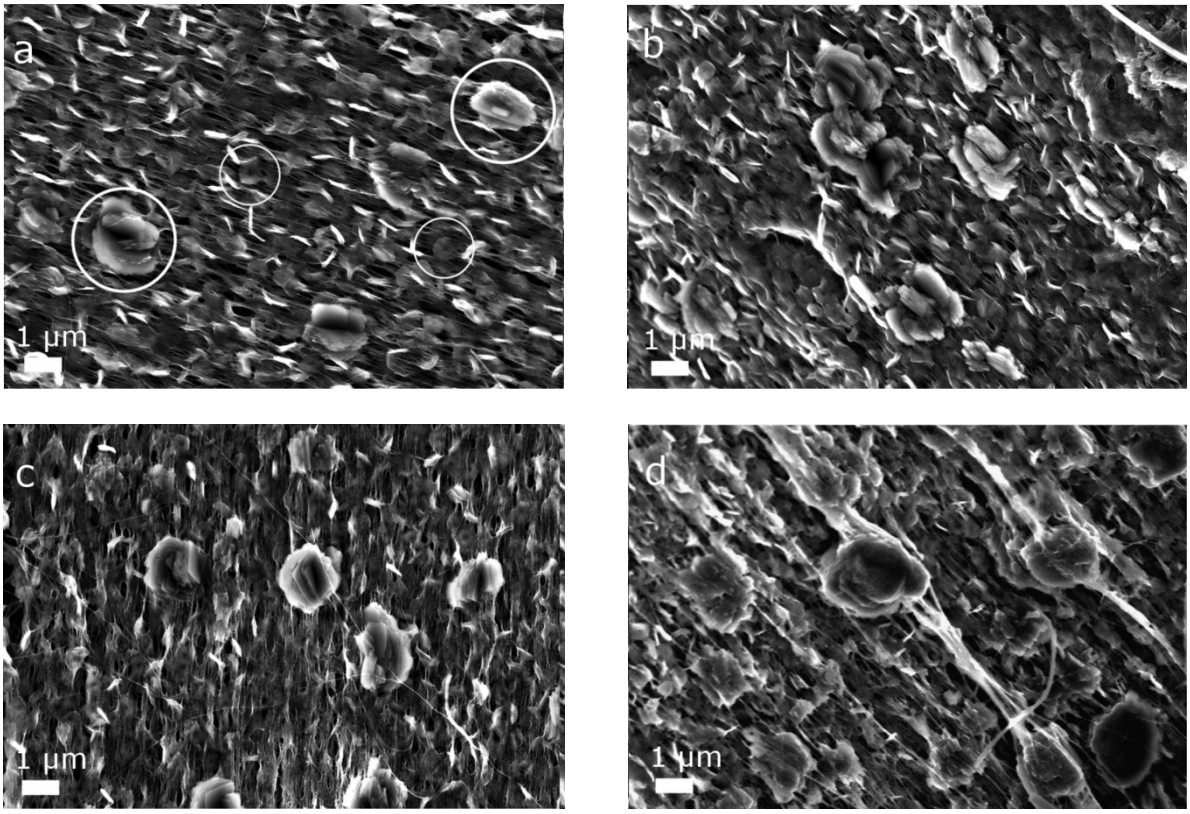

Figure 2.2.2: Scanning Electron Micrographs of Discharged Li-O_2 Electrodes in DMSO CNT electrode discharged at 25 mA/g_{CNT} to ~4000 mAh/g_{CNT} in 0.1 M $LiClO_4$ DMSO. Scanning electron microscopy was performed after a) ~30 minutes, b) ~12 hours, c) ~24 hours, and d) ~576 hours of aging after the end of discharge. Samples of LiOH flakes are marked by large circles and Li_2O_2 toroids are marked by small circles[19].

To gain further insight into the XRD results, a series of scanning electron microscopy (SEM) micrographs were collected at various time intervals after the end of discharge. A low rate (25 mA/g_{CNT}) was used at which the characteristic toroidal morphology of Li_2O_2 should be readily recognizable by SEM. Electrodes were removed from the cell after discharge and allowed to sit in the discharge solvent

in an argon environment glove-box until imaging. Electrodes were transported to the microscope sealed in an argon environment and rapidly transferred to vacuum in the SEM to minimize exposure to the ambient atmosphere. When imaged after ~30 minutes subsequent to discharge, the sample had both ~100 nm toroids typical of Li_2O_2 and ~1 µm flake-like particles (Figure 2.2.2a). We attribute the flake-like particles to LiOH based on our XRD results. As the sample is allowed to age in argon for progressively longer times (Figure 2.2.2b,c,d) the flakes become more dominant and toroids less evident. After ~576 hours (Figure 2.2.2d), the flakes are the primary features visible in the electrode and few toroids are observed. This is consistent with the observation in XRD of the conversion of electrochemically-formed Li_2O_2 to LiOH after aging in DMSO.

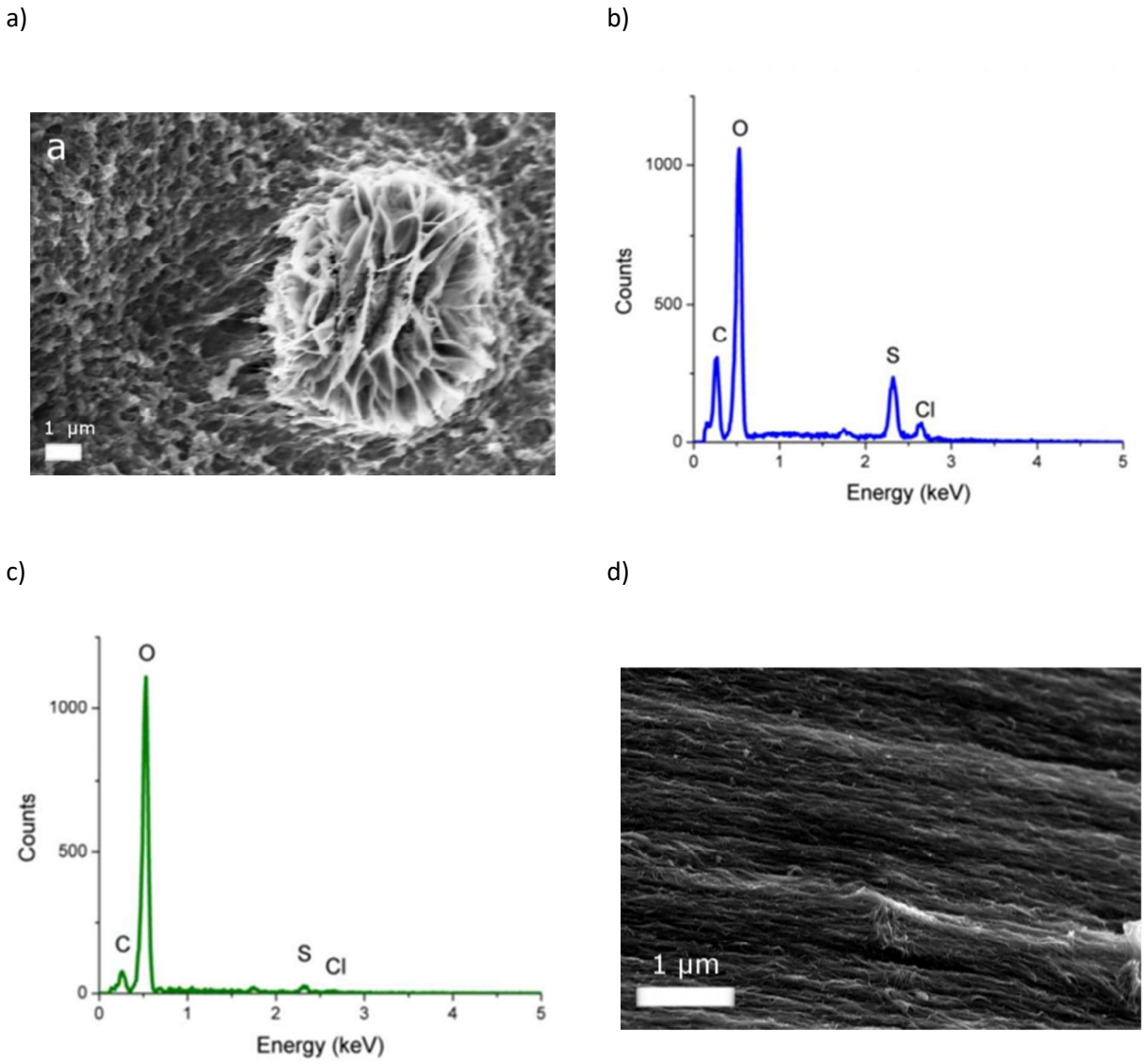

Figure 2.2.3: SEM Characterization of Flake-like Particles a) Energy dispersive X-ray spectroscopy (EDS) was performed on a flake-like particle in the SEM image shown from a sample discharge at 25 mA/g_{CNT} to ~4000 mAh/g_{CNT} in 0.1 M $LiClO_4$ DMSO b) EDS in a region of the electrode without flakes c) EDS taken in a region of the flake-like particle d) CNT carpet soaked in 0.1 M $LiClO_4$ DMSO for ~48 hours[19].

In order to check that flakes were the result of the formation of LiOH and not due to precipitation of $LiClO_4$ as DMSO evaporates, energy dispersive X-ray spectroscopy (EDS) was performed

on regions of a sample with and without flakes (Figure 2.2.3a). EDS can characterize the elemental composition of an imaged region of a sample. The flakes showed a lower peak for chlorine, indicating that the flakes were an oxygen-based compound (Figure 2.2.3b,c). EDS cannot detect hydrogen or lithium, so these results are consistent with either Li_2O_2 or LiOH. Coupling these results with XRD results strongly suggests that the flakes are LiOH. Further evidence was provided by imaging CNTs which had been soaked in $LiClO_4$ DMSO that showed no evolution of flake-like precipitates from $LiClO_4$ precipitation (Figure 2.2.3d).

Another possible source of error was high water content causing a reaction between water and either superoxide or lithium peroxide to form lithium hydroxide. However, the water content of 0.1 M $LiClO_4$ DMSO was measured by Karl Fischer titration and found to be below ~30 ppm. Complete reaction of this amount of water with Li_2O_2 to form LiOH would only result in the conversion about 1% of the Li_2O_2[19].

2.3 Commercial Li_2O_2 Powder in Dimethyl Sulfoxide

XRD and SEM studies of Li_2O_2 conversion to LiOH in discharged electrodes in the presence of DMSO suggests that DMSO has a role in the instability of Li_2O_2. However, further study was needed to determine if a direct reaction between DMSO and Li_2O_2 was occurring. Mixtures of DMSO and commercially available ball-milled Li_2O_2 were prepared and allowed to age.

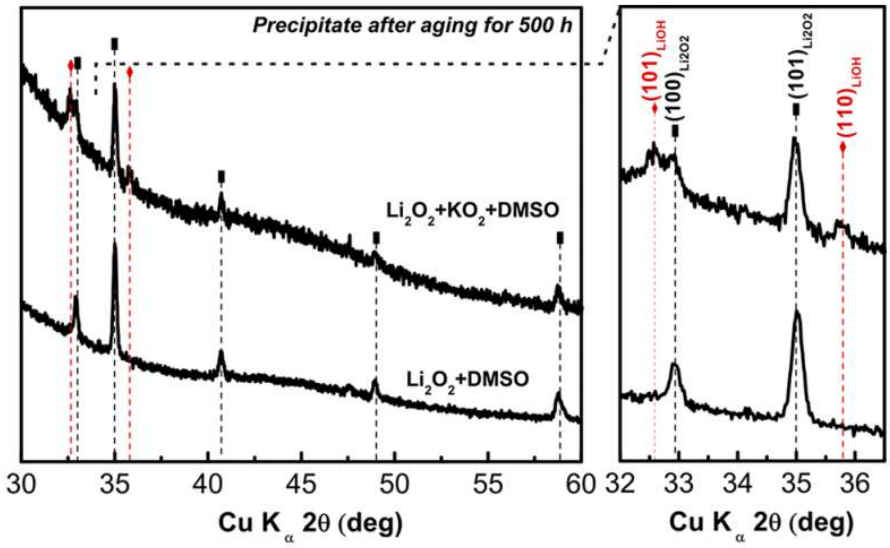

Figure 2.3.1: XRD Measurements of Li_2O_2 and DMSO Mixtures The bottom spectrum is of a mixture of Li_2O_2 and DMSO aged for ~500 hours in a ratio of 1:100 and the top spectrum is of a mixture of KO_2, Li_2O_2, and DMSO aged for ~500 hours in a ratio of 1:1:100. The plot on the right is a magnification of the plot on the left[19].

A 1:100 mixture of Li_2O_2 and DMSO was prepared and continuously stirred for ~500 hours before centrifugation and XRD measurement of the solid (Figure 2.3.1). The characteristic peaks for Li_2O_2 were observed while the characteristic peaks for LiOH were not observed. This suggests that commercial Li_2O_2 is more stable in DMSO than electrochemically formed Li_2O_2. One possible explanation is that the surface of electrochemically formed Li_2O_2 is known to be oxygen-rich and behave like superoxide[20]. To reflect the influence of superoxide on the decomposition of electrochemical Li_2O_2 in DMSO, a mixture of 1:1:100 KO_2:Li_2O_2:DMSO was prepared and stirred for ~500 hours. In this sample, peaks for both LiOH and Li_2O_2 are clearly evident, suggesting that superoxide has a critical role in Li_2O_2 decomposition to LiOH.

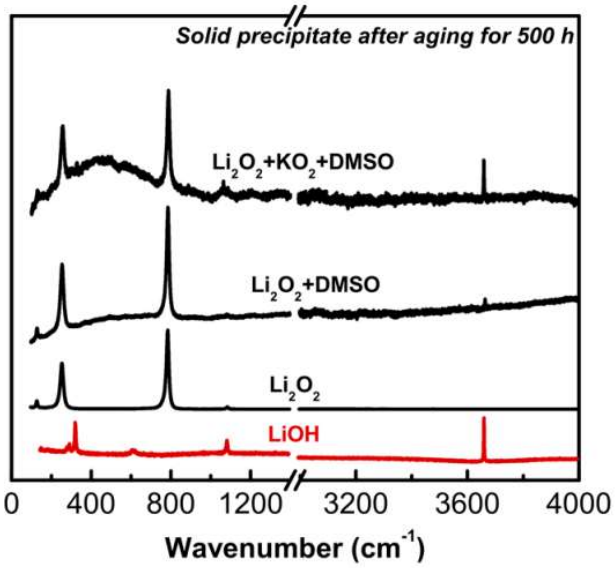

Figure 2.3.2: Raman Spectroscopy Measurements of Li_2O_2 and DMSO Mixtures The bottom spectrum is of a mixture of Li_2O_2 and DMSO aged for ~500 hours in a ratio of 1:100 and the top spectrum is of a mixture of KO_2, Li_2O_2, and DMSO aged for ~500 hours in a ratio of 1:1:100[19].

Raman spectroscopy measurements of the solid precipitate after aging and centrifugation yield similar results as characterization by XRD, except a small peak for LiOH was detected in the mixture without KO_2, suggesting some reactivity even in the absence of superoxide molecules (Figure 2.3.2). While these measurements clearly demonstrate that superoxide in DMSO promotes the decomposition of Li_2O_2 to LiOH, further experiments were needed to determine by what mechanism.

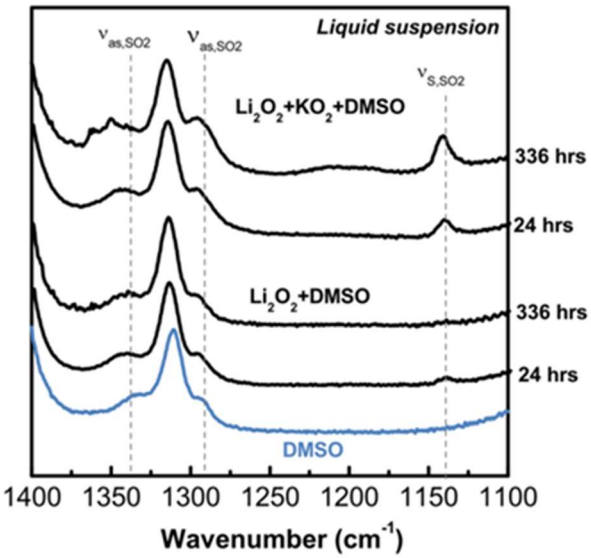

Figure 2.3.3: Fourier-Transform Infrared Spectroscopy of Li_2O_2 and DMSO Mixtures The blue line is a FT-IR standard spectrum for DMSO. FT-IR results are shown for 1:100 Li_2O_2 and DMSO mixtures after 24 and 336 hours of aging and 1:1:100 KO_2, Li_2O_2, and DMSO mixtures after 24 and 336 hours[19].

In order to determine if DMSO was participating in the conversion of Li_2O_2 to LiOH, Fourier-transform infrared (FT-IR) spectroscopy was performed on the liquid supernatant of 1:100 mixtures of Li_2O_2 and DMSO after aging and centrifugation (Figure 2.3.3). Fourier-transform infrared spectroscopy allows for the characterization of the bonding of the molecules based on absorption spectra of different frequencies of light. No significant changes were observed in the spectra of the Li_2O_2 and DMSO mixture after aging for 24 hours and 336 hours. However, when the same experiment was performed with a mixture of 1:1:100 KO_2, Li_2O_2, and DMSO, a peak corresponding to the sulfone group evolved as the time of aging increased. This indicates that as Li_2O_2 converts to LiOH, dimethyl sulfoxide converts to dimethyl sulfone.

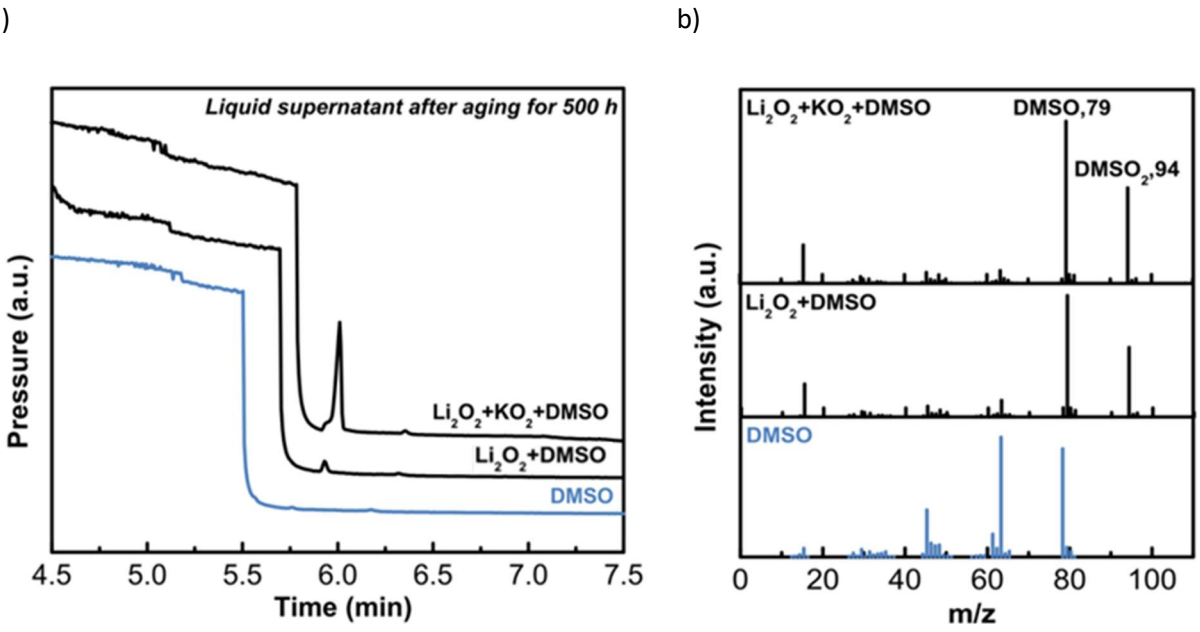

Figure 2.3.4 Gas Chromatography of Li_2O_2 and DMSO Mixtures a) Gas chromatography results for mixtures of 1:100 Li_2O_2 and DMSO and 1:1:100 KO_2, Li_2O_2, and DMSO after aging for 500 hours and centrifugation b) Mass spectra of these mixtures[19].

In order to further analyze the evolution of dimethyl sulfone, gas chromatography measurements were taken of liquid supernatant of 1:100 Li_2O_2 and DMSO and 1:1:100 KO_2, Li_2O_2, and DMSO mixtures after aging for 500 hours and centrifugation (Figure 2.3.4). Gas chromatography characterizes compounds in a mixture by flowing a carrier gas through a column with the mixture present. Different species will travel through the column with a characteristic retention time. In our experiments, new species evolved at ~6 min that were not observed in pure DMSO, indicating the presence of decomposition products in the liquid supernatant. Mass spectroscopy confirmed that the species evolving at this peak at ~6 min were dimethyl sulfone. Gas chromatography yields similar results as FT-IR spectroscopy but due to its greater signal is able to show that some amount of dimethyl sulfone is forming in the mixture without KO_2. This suggests that DMSO is not stable with Li_2O_2, but the presence of superoxide enhances the decomposition. It also explains why some reports observed stability

between Li_2O_2 and DMSO after long times, as these studies characterized the liquid suspension only with FT-IR and not gas-chromatography, which might have detected dimethyl sulfone[13,21].

2.4 Mechanisms of Dimethyl Sulfoxide and Li_2O_2 Decomposition

These experiments provided necessary insights into the mechanism of Li_2O_2 instability in DMSO. Mozhzhukhina et al. had previously proposed a reaction mechanism for the decomposition of DMSO to dimethyl sulfone by direct nucleophilic attack by superoxide[13] (Figure 2.4.1a). This mechanism was proposed based on their observation by FT-IR of the formation of dimethyl sulfone in the solvent subsequent to discharge. However, this study did not analyze the solid discharge product and did not observe the formation of LiOH, which is not accounted for by the proposed reaction mechanism. Sharon et al. reported a mechanism that results in the formation of both LiOH and dimethyl sulfone based on their observation of LiOH by XRD and dimethyl sulfone by nuclear magnetic resonance (NMR) spectroscopy[14] (Figure 2.4.1b). Our study suggests that this is the correct mechanism for decomposition of DMSO. The presence of lithium superoxide or superoxide-like oxygen rich surface sites in electrochemically formed Li_2O_2 promotes hydrogen abstraction from DMSO. Superoxide forms hydroperoxyl radicals with protons. This allows for the reaction of DMSO with hydroperoxyl species to form dimethyl sulfone and lithium hydroxide. Our study advances beyond what was reported by Sharon et al.[14] in that they suggest that the decomposition occurs during discharge while our experiments have shown chemical decomposition can occur subsequent to discharge by residual superoxide and superoxide-like sites on Li_2O_2. This suggests the promising results of Peng et al.[15] were due to rapid discharge and charge before the decomposition of DMSO could occur. It does not appear that the choice of electrode should affect the decomposition reaction as Peng et al. suggested.

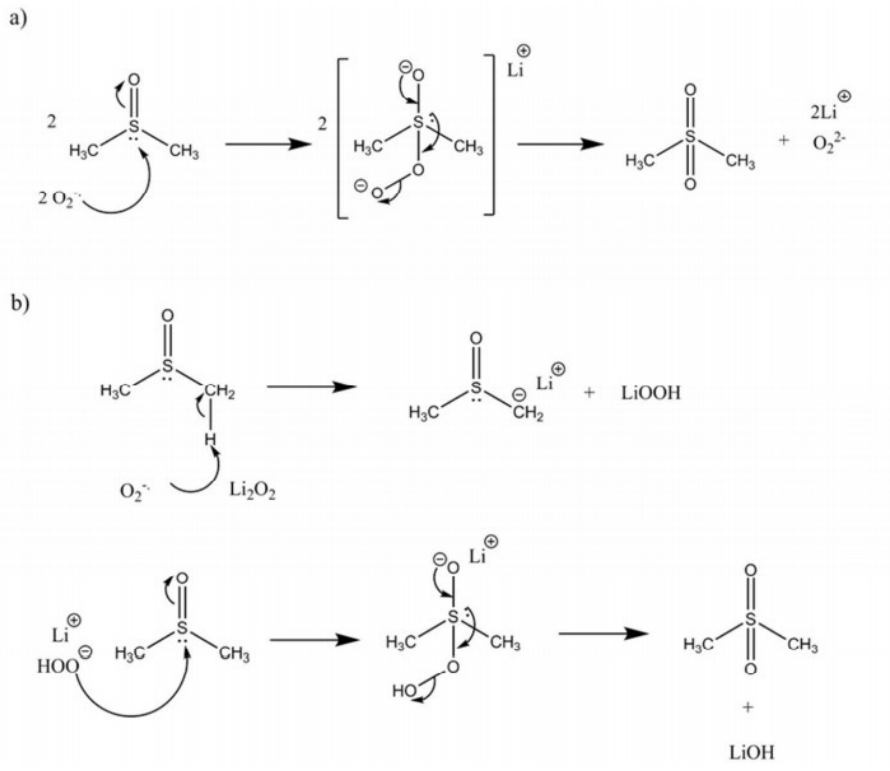

Figure 2.4.1 Schematic of Possible DMSO Decomposition Pathways a) Nucleophilic attack of DMSO by lithium superoxide b) Hydrogen abstraction from DMSO by superoxide causing the ultimate formation of LiOH and dimethyl sulfone[19].

Studies published subsequent to our report have largely confirmed the conclusion that DMSO is not chemically stable with superoxide and Li_2O_2. One report suggests that DMSO is stable in contact with Li_2O_2, but this report relies on FT-IR results and not higher precision gas chromatography measurements[21]. Marchini et al. observed decomposition of DMSO at the interface with Li_2O_2 on a highly-oriented pyrolytic graphite electrode by X-ray spectroscopy[22]. Sankarasubramanian et al. observed evidence of side reactions with superoxide in DMSO rotating ring-disk electrode experiments[23]. Mozhzhukhina et al. observed the formation of carbonates on gold electrodes during Li-

O_2 discharge[24]. These studies demonstrate that DMSO is chemically unstable with Li_2O_2 and superoxide reaction intermediates.

While DMSO is not suitable for commercial use, it can still be of insight for fundamental study under appropriate conditions. It can provide valuable insight into the behavior of Li-O_2 discharge under high Li^+-O_2^- solubility conditions[25,26]. Chemical reactions between Li_2O_2 and DMSO occur on long time scales and short time scale studies may not be greatly influenced by the side reactions. The studies of cycling on Au[15] and TiC[16] in DMSO occurred at a fast rate and to a limited depth of discharge, indicating Li_2O_2 and DMSO were stable under short time regimes. Mozhzhukhina et al. report no degradation of DMSO in the presence of KO_2 after 24 hours; the detection of conversion to dimethyl sulfone by FT-IR occurred after aging the mixture of DMSO and KO_2 for 2 months. Both Kwabi et al.[25] and Sharon et al.[14] report stable cycling of Li_2O_2 by using electrochemical quartz-crystal microbalance (EQCM) measurements. Under practical conditions for commercial use, Li-O_2 batteries must discharge over long periods of time and remain stable if left in the charged state. The long-time regime decomposition of Li_2O_2 and DMSO indicates that this is not possible. However, stable Li-O_2 discharge and cycling is possible when short time scales are used, excess solvent is present, and Li_2O_2 forms as a thin film with low solvent interface area. This enables the use of DMSO for laboratory scale fundamental study.

2.5 Conclusion

DMSO has received interest as an electrolyte for Li-O_2 batteries due to its high Li^+-O_2^- solubility and reports of high stability in some cases. However, conflicting reports existed about its chemical stability with lithium peroxide and superoxide. By performing time-series characterizations of commercial ball-milled Li_2O_2 and electrochemically formed Li_2O_2 we were able to determine that Li_2O_2 and DMSO are unstable when in contact with each other, forming LiOH and dimethyl sulfone. These

reactions are promoted by the presence of superoxide and can continue to occur long after discharge has ended. Characterization of the discharge product as Li_2O_2 or LiOH will depend on the duration of the discharge and aging of the electrode prior to measurement. While DMSO is not feasible for commercial use, the decomposition reaction is slow and DMSO can be valuable for fundamental study of Li-O_2 discharge mechanisms under appropriate conditions.

References

1. McCloskey, B. D., Bethune, D. S., Shelby, R. M., Girishkumar, G. & Luntz, A. C. Solvents' Critical Role in Nonaqueous Lithium–Oxygen Battery Electrochemistry. *J. Phys. Chem. Lett.* **2,** 1161–1166 (2011).
2. Xu, D., Wang, Z., Xu, J., Zhang, L. & Zhang, X. Novel DMSO-based electrolyte for high performance rechargeable Li-O2 batteries. *Chem. Commun. (Camb).* **48,** 6948–50 (2012).
3. Walker, W. *et al.* A rechargeable Li-O2 battery using a lithium nitrate/ N,N-dimethylacetamide electrolyte. *J. Am. Chem. Soc.* **135,** 2076–2079 (2013).
4. Laoire, C. O., Mukerjee, S., Abraham, K. M., Plichta, E. J. & Hendrickson, M. A. Influence of nonaqueous solvents on the electrochemistry of oxygen in the rechargeable lithium-air battery. *J. Phys. Chem. C* **114,** 9178–9186 (2010).
5. Herranz, J., Garsuch, A. & Gasteiger, H. A. Using rotating ring disc electrode voltammetry to quantify the superoxide radical stability of aprotic Li-air battery electrolytes. *J. Phys. Chem. C* **116,** 19084–19094 (2012).
6. Allen, C. J., Mukerjee, S., Plichta, E. J., Hendrickson, M. A. & Abraham, K. M. Oxygen Electrode Rechargeability in an Ionic Liquid for the Li–Air Battery. *J. Phys. Chem. Lett.* **2,** 2420–2424 (2011).
7. Abraham, K. M. A Polymer Electrolyte-Based Rechargeable Lithium/Oxygen Battery. *J. Electrochem. Soc.* **143,** 1 (1996).
8. Kitaura, H. & Zhou, H. Electrochemical Performance of Solid-State Lithium-Air Batteries Using Carbon Nanotube Catalyst in the Air Electrode. *Adv. Energy Mater.* **2,** 889–894 (2012).
9. Gallant, B. M. *et al.* Chemical and Morphological Changes of Li–O2 Battery Electrodes upon Cycling. *J. Phys. Chem. C* **116,** 20800–20805 (2012).
10. Johnson, L. *et al.* The role of LiO2 solubility in O2 reduction in aprotic solvents and its consequences for Li-O2 batteries. *Nat. Chem.* **6,** 1091–1099 (2014).
11. Trahan, M. J., Mukerjee, S., Plichta, E. J., Hendrickson, M. A. & Abraham, K. M. Studies of Li-Air Cells Utilizing Dimethyl Sulfoxide-Based Electrolyte. *J. Electrochem. Soc.* **160,** A259–A267 (2012).

12. Laoire, C. O., Mukerjee, S., Abraham, K. M., Plichta, E. J. & Hendrickson, M. A. Elucidating the Mechanism of Oxygen Reduction for Lithium-Air Battery Applications. *J. Phys. Chem. C* **113,** 20127–20134 (2009).

13. Mozhzhukhina, N., Méndez De Leo, L. P. & Calvo, E. J. Infrared spectroscopy studies on stability of dimethyl sulfoxide for application in a Li-air battery. *J. Phys. Chem. C* **117,** 18375–18380 (2013).

14. Sharon, D. *et al.* Oxidation of Dimethyl Sulfoxide Solutions by Electrochemical Reduction of Oxygen. *J. Phys. Chem. Lett.* **4,** 3115–3119 (2013).

15. Peng, Z., Freunberger, S. A., Chen, Y. & Bruce, P. G. A reversible and higher-rate Li-O2 battery. *Science* **337,** 563–6 (2012).

16. Ottakam Thotiyl, M. M. *et al.* A stable cathode for the aprotic Li-O2 battery. *Nat. Mater.* **12,** 1050–6 (2013).

17. McCloskey, B. D. *et al.* Combining Accurate O 2 and Li 2 O 2 Assays to Separate Discharge and Charge Stability Limitations in Nonaqueous Li–O 2 Batteries. *J. Phys. Chem. Lett.* **4,** 2989–2993 (2013).

18. Mitchell, R. R., Gallant, B. M., Shao-Horn, Y. & Thompson, C. V. Mechanisms of Morphological Evolution of Li 2 O 2 Particles during Electrochemical Growth. *J. Phys. Chem. Lett.* **4,** 1060–1064 (2013).

19. Kwabi, D. G. *et al.* Chemical Instability of Dimethyl Sulfoxide in Lithium–Air Batteries. *J. Phys. Chem. Lett.* **5,** 2850–2856 (2014).

20. Yang, J. *et al.* Evidence for lithium superoxide-like species in the discharge product of a Li-O2 battery. *Phys. Chem. Chem. Phys.* **15,** 3764–71 (2013).

21. Schroeder, M. A. *et al.* DMSO–Li $_2$ O $_2$ Interface in the Rechargeable Li–O $_2$ Battery Cathode: Theoretical and Experimental Perspectives on Stability. *ACS Appl. Mater. Interfaces* **7,** 11402–11411 (2015).

22. Marchini, F., Herrera, S. E., Calvo, E. J. & Williams, F. J. Surface studies of lithium-oxygen redox reactions over HOPG. *Surf. Sci.* **646,** 154–159 (2016).

23. Sankarasubramanian, S., Seo, J., Mizuno, F., Singh, N. & Prakash, J. Rotating Ring-Disc Electrode Investigation of the Aprotic Superoxide Radical Electrochemistry on Multi-Crystalline Surfaces and Correlation with Density Functional Theory Modeling: Implications for Lithium-Air Cells. *J. Electrochem. Soc.* **163,** A2377–A2384 (2016).

24. Mozhzhukhina, N. *et al.* Insights into dimethyl sulfoxide decomposition in Li-O2battery: Understanding carbon dioxide evolution. *Electrochem. commun.* **80,** 16–19 (2017).

25. Kwabi, D. G. *et al.* Controlling Solution-Mediated Reaction Mechanisms of Oxygen Reduction Using Potential and Solvent for Aprotic Lithium-Oxygen Batteries. *J. Phys. Chem. Lett.* **7,** 1204–1212 (2016).

26. Bondue, C. J., Hegemann, M., Molls, C., Thome, E. & Baltruschat, H. A Comprehensive Study on Oxygen Reduction and Evolution from Lithium Containing DMSO Based Electrolytes at Gold Electrodes. *J. Electrochem. Soc.* **163,** A1765–A1775 (2016).

Chapter Three: Effect of Water Content on Li-O_2 Discharge Morphology and Solvent Stability

3.1 Water as a Li-O_2 Solvent Additive

Achieving both high stability and high capacity is an ongoing goal in the development of Li-O_2 batteries. Solvents that allow for high capacity by copious Li_2O_2 toroid formation often have a propensity for side reactions. Khetan et al. demonstrated that as a general trend, solvents with higher Li^+-O_2^- solubility capable of higher capacities are also more susceptible to side reactions due to nucleophilic attack by superoxide[1]. One possible strategy is to use a solvent with lower Li^+-O_2^- solubility for increased stability and include a stable solvent additive that promotes the solubility of Li^+-O_2^-.

This strategy was explored by using water as an additive. Introducing water to a non-aqueous Li-O_2 battery is not suitable for commercial use. In particular, water can be decomposed at the anode to form hydrogen and it is almost entirely consumed during charge[2]. However, adding water to the solvent can provide fundamental understanding of how additives influence Li-O_2 discharge. Water has a much higher acceptor number than non-aqueous electrolyte solvents (Table 3.1.1). Acceptor number and donor number are measures of the Lewis acidity and Lewis basicity, respectively, of a given molecule. Acceptor number is calculated by measuring the nuclear magnetic resonance (NMR) spectroscopic shift for P^{31} in triethyl phosphine oxide in solution with dichloroethane when a given molecule is added. Acceptor number is the ratio of this shift to the shift caused by adding $SbCl_5$ to the dichloroethane solution[3]. Donor number is measured by the enthalpy of the interaction of a given molecule with $SbCl_5$ in a solution of dichlorethane[3]. A high donor number solvent, such as DMSO, favors the solvation of Li^+ ion[4]. A high acceptor number solvent, such as water, favors the solvation of O_2^-[5]. High donor number and high acceptor number have been shown to correlate with increased combined solvation energy for Li^+-O_2^-[6].

Table 3.1.1 Donor and Acceptor Number of Li-O_2 Solvents

Solvent Name		Donor Number (kcal/mol)	Acceptor Number (unitless)
Dimethyl sulfoxide	DMSO	29.8 [3]	19.3 [3]
Dimethoxyethane	DME	20.0[7]	10.2 [7]
Acetonitrile	MeCN	14.1 [3]	18.9 [3]
Water	H_2O	18.0 [3]	54.8 [3]

The use of water as a solvent additive has been shown to enhance first discharge capacity[5,8]. Meini et al. first reported an effect of solvent humidity on Li-O_2 capacity[8]. Guo et al. reproduced the water-induced increase in capacity coupled with changes in discharge morphology, solvent stability, and loss of cyclability[9]. Aetukuri et al. demonstrated that the addition of water to a variety of electrolyte solvents such as dimethoxyethane (DME), dimethyl sulfoxide (DMSO), and tetraglyme (TEGDME) causes the promotion of Li_2O_2 toroids and increases discharge capacity[5]. Schwenke et al. reported the effect of water in promoting toroids and capacity and in addition observed that the effect of adding water had a discharge rate dependence[2]. Adding water increased toroid formation to a great degree at low discharge rates but minimally at high discharge rates. Schwenke et al. also used online-electrochemical mass spectroscopy to demonstrate that adding water does not prevent the stable formation of Li_2O_2.

These studies pointed toward a promising strategy of optimizing between solvent capacity and solvent stability, provided the factors that determined the stability of the solvent additive were determined. In order to study this question, we performed Li-O_2 discharges in different solvents with and without the addition of water. We analyzed the effect of adding water on morphology, stability, and capacity by examining the properties of the solvent and water interaction. Additionally, we considered the effect of water on Li_2O_2 film formed through the surface Li-O_2 discharge pathway, as the focus of the prior reports had been on the effect on toroids formed through the solvent pathway.

3.2 Stable Discharge in Dimethoxyethane with Water Additive

a)

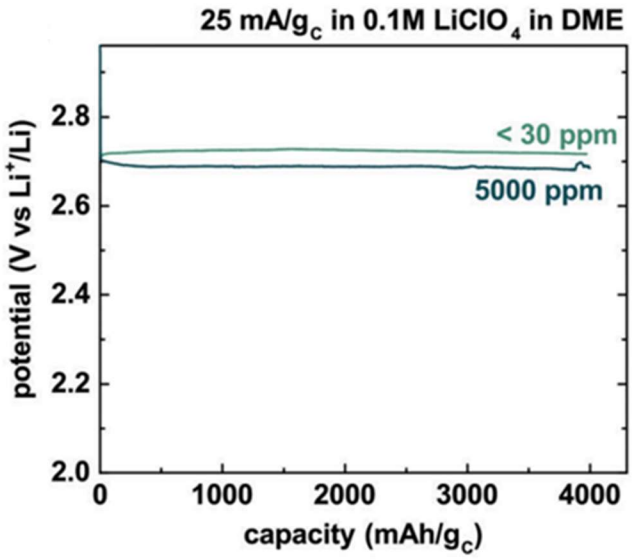

b)

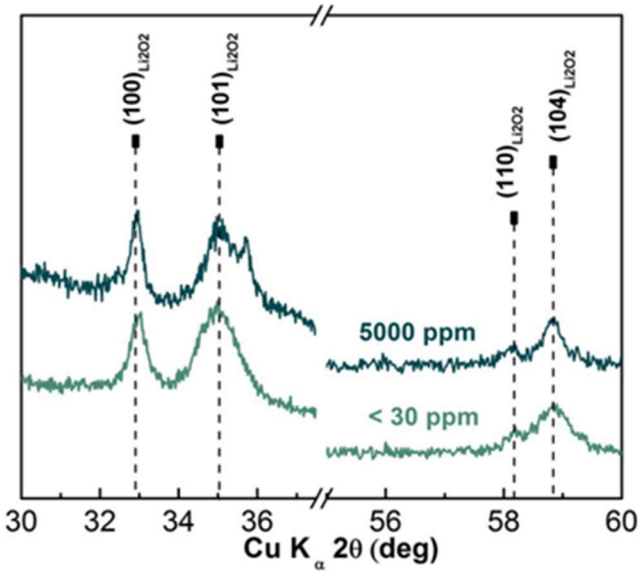

Figure 3.2.1: Effect of Added Water on Discharge Stability in DME a) Galvanostatic discharge profiles of carbon nanotube electrodes discharged in 0.1 M $LiClO_4$ DME at 25 mA/g_{CNT} to 4000 mAh/g_{CNT} in the anhydrous condition of ~< 30 ppm H_2O and with 5000 ppm H_2O added b) X-ray diffraction spectra of

carbon nanotube electrodes discharged in 0.1 M $LiClO_4$ DME at 25 mA/g_{CNT} to 4000 mAh/g_{CNT} in the anhydrous condition of ~< 30 ppm and with 5000 ppm H_2O added[10].

We chose to study the effect of water in the solvent dimethoxyethane (DME), because while DME is not completely stable during Li-O_2 discharge it is more stable compared to many other solvents on first discharge[11]. DME has a low Li^+-O_2^- solubility due to its low donor number. Adding water should enhance this solubility due to the high acceptor number of water. We performed these experiments in high surface-area carbon nanotube carpet electrodes, which allow for higher capacities and more extensive imaging by scanning electron microscopy (SEM) and transmission electron microscopy (TEM) compared to prior studies.

We performed discharges to 4000 mAh/g_{CNT} at a low discharge rate of 25 mA/g_{CNT} in samples without added water and with 5000 ppm water added (Figure 3.2.1a). The discharge potentials were roughly comparable in both samples. X-ray diffraction tested for the formation of Li_2O_2 and LiOH. Only Li_2O_2 was detected in both cases (Figure 3.2.1b), indicating that the addition of water to DME does not lead to significant side reactions on discharge, consistent with the reports of Schwenke et al[2].

a)

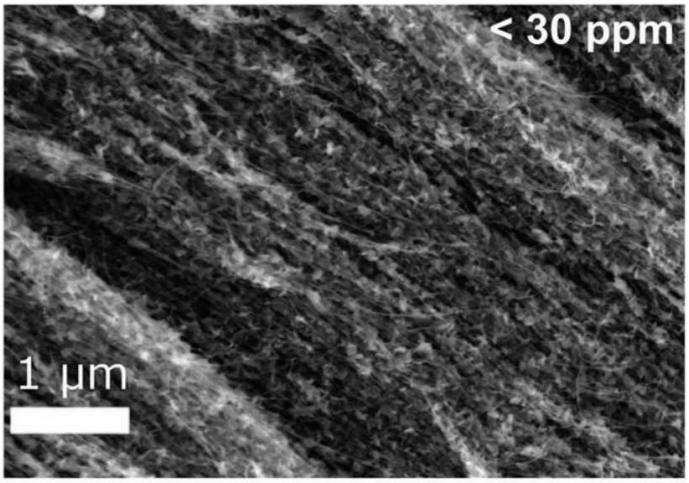

b)

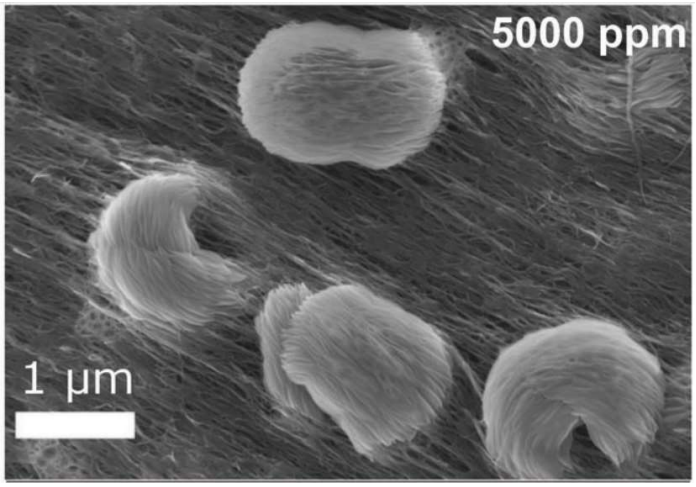

Figure 3.2.2 Effect of Water on Discharge Morphology in DME a) SEM image of a carbon nanotube electrode discharged in <30 ppm H_2O 0.1 M $LiClO_4$ DME at 25 mA/g_{CNT} to 4000 mAh/g_{CNT} b) SEM image of a nanotube electrode discharged in 5000 ppm H_2O 0.1 M $LiClO_4$ DME at 25 mA/g_{CNT} to 4000 mAh/g_{CNT}[10].

We complemented X-ray diffraction characterization by studying the effect on morphology of additional water. SEM images were collected for electrodes discharged at 25 mA/g_{CNT} both with and without the addition of 5000 ppm H_2O. In the case with <30 ppm H_2O, copious small toroids were observed with a diameter on the order of 100 nm (Figure 3.2.2a). When 5000 ppm H_2O were added,

toroid sizes with diameters of ~1 μm were observed (Figure 3.2.2b). These results are consistent with water increasing the solubility of Li^+-O_2^- in the solvent. This has been shown to promote toroid formation and also allow for larger toroid sizes as Li^+-O_2^- spends a longer time in solution to aggregate and disproportionate into larger Li_2O_2 agglomerates[2].

Li-O_2 discharges are stable in DME even with the presence of H_2O. In order to better understand what properties allowed DME to support stable Li_2O_2 evolution without side reactions due to higher water content, we sought to study a solvent that was stable during Li-O_2 discharge without added water but unstable with water.

3.3 Unstable Li-O_2 Discharge in Acetonitrile with Water Additive

Similar to DME, acetronitrile (MeCN) is a common battery solvent with low Li^+-O_2^- solubility but comparatively high stability[1,12]. The low solubility of Li^+-O_2^- in acetonitrile is attributed to its low donor number, though its acceptor number is comparable to DMSO (Table 3.1.1). Acetonitrile is not stable with lithium foil, so $LiCoO_2$ was used as an anode. Potentials were corrected to be reported vs Li^+/Li.

a)

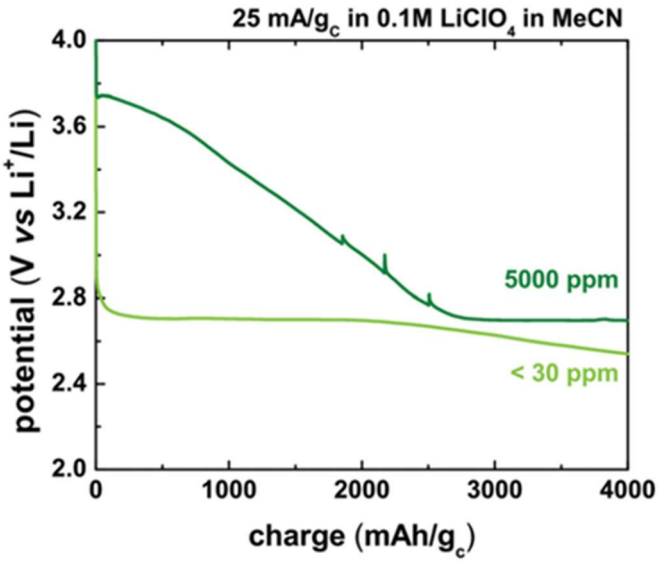

b)

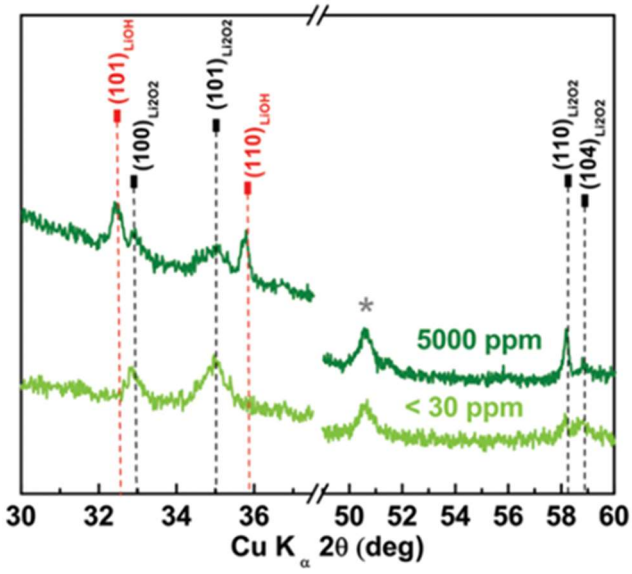

Figure 3.3.1: Effect of Added Water on Discharge Stability in MeCN a) Galvanostatic discharge profiles of carbon nanotube electrodes discharged in 0.1 M $LiClO_4$ MeCN against $LiCoO_2$ anodes at 25 mA/g_{CNT} to 4000 mAh/g_{CNT} in the anhydrous condition of ~< 30 ppm and with 5000 ppm H_2O added b) X-ray diffraction spectra of carbon nanotube electrodes discharged in 0.1 M $LiClO_4$ DME at 25 mA/g_{CNT} to 4000 mAh/g_{CNT} in the anhydrous condition of ~< 30 ppm and with 5000 ppm H_2O added[10].

When a discharge was performed in 0.1 M $LiClO_4$ MeCN at 25 mA/g_{CNT} to 4000 mAh/g_{CNT} without the addition of water, a stable discharge plateau was observed, similar to results for 0.1 M $LiClO_4$ DME (Figure 3.3.1a). However, when the same discharge was performed with the addition of 5000 ppm water, discharge began at much higher potentials which progressively declined. Schwenke et al. observed a similar increase in discharge potential when protons were used as an additive to DME, which they attribute to the reaction of protons with oxygen to form either water or hydroperoxyl radicals ($HOO^{\cdot}$)[2]. These discharge profiles suggest that side reactions occur in MeCN with added water but not in the anhydrous case. This was confirmed by performing XRD (Figure 3.3.1b). Only Li_2O_2 was observed in the anhydrous sample, while both Li_2O_2 and LiOH were observed in the sample with 5000 ppm H_2O.

a)

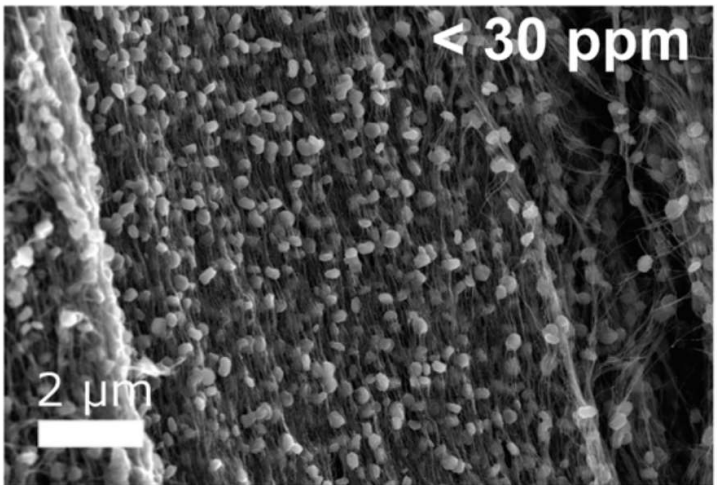

b)

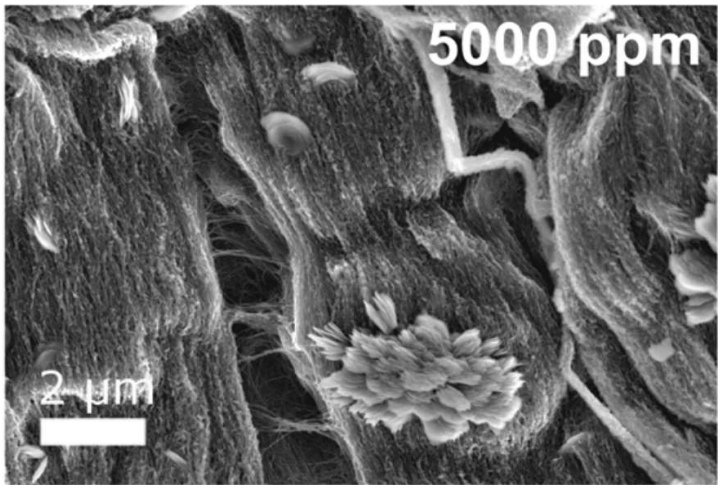

Figure 3.3.2 Effect of Water on Discharge Morphology in MeCN SEM images of carbon nanotube electrodes discharged in 0.1 M $LiClO_4$ MeCN against $LiCoO_2$ anodes at 25 mA/g_{CNT} to 4000 mAh/g_{CNT} in a) the anhydrous condition of ~< 30 ppm and b) with 5000 ppm H_2O added[10].

In order to better understand discharge mechanisms in acetonitrile, discharged electrodes were examined with SEM. Samples discharged at 25 mA/g_{CNT} to 4000 mAh/g_{CNT} in 0.1 M $LiClO_4$ MeCN without water exhibited copious toroids (Figure 3.3.2a). This is consistent with XRD results demonstrating the formation of Li_2O_2 in the absence of water. Samples discharged with 5000 ppm H_2O had some toroids typical of Li_2O_2, but also exhibited clusters of flake-like particles ~>1 µm in diameter (Figure 3.3.2b).

These collections of flakes are similar to the flake-like LiOH morphologies observed in aged DMSO discharged electrodes[13]. Classifying the flakes as LiOH is consistent with XRD results, which showed both Li_2O_2 and LiOH in discharged electrodes. Adding water to MeCN promotes the formation of LiOH instead of Li_2O_2.

3.4 Mechanisms of Solvent Stability or Instability in the Presence of Water

We observed that DME and MeCN can both produce Li_2O_2 without significant side reactions in the anhydrous condition. However, with the addition of water only DME is stable while significant amounts of LiOH form in MeCN. We sought to explain what mechanisms could account for LiOH formation in MeCN and explain why these mechanisms do not occur in DME by comparing the solvent properties of DME and MeCN.

Since a direct reaction between Li_2O_2 and H_2O to form LiOH is not energetically favorable (+41 kJ/mol)[2] and the initial discharge profile for 5000 ppm H_2O MeCN occurred at a higher potential consistent with the consumption of protons[2], we proposed a mechanism based on the solvent-dependent dissociation of protons from water. These protons react with superoxide intermediate to form hydroperoxyl radicals. This reaction between protons and superoxide was first proposed by Sawyer and Valentine[14] and later applied to Li-O_2 discharge by Schwenke et al[2].

$$H_2O \rightarrow H^+ + OH^-$$

$$O_2 + e^- \rightarrow O_2^-$$

$$H^+ + O_2^- \rightarrow HOO^{\cdot}$$

Further reactions of this radical with superoxide yield LiOH.

$$HOO^{\cdot} + O_2^- \rightarrow HOO^- + O_2$$

$$Li^+ + H_2O + HOO^- \rightarrow LiOH + H_2O_2$$

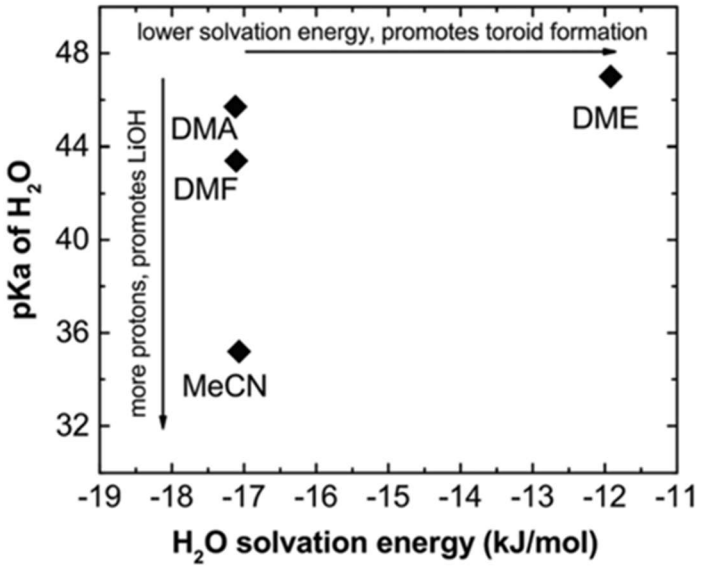

Figure 3.4.1: Morphology and Stability Trends for Water in Solvents Computed pKa of H_2O is plotted against computed water solvation energy for a variety of common battery solvents: MeCN, DME, dimethylacetamide (DMA), and dimethylformamide (DMF)[10].

This mechanism provides a reasonable pathway for the formation of LiOH in MeCN with added water. The absence of this side reaction in DME with the same amount of added water suggests that water deprotonates less readily in DME. If protons are the source of the side reaction in high water content solvents, solvents that readily deprotonate water molecules should be less stable for Li-O_2 discharge. To test this idea, first principles calculations of the deprotonation energy and pKa of water in DME and MeCN were performed (for details on computations see Kwabi et al.[10]). It was shown that deprotonation of water is much less favorable in DME than in MeCN (Figure 3.4.1). This indicates that the deprotonation energy of water in a given solvent is critical in determining if added water content will prevent the stable formation of Li_2O_2. In addition, it was demonstrated that the solvation energy of water was inversely related to toroid formation. When the solvent molecules interact less strongly with

water, water is freer to interact with Li^+-O_2^- and promote Li_2O_2 toroid formation. The interactions between the solvent molecules and water molecules have a profound effect on both the stability of the solvent and to what degree water will promote capacity.

3.5 Effect of Water on the Li-O_2 Surface Pathway Mechanism

Adding water affects the solubility of superoxide, size of toroid formation, and stability of the discharge processes. All of these mechanisms are related to the solvent pathway mechanism. What is less clear is the degree to which water affects Li-O_2 surface pathway processes. While capacity increases with water content, these capacity gains could be due to either a faster rate of solvation of Li^+-O_2^- or an inhibited rate of formation of Li_2O_2 film. Performing discharges to full capacity in carbon nanotube electrodes provided a way to test how the surface pathway influenced the effect of water on capacity, as carbon nanotubes have a significantly higher surface area than most other electrodes and unique surface properties.

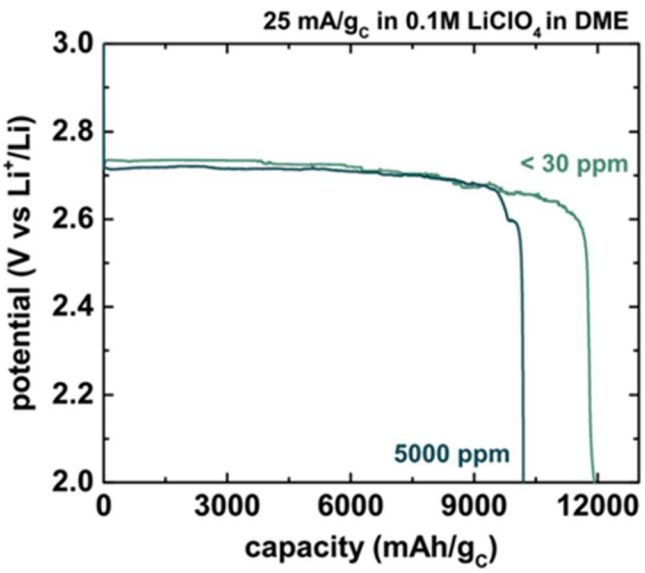

Figure 3.5.1 Effect of Water on Discharge Capacity in DME Galvanostatic discharge profiles of carbon nanotube electrodes discharged in 0.1 M $LiClO_4$ DME at 25 mA/g_{CNT} to a cut-off potential of 2.0 V vs Li^+/Li in the anhydrous condition of ~< 30 ppm and with 5000 ppm H_2O added[10].

In order to observe the effect on capacity of water in DME, carbon nanotube electrodes in 0.1 M $LiClO_4$ DME with both <30 ppm and 5000 ppm H_2O were discharged at a rate of 25 mA/g_{CNT} to a cut-off potential of 2.0 V vs Li^+/Li (Figure 3.5.1). While both Aetukuri et al.[5] and Schwenke et al.[2] report large increases in capacity as the water content is increased, we saw no significant difference. In both the anhydrous sample and 5000 ppm water sample the discharge capacity was ~10,000 mAh/g_{CNT}. This discrepancy was attributed to the properties of the carbon nanotube electrode, as all other conditions were similar to those used in Aetukuri et al[5]. In order to rationalize this difference, the morphology of the Li_2O_2 at end of discharge was studied.

a)

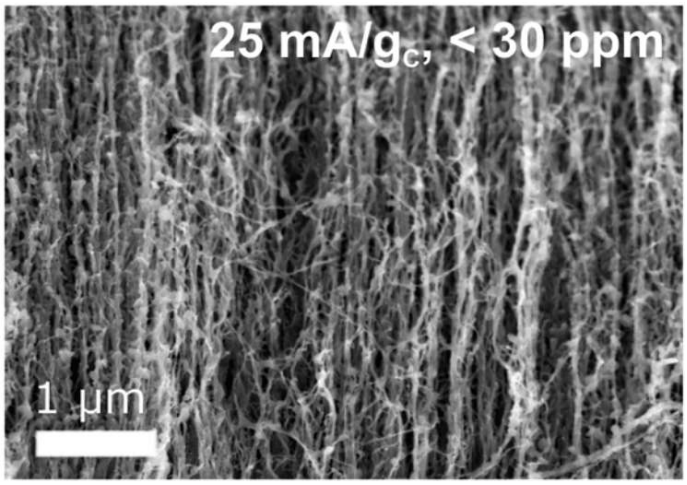

b)

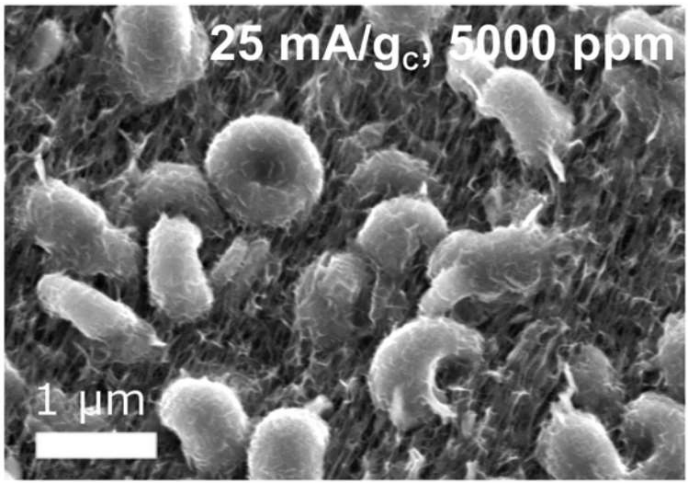

Figure 3.5.2 Effect of Water on Morphology at Full Discharge in DME SEM images of carbon nanotube electrodes discharged in 0.1 M $LiClO_4$ DME at 25 mA/g_{CNT} to a cut-off potential of 2.0 V vs Li^+/Li in the anhydrous condition of ~< 30 ppm and with 5000 ppm H_2O added[10].

While the addition of 5000 ppm H_2O did not cause a significant difference in the discharge capacity of carbon nanotube electrodes in 0.1 M $LiClO_4$ DME, a large change in Li_2O_2 toroid size occurred (Figure 3.5.2). This indicates that while water promoted Li^+-O_2^- solubility which caused larger toroid

formation, Li_2O_2 toroids represented a small portion of the overall discharge product such that changes in their amount did not significantly affect the overall capacity. The surface pathway is dominant even at high water content in carbon nanotube electrodes.

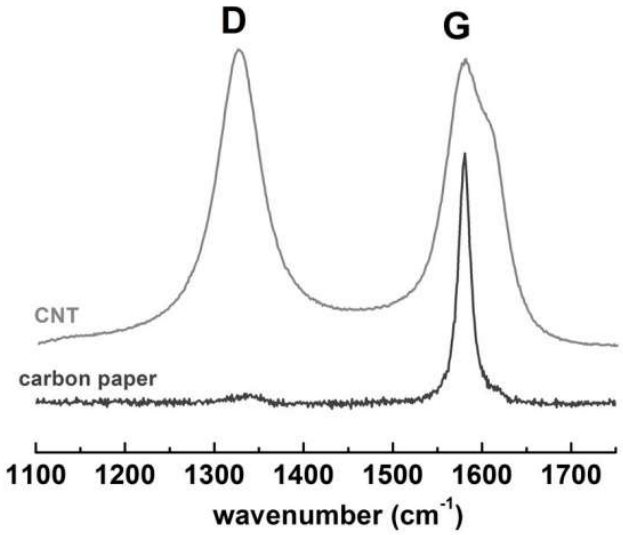

Figure 3.5.3 Raman Spectroscopy Spectra of Carbon Electrodes Raman spectroscopy spectra of carbon nanotubes (light gray) and carbon paper (dark gray)[10].

The dominance of the surface pathway in carbon nanotubes is due to their high defect density. Raman spectroscopy of carbon nanotubes and a typical carbon electrode, carbon paper, shows that the defect density of carbon nanotubes is substantially higher (Figure 3.5.3). The G band corresponds to graphitic sp^2 carbon while the D band broadly corresponds to sp^3 carbon and other defects[15]. The greater defect density of carbon nanotubes, indicated by the high D band peak compared to carbon paper, should increase the activity of the electrode surface.

The surface area normalized capacity is roughly 10x greater for carbon nanotubes than other electrodes in previous reports which used carbon paper, Vulcan carbon, or Super P carbon[2,5,8,10,16,17]. As

the surface can support a much greater amount of Li_2O_2, the influence of altering toroid formation through the addition of water is less.

a)

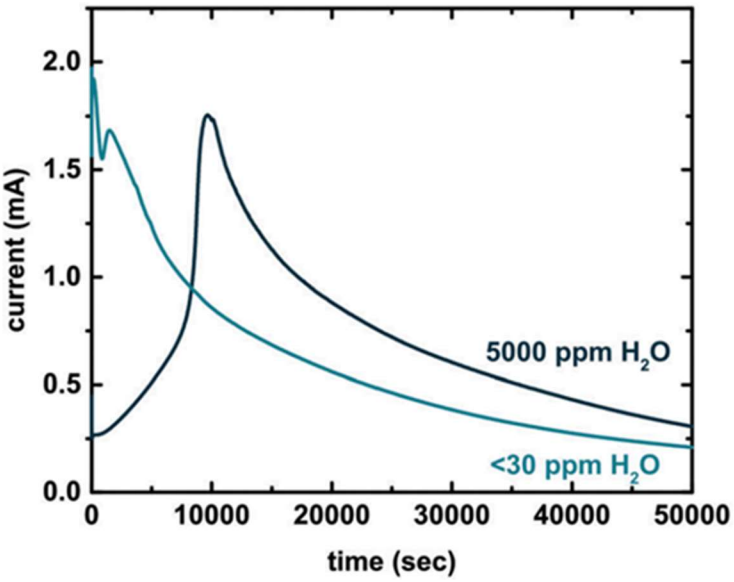

b)

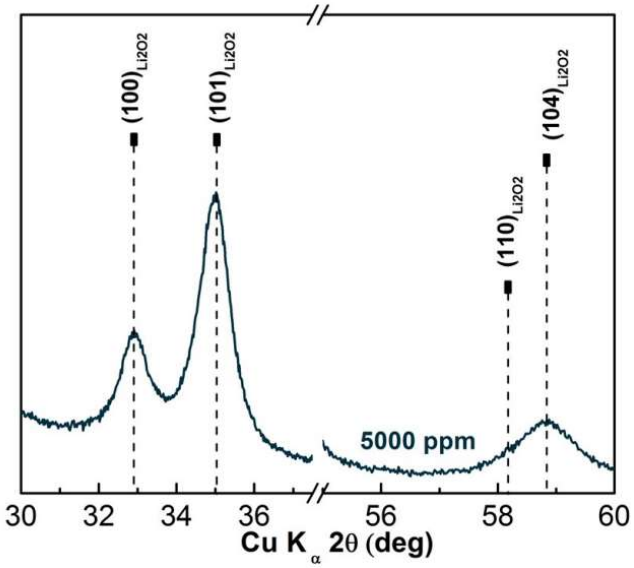

Figure 3.5.4 Effect of Water on Li-O_2 Surface Nucleation a) Carbon paper electrode discharged at 2.0 V vs Li^+/Li with 0.1 M $LiClO_4$ DME with <30 ppm H_2O and 5000 ppm H_2O b) XRD spectrum for carbon paper electrode discharged at 2.0 V vs Li^+/Li with 0.1 M $LiClO_4$ DME with 5000 ppm H_2O[10].

While these results suggest that water content is less critical when the surface pathway formation of Li_2O_2 film is dominant, they do not offer insight into whether the addition of water is affecting the rate of nucleation and growth of the film. In order to gain intuition into this effect, carbon paper electrodes were discharged at 2.0 V vs Li^+/Li in 0.1 M $LiClO_4$ DME with and without the addition of 5000 ppm H_2O (Figure 3.5.4a). XRD was used to confirm that the discharge product under these conditions was Li_2O_2 (Figure 3.5.4b). Discharging in a potentiostatic condition allows for the interpretation of current-time transients by well-established models for nucleation and growth. Carbon paper electrodes were used to provide a flat surface to observe film evolution by microscopy. This technique had been reported for Li-S (lithium-sulfur) batteries[18,19], but most Li-O_2 studies have relied on interpreting nucleation behavior based on galvanostatic discharge[20]. Peaks in current vs time transients are generally indicative of nucleation and growth behavior[21,22]. The time of the current peak is related to the favorability of nucleation and growth kinetics. Shorter peak times correspond to faster nucleation and growth kinetics. For both the anhydrous and 5000 ppm case, peaks were observed in the current-time transient, indicating a nucleation and growth process at the surface. Increasing the water content of 0.1 M $LiClO_4$ DME caused the time of the peak to greatly increase, indicating slower Li_2O_2 film nucleation and growth. This suggests that the water content has an effect on the surface pathway as well as the solvent pathway. However, it is not possible to directly measure the contribution of the solvent pathway and surface pathway in these 2-electrode cell experiments. A more rigorous study of the kinetics and solvent property dependence of the surface pathway will be conducted in Chapter Four.

3.6 Conclusion

The effect of water on the stability and capacity of two different Li-O_2 electrolyte solvents was studied on high surface area carbon nanotube electrodes. Li-O_2 discharges occurred with minimal side

reactions in DME even with the addition of 5000 ppm H_2O. In MeCN, discharge became unstable once water was added. This was attributed to greater deprotonation of water in MeCN, resulting in reactions between superoxide and protons. The high defect density of the carbon nanotube electrode caused the surface discharge pathway to dominate, leading the discharge capacity to remain fixed even as toroid size increased. Potentiostatic measurements demonstrated that adding water causes a slower rate of passivation of the carbon electrode. This study suggests that while additives such as water can promote discharge capacity, interactions with solvent molecules and electrode properties must be carefully considered.

References

1. Khetan, A., Luntz, A. & Viswanathan, V. Trade-offs in capacity and rechargeability in nonaqueous Li-O2 batteries: Solution-driven growth versus nucleophilic stability. *J. Phys. Chem. Lett.* **6,** 1254–1259 (2015).
2. Schwenke, K. U., Metzger, M., Restle, T., Piana, M. & Gasteiger, H. A. The Influence of Water and Protons on Li2O2 Crystal Growth in Aprotic Li-O2 Cells. *J. Electrochem. Soc.* **162,** A573–A584 (2015).
3. Gutmann, V. Solvent effects on the reactivities of organometallic compounds. *Coord. Chem. Rev.* **18,** 225–255 (1976).
4. Johnson, L. *et al.* The role of LiO2 solubility in O2 reduction in aprotic solvents and its consequences for Li-O2 batteries. *Nat. Chem.* **6,** 1091–1099 (2014).
5. Aetukuri, N. B. *et al.* Solvating additives drive solution-mediated electrochemistry and enhance toroid growth in non-aqueous Li-O2 batteries. *Nat. Chem.* **7,** 50–56 (2015).
6. Kwabi, D. G. *et al.* Experimental and Computational Analysis of the Solvent-Dependent O2/Li+-O2− Redox Couple: Standard Potentials, Coupling Strength, and Implications for Lithium-Oxygen Batteries. *Angew. Chemie* **128,** 3181–3186 (2016).
7. Marcus, Y. The properties of organic liquids that are relevant to their use as solvating solvents. *Chem. Soc. Rev.* **22,** 409 (1993).
8. Meini, S., Piana, M., Tsiouvaras, N., Garsuch, A. & Gasteiger, H. A. The Effect of Water on the Discharge Capacity of a Non-Catalyzed Carbon Cathode for Li-O2 Batteries. *Electrochem. Solid-State Lett.* **15,** A45 (2012).
9. Guo, Z., Dong, X., Yuan, S., Wang, Y. & Xia, Y. Humidity effect on electrochemical performance of

Li-O2batteries. *J. Power Sources* **264,** 1–7 (2014).

10. Kwabi, D. G. *et al.* The effect of water on discharge product growth and chemistry in Li–O_2 batteries. *Phys. Chem. Chem. Phys.* **18,** 24944–24953 (2016).

11. McCloskey, B. D., Bethune, D. S., Shelby, R. M., Girishkumar, G. & Luntz, A. C. Solvents' Critical Role in Nonaqueous Lithium–Oxygen Battery Electrochemistry. *J. Phys. Chem. Lett.* **2,** 1161–1166 (2011).

12. Laoire, C. O., Mukerjee, S., Abraham, K. M., Plichta, E. J. & Hendrickson, M. A. Elucidating the Mechanism of Oxygen Reduction for Lithium-Air Battery Applications. *J. Phys. Chem. C* **113,** 20127–20134 (2009).

13. Kwabi, D. G. *et al.* Chemical Instability of Dimethyl Sulfoxide in Lithium–Air Batteries. *J. Phys. Chem. Lett.* **5,** 2850–2856 (2014).

14. Sawyer, D. T. & Valentine, J. S. How Super Is Superoxide? *Acc. Chem. Res.* **14,** 393–400 (1981).

15. Dresselhaus, M. S., Dresselhaus, G., Saito, R. & Jorio, A. Raman spectroscopy of carbon nanotubes. *Phys. Rep.* **409,** 47–99 (2005).

16. Nazar, L. *et al.* Current Density Dependence of Peroxide Formation in the Li-O2 Battery and its Effect on Charge. *Energy Environ. Sci.* **6,** 1772–1778 (2013).

17. Lau, S. & Archer, L. A. Nucleation and Growth of Lithium Peroxide in the Li-O2 Battery. *Nano Lett.* **15,** 5995–6002 (2015).

18. Fan, F. Y., Carter, W. C. & Chiang, Y.-M. Mechanism and Kinetics of Li_2S Precipitation in Lithium-Sulfur Batteries. *Adv. Mater.* **27,** 5203–5209 (2015).

19. Gerber, L. C. H. *et al.* Three-Dimensional Growth of Li2S in Lithium-Sulfur Batteries Promoted by a Redox Mediator. *Nano Lett.* **16,** 549–54 (2016).

20. Yin, Y., Torayev, A., Gaya, C., Mammeri, Y. & Franco, A. A. Linking the Performances of Li-O2Batteries to Discharge Rate and Electrode and Electrolyte Properties through the Nucleation Mechanism of Li2O2. *J. Phys. Chem. C* **121,** 19577–19585 (2017).

21. Avrami, M. Kinetics of phase change. II Transformation-time relations for random distribution of nuclei. *J. Chem. Phys.* **8,** 212–224 (1940).

22. Fleischmann, M. & Thirsk, H. R. Electrochemical kinetics of formation of monolayers of solid phases. *Electrochim. Acta* **9,** 757–771 (1964).

Chapter Four: Modeling the Discharge Pathways of Li-O_2 Batteries

4.1 Introduction

Li-O_2 batteries could become widely adopted if they can provide significant energy storage gains relative to Li-ion batteries. This requires optimizing performance to achieve capacities close to their high theoretical limit. The capacity of a Li-O_2 battery is determined by how efficiently Li_2O_2 discharge product fills the void space of the cathode. Li_2O_2 is an insulating solid that deposits on the surface of the electrode. These deposits passivate the electrode surface and prevent further reduction of O_2 to Li_2O_2[1,2].

The efficiency of void filling is determined by the morphology and size of Li_2O_2, which can form either as a thin film of ~10 nm thickness or toroids with diameter ~100-1,000 nm[3,4]. As previously described in Chapter One, these morphologies can be attributed to two competing pathways that operate during discharge[5–7]. The surface pathway involves an initial reduction of oxygen to form Li^+-O_2^- intermediate, which is further reduced by another electron transfer to form Li_2O_2 (Equation 4.1).

Equation 4.1: Surface Pathway

(i) $$Li^+ + O_2 + e^- \rightarrow (Li^+ - O_2^-)_{surf}$$

(ii) $$(Li^+ - O_2^-)_{surf} + Li^+ + e^- \rightarrow Li_2O_2$$

The solvent pathway involves the same initial step of reduction to form Li^+-O_2^-, but lithium superoxide is then solvated by solvent molecules and disproportionates to form Li_2O_2 toroids (Equation 4.2).

Equation 4.2: Solvent Pathway

(i) $$Li^+ + O_2 + e^- \rightarrow (Li^+ - O_2^-)_{surf}$$

(ii) $$(Li^+ - O_2^-)_{surf} \rightarrow (Li^+ - O_2^-)_{solv}$$

(iii) $$2(Li^+ - O_2^-)_{solv} \rightarrow Li_2O_2 + O_2$$

Because the third step does not require access to the electrode surface for an electron transfer, larger length scales of Li_2O_2 discharge product are possible.

Since promoting the toroidal morphology as opposed to the thin film morphology is critical to achieving high capacity, precise control and understanding of the two mechanistic pathways are necessary. Trends with various discharge conditions have been reported that either favor the surface or solvent pathway. At high overpotential or high current density, the surface pathway is dominant and thin film Li_2O_2 primarily forms[4,6,8]. At low overpotential or low current density, the solvent pathway is dominant and primarily Li_2O_2 toroids form. Higher solubility of Li^+-O_2^- causes more toroids to form. This can occur by adjusting the solvent type[5,9], water content[7,10], salt anion[11], and salt concentration[12]. The increase of toroids and dominance of the solvent pathway have been attributed to an enhanced Li^+-O_2^- solvation rate[10] as well as the possibility of inhibiting the surface passivation rate[13]. The trends with potential or current density and lithium superoxide solubility are interdependent; the promotion of toroids occurs to a greater degree at low current density than high current density[10]. While these trends have been identified, it is not clear whether the dominant mechanistic reason for toroid promotion is an enhanced solvation rate of lithium superoxide or an inhibited surface lithium superoxide reduction rate and how each of these rates are dependent on parameters such as potential and Li^+-O_2^- solubility. In this study, we develop a model of Li-O_2 discharge mechanisms in order to examine the dependence of the solvent pathway rate and surface pathway rate on each other and on various discharge parameters. Precise knowledge of pathway promotion or inhibition mechanisms can help to guide cell design for optimal capacity.

Modeling the competing discharge mechanistic pathways in a Li-O_2 cell should have several features to ensure physically reasonable assumptions and broadly applicable results. 1) The model should describe separate processes for the surface pathway and the solvent pathway in order to determine their dependence on different experimental parameters. 2) The model should be readily

quantitatively compared to time-resolved experimental measures of the solvent pathway and surface pathway to ensure that modeling assumptions are physically reasonable. 3) Modeling in the potentiostatic condition allows for more fundamental understanding of the nucleation and growth processes in the surface pathway as the potential for electron transfers is fixed. Numerous models exist which capture various experimentally observed properties of Li-O_2 discharge[7,14–19] but most were not designed to model the separate dependence of each mechanistic pathway and lack at least one of these desired modeling features. Many rely on a fit of experimental galvanostatic discharge curves[14,16,18] or potential scans[7], in which the contributions of the surface and solvent pathway must be inferred from the overall result rather than directly measured. Common experimentally observed features of Li-O_2 discharge are ignored in some reports, such as passivation by Li_2O_2[15,19], nucleation and growth of the film[7], and the separate contribution of the surface pathway to Li_2O_2 film/small particle growth[14]. In order to address all of these criteria, we chose to design a model that would consider the time-resolved evolution of each pathway during potentiostatic discharge in a rotating-ring disk electrode (RRDE) experiment, which allows for the direct measure of the solvent pathway and separation of the contribution of each pathway.

Rotating ring-disk electrode experiments involve a four-electrode setup. In addition to a counter and reference electrode, a rotating rod with two concentric electrodes is placed at the surface of the electrolyte solvent (Figure 4.1.1). The reduction reactions of interest occur at the central disk electrode and produce either insoluble or soluble products. The outer electrode is a concentric ring set to a potential that will oxidize the soluble products produced at the disk. Soluble species are swept away from the disk by convection, oxidized by the ring, and produce a current that is a measure of the percentage of soluble species to total species formed at the disk. RRDE has been shown to be a valuable method to study Li-O_2 discharge properties[5,6,19–25]. During discharge, reduction reactions at the disk produce either solvated Li^+-O_2^- by the solvent pathway or solid Li_2O_2 by the surface pathway. The ring is

set to a constant oxidizing potential to measure the amount of Li^+-O_2^- produced. We assume that the transfer of Li^+-O_2^- to the ring and the subsequent oxidation reaction occur much faster than parasitic side reactions or disproportionation. Since the disk current is a sum of the contribution of surface and solvent pathways, and the ring current is a measure only of the solvent pathway, the contribution of each pathway can be determined throughout discharge.

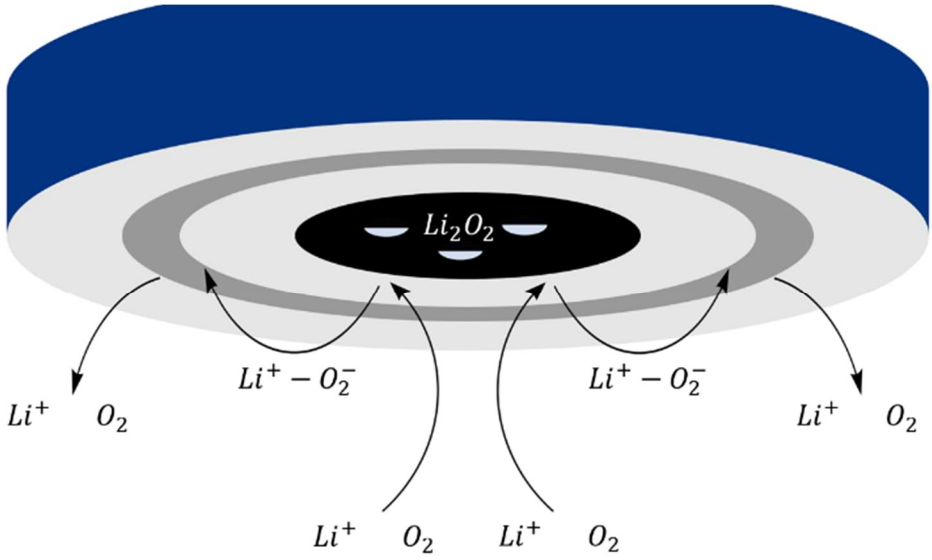

Figure 4.1.1 Schematic of a Rotating Ring Disk Electrode Schematic of Li-O_2 discharge reactions at the disk and ring electrode in an RRDE experiment. The dark grey region is the ring electrode; the black region is the disk electrode; the blue region is the body of the RDE rotor.

In this study, we develop a model of Li-O_2 discharge in a RRDE setup in order to experimentally validate modeled assumptions about the nature of the solvent pathway and surface pathway. We use the model to determine the rate of each pathway under a wide array of discharge parameters. We find that the rate of the solvent pathway is broadly insensitive to potential and solvent Li^+-O_2^- solubility. Inhibiting the rate of the surface pathway is the key determinant in promoting toroid morphology and maximizing Li-O_2 discharge capacity.

4.2 Experimental Methods

Rotating ring-disk electrode experiments were conducted using a Pine rotating disk electrode setup connected to a Biologic SP300 potentiostat. For Li-O_2 experiments, the disk electrode was glassy carbon (diameter: 5mm), the ring electrode was platinum (inner diameter: 6.5 mm), and the counter and reference electrodes were lithium foil. ~20 mL of solvent were used in a 50 mL flask and tested by Karl Fischer titration after experiments to measure water content. Solvents with a water content below ~30 ppm were considered to be nominally anhydrous. Oxygen was bubbled into the solvent for ~20 minutes to saturate the solvent prior to experiments. Oxygen flow blanketed the solvent during discharge to preserve oxygen saturation. Discharges were performed at a fixed disk reduction potential for 2 minutes (unless otherwise noted). The ring was held at 3.5 V vs Li^+/Li for all experiments, having previously been determined to be optimal for collection of soluble species[6]. After each discharge, the product on the surface was oxidized by performing a potential scan from 3 to 4.3 V vs Li^+/Li twice.

To calibrate the ring collection efficiency, ferrocene was added to the solution to a concentration of ~ 5 mM. Argon gas was bubbled through the solvent in order to remove oxygen. The potential was scanned from 3.6 to 4.3 V vs Li^+/Li. The ring was held at 3.2 V vs Li^+/Li. Collection efficiency was measured by taking the average ring current above 4 V vs Li^+/Li divided by the average disk current during the same portion of the scan. The collection efficiency was determined to be ~23%.

4.3 Experimental Rotating Ring Disk Electrode Results

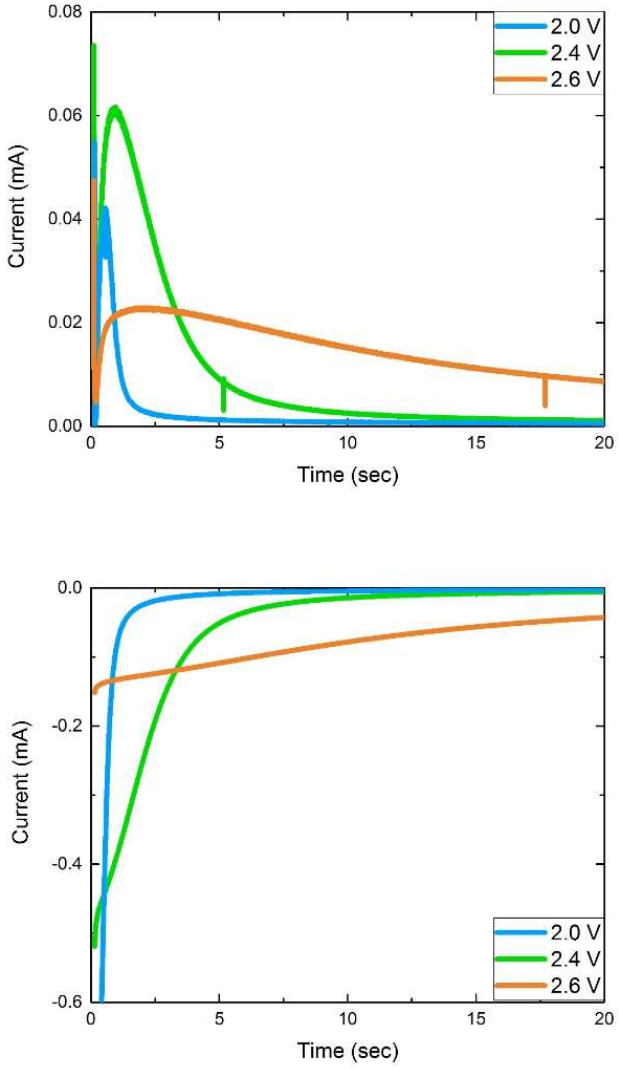

Figure 4.3.1: Experimental RRDE Trend with Discharge Potential Ring (top) and disk (bottom) current time transients for discharges in 0.1 M $LiClO_4$ DMSO at 1600 rpm at 2.0 V, 2.4 V, and 2.6 V vs Li^+/Li disk potentials. Open circuit potential is 2.96 V vs Li^+/Li for the formation of Li_2O_2[26].

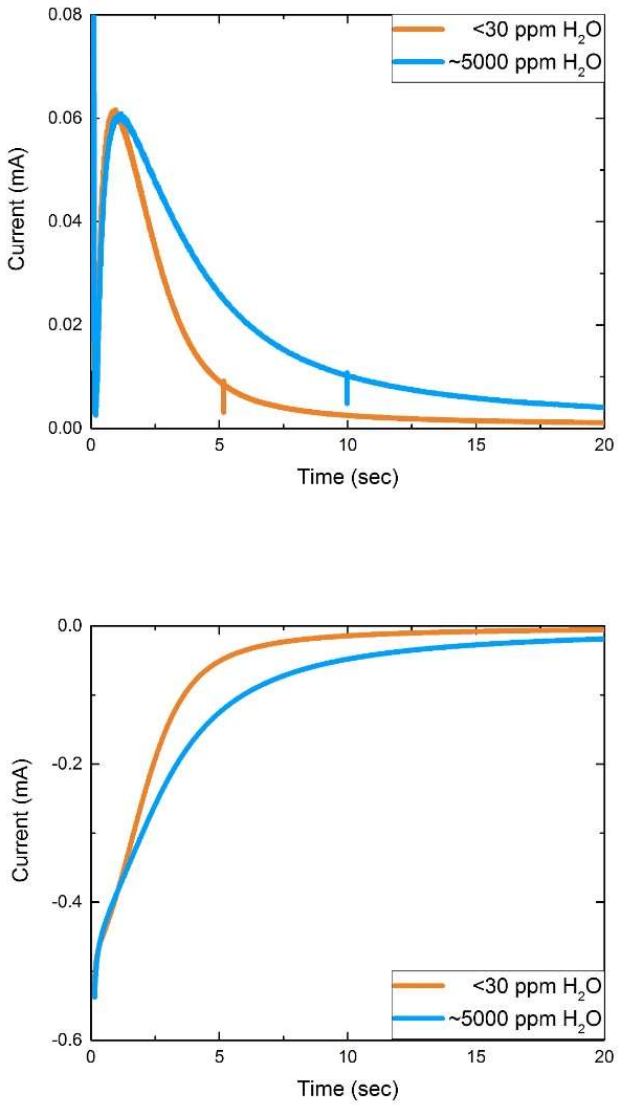

Figure 4.3.2 Experimental RRDE Trend for Water Content Ring (top) and disk (bottom) current time transients for discharges in 0.1 M $LiClO_4$ DMSO at 1600 rpm at 2.4 V vs Li^+/Li disk potential with ~< 30 ppm H_2O and ~5000 ppm H_2O.

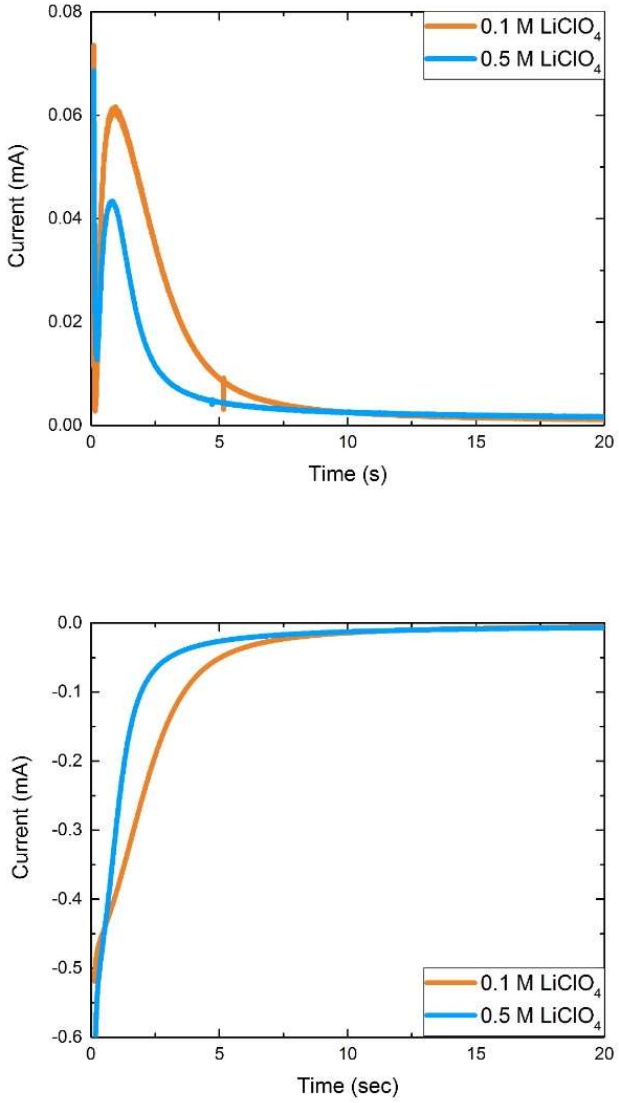

Figure 4.3.3 Experimental RRDE Trend for Salt Concentration Ring (top) and disk (bottom) current time transients for discharges in 0.1 M and 0.5 M $LiClO_4$ DMSO at 1600 rpm at 2.4 V vs Li^+/Li disk potential.

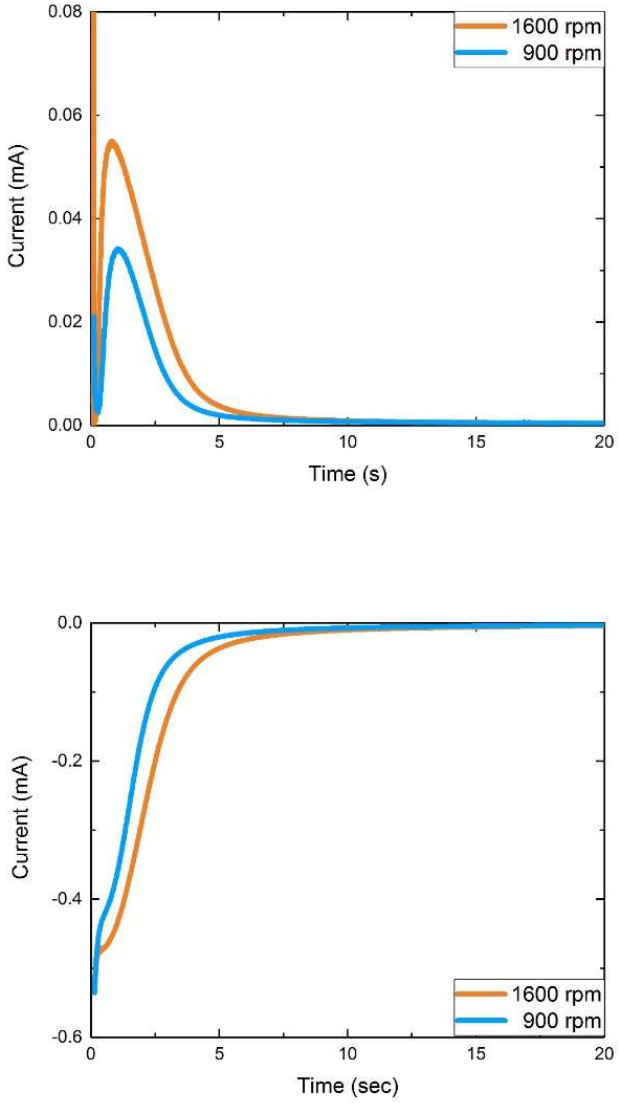

Figure 4.3.4 Experimental RRDE Trend for Rotation Rate Ring (top) and disk (bottom) current time transients for discharges in 0.1 M $LiClO_4$ DMSO at 900 and 1600 rpm at 2.4 V vs Li^+/Li disk potential.

RRDE potentiostatic trends against disk potential, water content, salt concentration, and rotation rate were collected to serve as an experimental set to check modeled results against. The results are consistent with prior reports of trends in Li-O_2 RRDE experiments[6,12,22]. It is assumed that side reactions are negligible and that disproportionation is much slower than the time it takes for solvated Li^+-O_2^- to be swept away from the disk and oxidized at the ring. Dimethyl sulfoxide (DMSO) and

dimethoxyethane (DME) have been demonstrated to stably form Li_2O_2 by electrochemical quartz microbalance (EQCM) measurements under similar discharge conditions to this experiment[6,27], and the rate constant for disproportionation, as measured by Johnson et al., is slow compared to estimated rate constants for reduction[5,6]. The disk oxidation scan possessed peaks characteristic of Li^+-O_2^- and Li_2O_2, even in the presence of water (Figures A.1 and A.2), suggesting reasonable discharge stability[24]. Figure 4.3.1 demonstrates the potential dependence for 0.1 M $LiClO_4$ DMSO at 1600 rpm. The disk current has a higher initial value with increased overpotential but decreases more rapidly with time, indicating faster passivation of the disk by Li_2O_2. The ring current begins with an initial non-faradaic response at ~<100 milliseconds followed by a transit time and build-up to a peak representing the delay between solvated Li^+-O_2^- production at the disk and oxidation at the ring[28]. The peak in the ring current has a maximum at intermediate overpotential. The ring current decay mirrors that of the disk current as fewer soluble species are produced as the passivation of the disk electrode by the Li_2O_2 film progresses. Increasing the water content causes a slower decay in the disk current and a higher ring current (Figure 4.3.2). Increasing the concentration of $LiClO_4$ from 0.1 M to 0.5 M causes a faster decay in the disk current and a lower ring current (Figure 4.3.3). Reducing the rotation rate causes a lower initial disk current, a faster decay in the disk current, and a reduced ring current (Figure 4.3.4). Assuming that the slope of the disk current corresponds to the rate of surface pathway formation of Li_2O_2 and that the ring current represents the rate of production of solvated Li^+-O_2^- by the solvent pathway allows for some qualitative inferences to be made from these experimental results. The changing decay of the disk current suggests that the surface pathway rate increases with higher overpotential, lower water content, higher salt concentration, and lower rotation rate. In order to further interpret these qualitative experimental trends, it was necessary to fit these data with a model of the Li-O_2 discharge mechanism pathways.

4.4 Constructing the Model

a) Nucleation and Growth

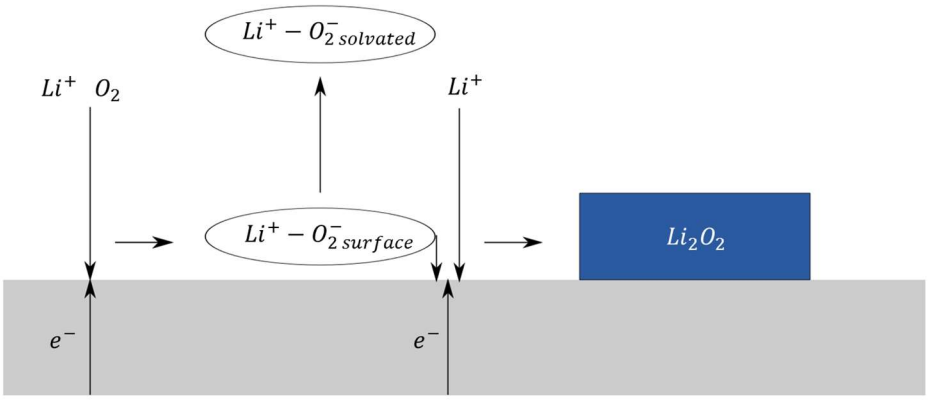

b) Tunneling

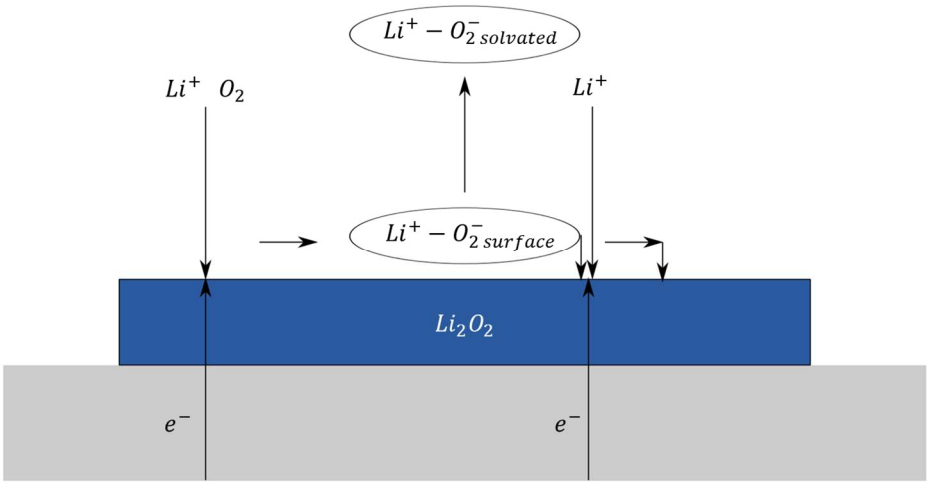

Figure 4.4.1: Schematics of Model Assumptions a) Schematic of mechanisms for radial growth of Li_2O_2 islands b) Schematic of mechanisms for thickening of Li_2O_2 islands by tunneling. The gray region is the electrode; the blue region is a sample Li_2O_2 island.

The primary mechanisms for Li_2O_2 film evolution previously reported are nucleation and growth[13,14] and tunneling[2,7]. To approximate the combined effect of both of these processes, we assume that the film nucleates instantaneously at some number of active sites at a fixed film height and then

grows radially (Figure 4.4.1a). Once created, each area increment of Li_2O_2 will then thicken by electron transport through tunneling (Figure 4.4.1b). The initial height is estimated from examining a time progression of capacities measured by oxidation at the disk subsequent to discharge (Figure A.3). This height represents the critical height at which the tunneling current begins to exponentially decay[2]. The goal of the model will be to predict how much solvation occurs as both the nucleation and growth and thickening by tunneling of the Li_2O_2 proceed.

The model relies on calculating and comparing the rate of creation of surface Li^+-O_2^- by oxygen reduction and the rate of depletion of surface Li^+-O_2^- by either reduction or solvation. Full derivations of the following expressions are provided in Discussion A.1. The Koutecky-Levich equation[28] is applied in order to calculate the rate of oxygen reduction (Equation 4.3). Since the concentration of Li^+ is ~100x that of O_2 with comparable diffusivity[29], oxygen is assumed to be the transport limiting species.

Equation 4.3: Rate of Oxygen Reduction at the Electrode Surface

$$r_1 = \left(\frac{1}{k_1^0 \exp\left(\frac{-\alpha_1 F}{RT}\eta\right)} + \frac{1}{.62\left(D_{O_2}{}^{2/3}\omega^{1/2}\upsilon_{kin}^{-1/6}\right)}\right)^{-1} * C_{O_2}^{bulk}$$

r_1 is the rate of oxygen reduction in mol O_2/(m^2*s), k_1^0 is the rate constant for oxygen reduction in m/s, α_1 is the transfer coefficient for oxygen reduction, η is the overpotential in V, D_{O_2} is the diffusivity of oxygen in the solvent in m^2/s, ω is the rotation rate in radians/s, ν_{kin} is the kinematic viscosity of the solvent in m^2/s, and $C_{O_2}^{bulk}$ is the solubility of oxygen in the solvent in mol/m^3. A correction factor of $\left[1 + \exp(-.386 * \pi^2\omega(\frac{D_{O_2}}{\nu_{kin}})^{\frac{1}{3}}t) + \exp(-1.54 * \pi^2\omega(\frac{D_{O_2}}{\nu_{kin}})^{\frac{1}{3}}t)\right]$ is applied to account for non-steady state effects at the ~100 millisecond time regime (Discussion A.1)[28,30]. The reduction of oxygen is considered to be independent of the surface concentration of Li^+-O_2^- since the initial electron transfer to oxygen is an outer sphere reaction[24].

The solvation of Li^+-O_2^- is modeled as a first order reaction with the concentration of surface Li^+-O_2^-.

Equation 4.4: Solvation Rate of Surface Li^+-O_2^-

$$r_{solv} = k_{solv} * C_{Li^+-O_2^-}^{surf}$$

k_{solv} is the rate constant for solvation in s^{-1} and $C_{Li^+-O_2^-}^{surf}$ is the concentration of surface Li^+-O_2^- in mol/m^2. Li^+-O_2^- solvated in a given time increment at the disk is considered to arrive at the ring following a uniform transit time. The ring current is adjusted by the ring collection efficiency of 23%. The transit time was on a sufficiently shorter time scale than the build-up time that it could be reasonably approximated as instantaneous (Figure A.4).

The nucleation and growth process is described by an adaptation of the Johnson-Mehl-Avrami-Kolmogorov framework[13,14,31]. The radial growth rate will depend on the concentration of surface Li^+-O_2^- and potential.

Equation 4.5: Radial Growth Rate of Li_2O_2 Film

$$v = \frac{M}{\rho} C_{LiO2}^{surf} k_2^0 \exp\left(\frac{-\alpha_2 F}{RT}\eta\right)$$

v is the radial growth rate of an individual island of Li_2O_2 in m/s, M is the molar mass of Li_2O_2 in g/mol, ρ is the density of Li_2O_2 in g/m^3, k_2^0 is the rate constant for reduction of lithium superoxide in s^{-1}, and α_2 is the transfer coefficient for lithium superoxide reduction. The islands of Li_2O_2 will grow outward and eventually impinge. To correct for the effect of impingement, we apply the Johnson-Mehl-Avrami-Kolmogorov framework[31] to calculate the fractional area coverage of the electrode by the Li_2O_2 film at a given time:

Equation 4.6: Area Coverage of Electrode by Li_2O_2

$$a_{film} = 1 - \exp(-\pi \frac{N}{A_e}(\sum_i (\nu_i \Delta t))^2)$$

a_{film} is the fraction of the electrode covered by Li_2O_2 film, N is the number of nuclei, A_e is the area of the electrode in m^2, ν_i is the radial growth in m/s at a given time increment i, and Δt is the size of each time increment in s. Because N and ν_i are both in the exponential factor of time squared, changes in $\sqrt{N}$ and k_2^0 are mathematically indistinguishable in this model, without some outside measure of the number of nucleation sites. Both N and k_2^0 reflect the favorability of Li^+-O_2^- reduction at the electrode surface. The product $\sqrt{N}k_2^0$ is treated as a single parameter in the model, which qualitatively represents how active the surface of the electrode is for Li^+-O_2^- reduction under a given set of conditions.

The reactions at the surface of the Li_2O_2 film are similar to the reactions at the surface of the electrode except the transport of electrons through the film by tunneling is rate limiting. The activity of oxygen reduction at the surface of Li_2O_2 is approximated as being equal to the activity at the electrode surface. The concentration of surface Li^+-O_2^- on the film is assumed to rapidly equilibrate with the concentration of surface Li^+-O_2^- on the electrode and the two concentrations are treated as equivalent. The rate of solvation is the same at the surface of the electrode and the film. The rate of electron tunneling is assumed to be an exponential decay with height from the initial rate at the film surface[2].

Equation 4.7: Rate of Electron Tunneling

$$r_{tunn} = r_1 * \exp(-\beta * (h - h^0))$$

r_{tunn} is the rate of electrons tunneled in mol/(m^2*s), β is the decay coefficient of the tunneling current with film thickness in m^{-1} [2], h is the thickness of the film in m, and h^0 is the initial thickness of the film upon nucleation and growth in m. It is assumed in a given time increment some fraction γ of the tunneled electrons reduce surface Li^+-O_2^- and 1- γ reduce oxygen. γ is calculated from the relative favorability of O_2 and Li^+-O_2^- reduction.

Equation 4.8: Fraction of Tunneled Electrons Reducing Lithium Superoxide

$$\gamma = \frac{k_2^{tunn} * C_{LiO_2}^{surf} * exp\left(\frac{-\alpha_2 F}{RT}\eta\right)}{k_2^{tunn} * C_{LiO_2}^{surf} * exp\left(\frac{-\alpha_2 F}{RT}\eta\right) + (\frac{1}{k_1^0 exp(\frac{-\alpha_1 F}{RT}\eta)} + \frac{1}{.62({D_{O_2}}^{2/3}\omega^{1/2}\upsilon_{ki}^{-1/6})})^{-1} * C_{O_2}^{bulk}}$$

k_2^{tunn} is the rate constant for lithium superoxide reduction on the Li_2O_2 film. The height of each area increment of Li_2O_2 changes according to the amount of lithium superoxide reduced at that area increment during the time increment.

Equation 4.9: Film Thickness Change for an Area Increment of Film during a Time Increment

$$\Delta h = \Delta t * \gamma * \frac{M}{\rho} * r_1 * \exp(-\beta * (h - h^0))$$

The concentration of surface lithium superoxide changes by the amount added through reduction of oxygen at either the surface of the electrode or Li_2O_2 film and the amount depleted by reduction of lithium superoxide at the surface of the electrode or Li_2O_2 film or depleted by the solvation of lithium superoxide from the electrode or Li_2O_2 surface.

Equation 4.10: Surface Li^+-O_2^- Concentration in each Time Increment

$$\Delta C_{LiO_2}^{surf} = \Delta t * \left(\left(1 - a_{film}\right) * r_1 + a_{film}*(r_{1,tunn} - r_{2,tunn}) - r_{solv}\right) - \Delta a_{film} * \frac{h\rho}{M}$$

The first term represents the amount of Li^+-O_2^- formed on the electrode surface, the second term represents the net reduction of oxygen or Li^+-O_2^- at the surface of the Li_2O_2 film, the third term represents the solvation of Li^+-O_2^-, and the fourth term represents the amount of Li_2O_2 formed through nucleation and growth.

Table 4.1: Experimental Parameters and Physical Constants

Symbol	*Definition*	*Value*	*Units*
η	Overpotential		V
M	Molar mass of Li_2O_2	45.881	g/mol
ρ	Density of Li_2O_2[32,33]	2.31 x 10^6	g/m^3
$C_{O_2}^{bulk}$	Bulk Oxygen Concentration (DMSO)[29]	2.1	mol/ m^3
$C_{O_2}^{bulk}$	Bulk Oxygen Concentration (DME)[34]	8.8	mol/ m^3
D_{O_2}	Diffusivity of Oxygen (DMSO)[29]	3.23 x 10^{-9}	m^2/s
D_{O_2}	Diffusivity of Oxygen (DME)[35]	4 x 10^{-9}	m^2/s
υ_{kin}	Viscosity of Solvent (DMSO)[36]	1.77 x 10^{-6}	m^2/s
υ_{kin}	Viscosity of Solvent (DME)[37]	5.2 x 10^{-7}	m^2/s
ω	Rotation Rate		1/s
β	Tunneling Decay Constant[2]	6.9 x 10^9	1/m

Table 4.2: Fitting Parameters and Estimated Parameters

Model Fitting Parameters		
Symbol	*Definition*	*Units*
$\sqrt{N}k_2^0$	Root of Nucleation Density * Superoxide reduction rate constant at electrode surface	1/s
k_{solv}	Superoxide solvation rate constant	1/s
Estimated Model Parameters		
Symbol	*Definition*	*Units*
k_1^0	Oxygen reduction rate constant	m/s
k_2^{tunn}	Superoxide reduction rate constant at Li_2O_2 film surface	1/s
α_1	Oxygen reduction transfer coefficient	unitless
α_2	Superoxide reduction transfer coefficient	unitless
h_0	Initial film height on nucleation and growth	m

Some of the parameters are not readily measured and require reasonable approximations. The initial height of the film after nucleation and growth and at the onset of tunneling decay was approximated using a progression of disk oxidation potential sweeps at different depths of discharge (Figure A.3). The exact nature of the transfer coefficients for oxygen and Li^+-O_2^- reduction are not fully understood. It has been reported that the value of α_1 is only reasonably approximated by the standard value of ~0.5 at very low overpotentials[9]. Tafel slopes of ~220 mV/decade have been reported for

DMSO[9] and ~290 mV/decade for DME[38] corresponding to oxygen reduction transfer coefficients of ~0.3 and ~0.2 respectively. The application of Marcus theory can account for these lower than expected transfer coefficients[19]. The Tafel slope for Li^+-O_2^- reduction has been measured as ~20-300 mV/decade greater than the slope for oxygen reduction[9], indicating a lower transfer coefficient. For this study, we approximate values of $\alpha_1 \cong .3$ and $\alpha_2 \cong .2$ for DMSO and $\alpha_1 \cong .2$ and $\alpha_2 \cong .1$ for DME (Discussion A.2). These approximate values of transfer coefficients could introduce some error at high overpotentials, but should provide reasonable estimates of qualitative potential dependence trends. k_1^0 was estimated by the initial disk current values for both 0.1 M $LiClO_4$ DMSO and DME using the estimates of α_1 noted above, giving values of $4*10^{-6}$ m/s for DMSO and $1*10^{-8}$ m/s for DME. η was calculated by taking the onset reduction potential for ~2.8 V vs Li^+/Li for 0.1M $LiClO_4$ DMSO and ~2.76 V vs Li^+/Li for 0.1 M $LiClO_4$ DME. Since the changes in η with changes in $LiClO_4$ concentration and H_2O content should be ~< 100 mV they were treated as negligible (Discussion A.3). As tunneling accounts for a small portion of the overall capacity during discharge, it was found to be sufficient to estimate k_2^{tunn} at the correct order of magnitude, which was ~1 s^{-1} for both solvents (Table A.1). $\sqrt{N}k_2^0$ and k_{solv} were treated as fitting parameters that are determined by fits to experimental data. The fitting process for DMSO samples involved scanning values of k_{solv} at increments of .25 s^{-1} and $\sqrt{N}k_2^0$ at increments of 10,000 s^{-1} and calculating the R^2 value for the fit of both experimental disk and corresponding ring current. The set of fitting parameters that maximized the sum of disk R^2 and ring R^2 was taken as the best fit.

4.5 Validating the Model by Experimental Fits

a) 0.1 M $LiClO_4$ DMSO Experiment

b) 0.1 M $LiClO_4$ DMSO Model

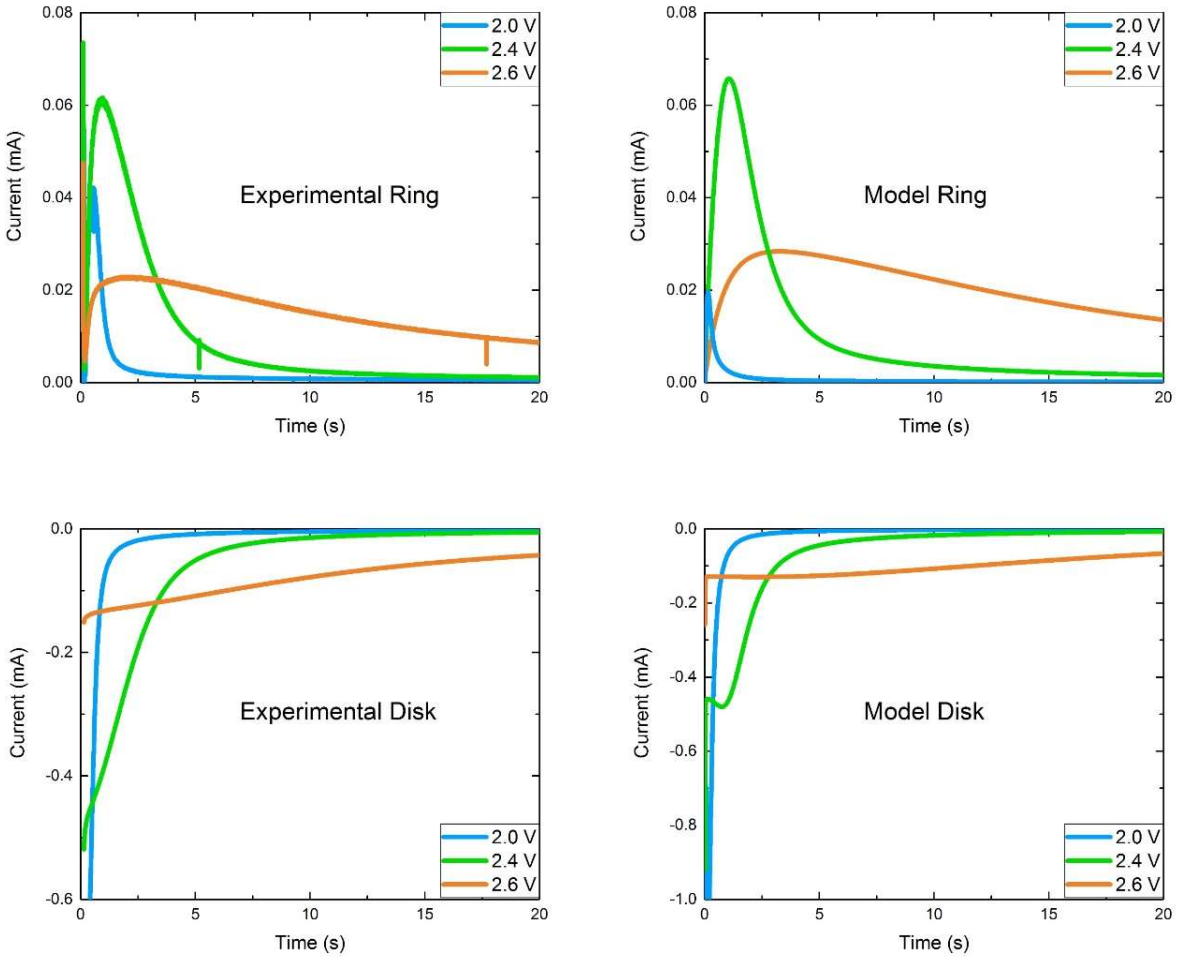

Figure 4.5.1: DMSO Experimental and Modeled Potential Dependence a) Disk and ring current time transients for discharges in 0.1 M $LiClO_4$ DMSO at 1600 rpm at 2.0 V, 2.4 V, and 2.6 V vs Li^+/Li b) Modeled disk and ring current transients for 0.1 M $LiClO_4$ DMSO at 1600 rpm at 2.0 V, 2.4 V, and 2.6 V vs Li^+/Li with fitting parameters k_{solv} = 1.25 s^{-1} and $\sqrt{N}k_2^0$ = 30,000 s^{-1}.

In order to ensure that the model contains physically reasonable assumptions, it is necessary to check that the model can fit and explain experimental trends. In particular, the model must be able fit the shape of a given disk current time transient and correctly predict the corresponding ring current time transient. It must also predict the proper trends with disk potential, water content, and salt

concentration. To model the potential dependence of 0.1 M $LiClO_4$ DMSO at 1600 rpm, the current transients at 2.4 V vs Li^+/Li were fit to obtain values of $\sqrt{N}k_2^0$ and k_{solv}. All parameters were then held constant and only the overpotential η was changed (Figure 4.5.1). The model confirms that the decay in disk current is consistent with the effect of passivation as a Li_2O_2 film nucleates and grows. The model shows that the maximum in the ring current at intermediate potential occurs because the surface concentration of Li^+-O_2^- is at an optimum between conditions of fast reduction and fast solvation. At high overpotentials, the rate of surface Li^+-O_2^- reduction is very large and the surface Li^+-O_2^- concentration is depleted. At low overpotentials, the relative rate of solvation to oxygen reduction is very large and the surface Li^+-O_2^- concentration is depleted. By equation 4.4 the ring current should be proportional to surface Li^+-O_2^- concentration and will also pass through an optimum at intermediate overpotential. The under-estimation of the ring current at the high overpotential of 2.0 V vs Li^+/Li is likely due to a potential dependence in the transfer coefficients that is not accounted for in this model. The model was shown to also be applicable for other solvents, as a qualitative fit of the potential dependence of discharges in 0.1 M $LiClO_4$ DME at 1600 rpm was achieved (Figure 4.5.2). It was not possible to check the fit for low overpotentials in DME because the low ring current was too close to the background current.

a) 0.1 M $LiClO_4$ DME Experiment

b) 0.1 M $LiClO_4$ DME Model

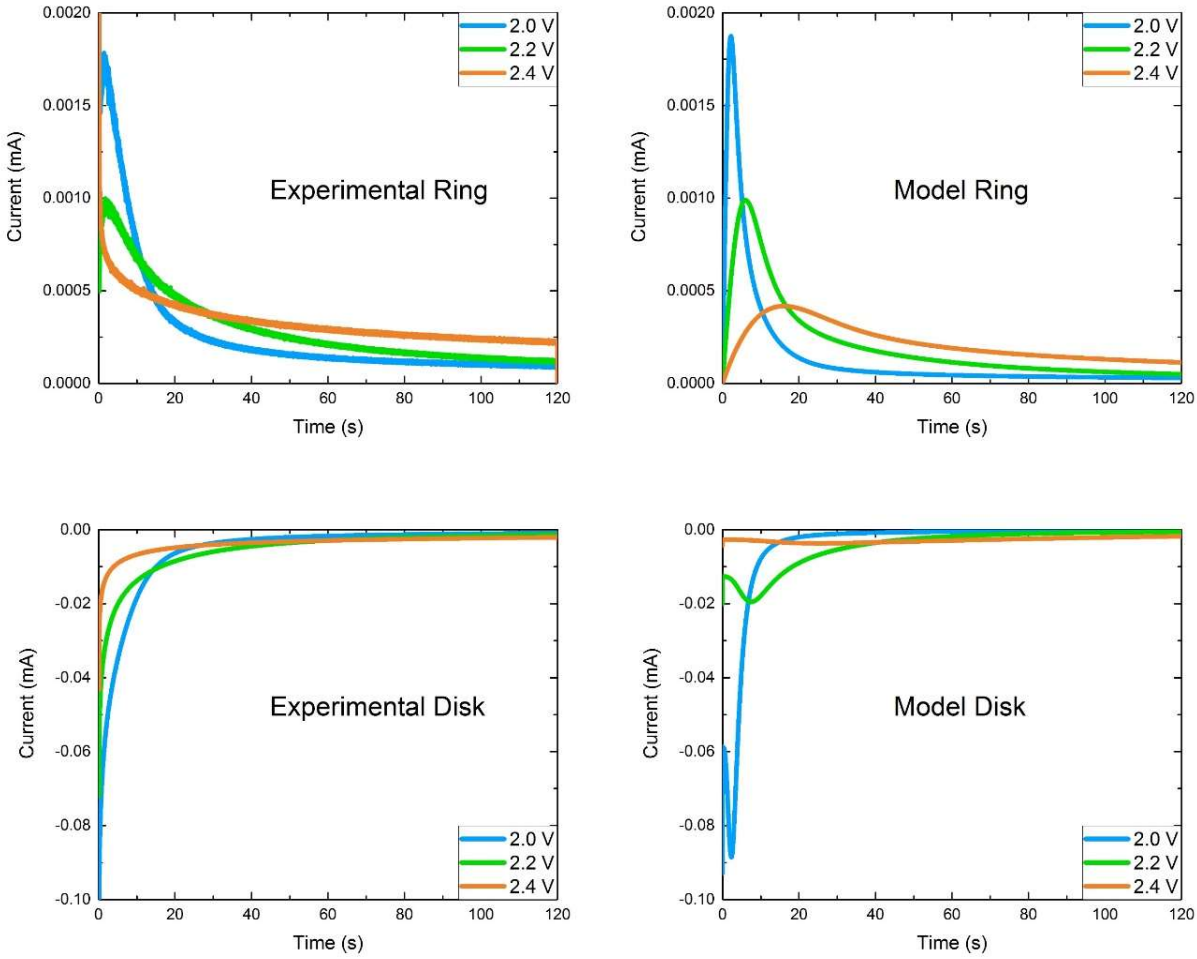

Figure 4.5.2 DME Experimental and Modeled Potential Dependence a) Disk and ring current time transients for discharges in 0.1 M $LiClO_4$ DME at 1600 rpm at 2.0 V, 2.2 V, and 2.4 V vs Li^+/Li b) Modeled disk and ring current transients for 0.1 M $LiClO_4$ DME at 1600 rpm at 2.0 V, 2.2 V, and 2.4 V vs Li^+/Li with fitting parameters k_{solv} = 0.1 s^{-1} and $\sqrt{N}k_2^0$ = 50,000 s^{-1}.

a) 0.1 M $LiClO_4$ DMSO 1600 rpm anhydrous

b) 0.1 M $LiClO_4$ DMSO 1600 rpm ~5000 ppm H_2O

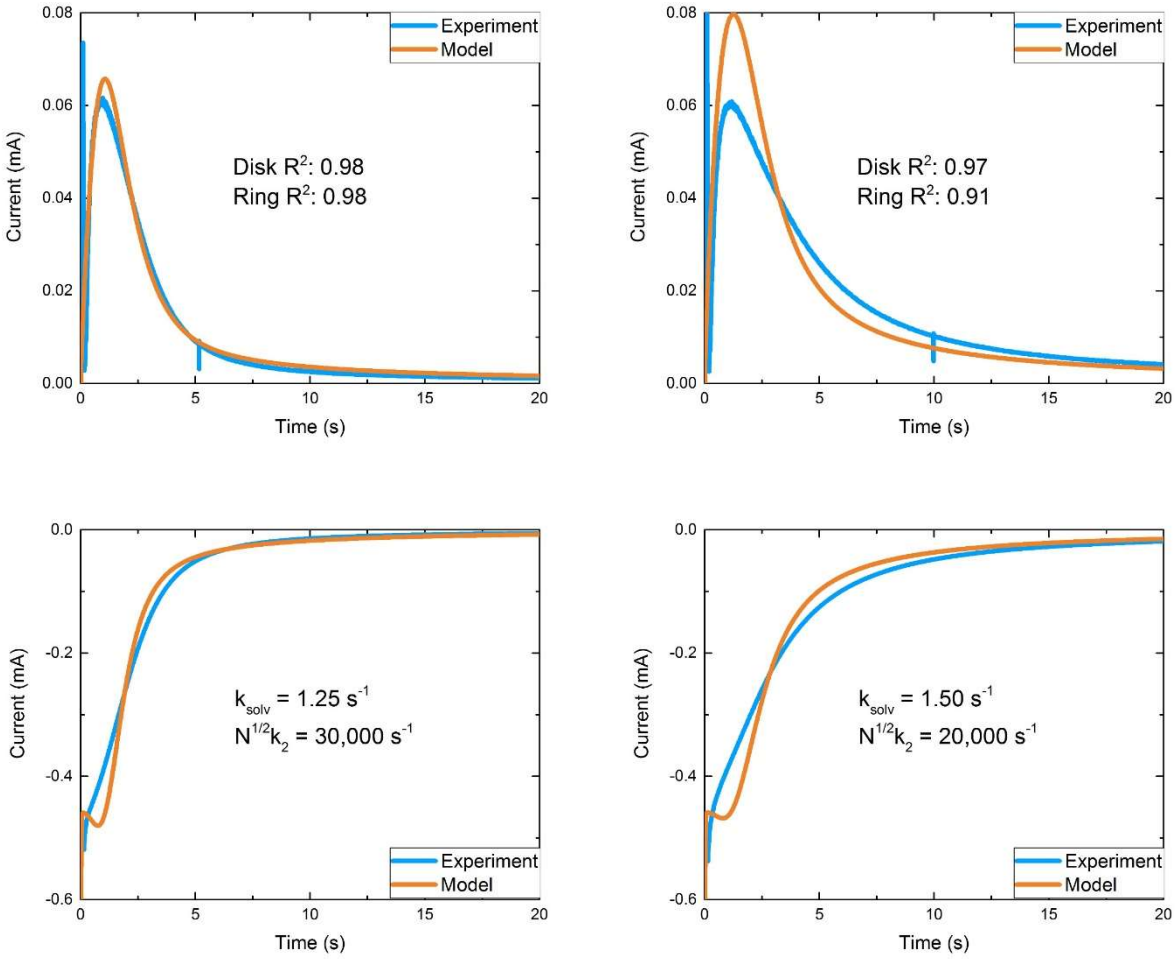

Figure 4.5.3: Fits of Experimental Discharge Curves for Water Content Trend: Fits were performed for data at 2.4 V vs Li^+/Li. a) Model fit of 0.1 M $LiClO_4$ DMSO at 1600 rpm anhydrous b) model fit of 0.1 M $LiClO_4$ DMSO at 1600 rpm with ~5000 ppm H_2O.

a) 0.1 M $LiClO_4$ DMSO 1600 rpm anhydrous

b) 0.5 M $LiClO_4$ DMSO 1600 rpm anhydrous

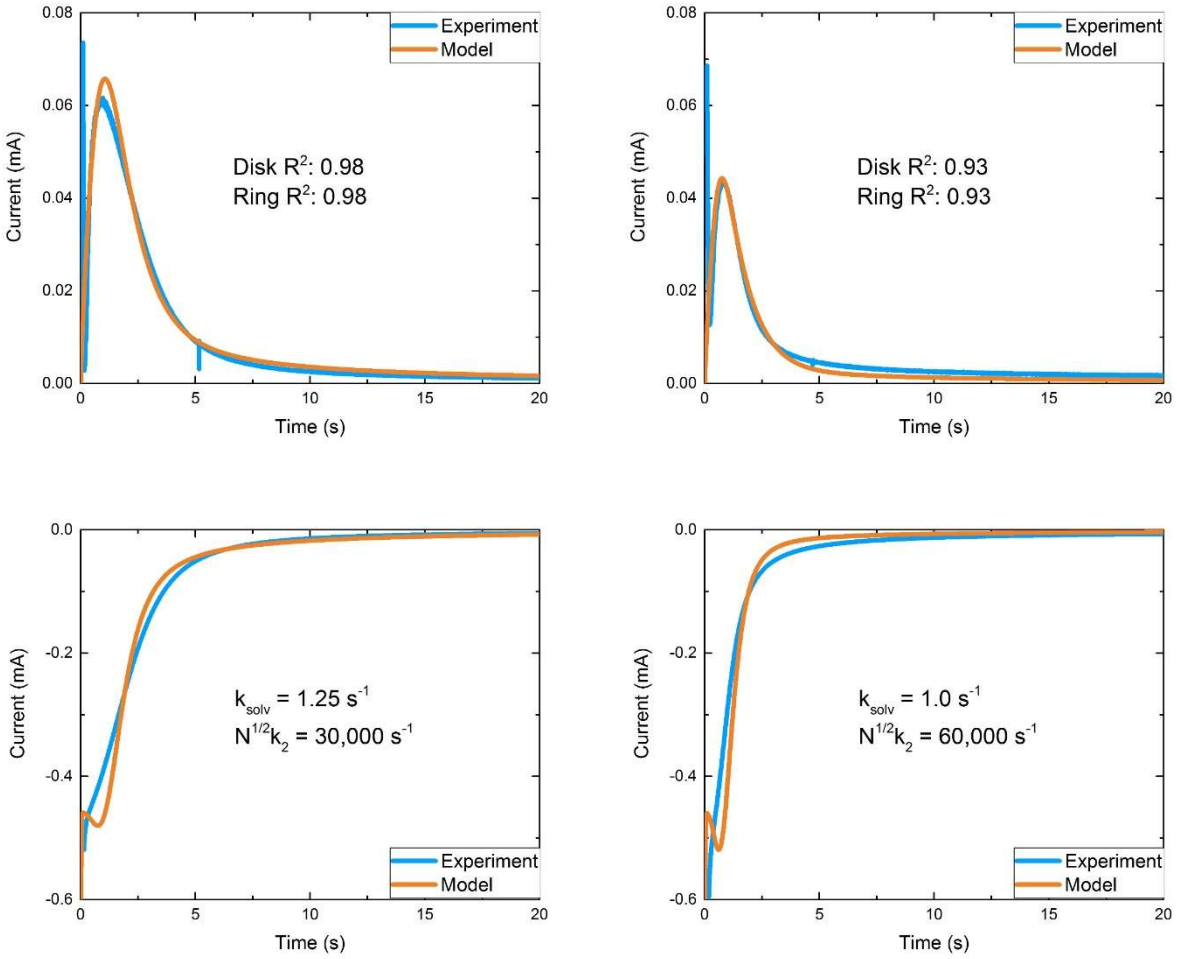

Figure 4.5.4: Fits of Experimental Discharge Curves for Salt Concentration Trend: Fits were performed for data at 2.4 V vs Li^+/Li. a) Model fit of 0.1 M $LiClO_4$ DMSO at 1600 rpm anhydrous and b) model fit of 0.5 M $LiClO_4$ DMSO at 1600 rpm.

a) 0.1 M $LiClO_4$ DMSO 1600 rpm anhydrous

d) 0.1 M $LiClO_4$ DMSO 900 rpm anhydrous

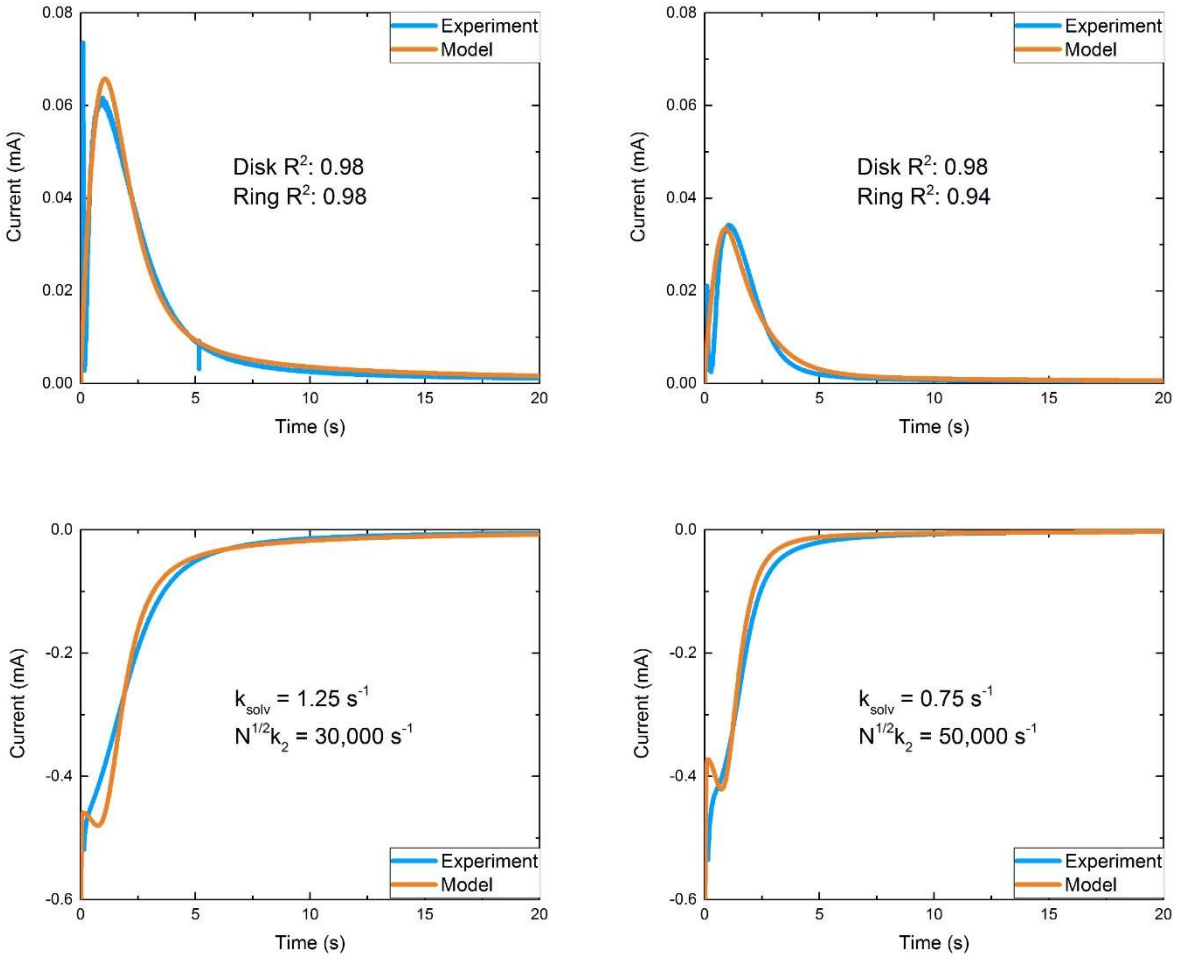

Figure 4.5.5: Fits of Experimental Discharge Curves by Model for Rotation Rate Trend: Fits were performed for data at 2.4 V vs Li^+/Li. a) Model fit of 0.1 M $LiClO_4$ DMSO at 1600 rpm anhydrous and b) model fit of 0.1 M $LiClO_4$ DMSO at 900 rpm.

Having replicated the disk potential dependence with the model, it was necessary to check that the model can also reproduce trends with solvent Li^+-O_2^- solubility. An addition of ~5000 ppm H_2O to the nominally anhydrous DMSO (~< 30 ppm H_2O) resulted in a shift of k_{solv} from 1.25 s^{-1} to 1.5 s^{-1} and a shift in the value of $\sqrt{N}k_2^0$ from 30,000 s^{-1} to 20,000 s^{-1} (Figure 4.5.3). The change in k_{solv} is likely due to the increase in acceptor number caused by adding water, which increases the favorability of solvation of Li^+-O_2^-. The change in $\sqrt{N}k_2^0$ could be caused by stronger interactions between solvent molecules and Li^+-

O_2^- and a weaker binding energy of Li^+ to O_2^-. These effects increase reorganization energy and inhibit the reduction reaction[23]. An increase in $LiClO_4$ concentration from 0.1 M to 0.5 M caused a shift in k_{solv} from 1.25 s^{-1} to 1.0 s^{-1} and a shift in $\sqrt{N}k_2^0$ from 30,000 s^{-1} to 60,000 s^{-1} (Figure 4.5.4). The decline in k_{solv} is due to fewer free solvent molecules, suppressing the solvation of Li^+-O_2^-. The increase in $\sqrt{N}k_2^0$ with increased Li^+ concentration is consistent with Li^+ being a reactant in the reduction of Li^+-O_2^-. A dependence of this step on Li^+ concentration has been previously reported[24]. Decreasing the rotation rate from 1600 rpm to 900 rpm decreases k_{solv} from 1.25 s^{-1} to .75 s^{-1} and increases $\sqrt{N}k_2^0$ from 30,000 s^{-1} to 50,000 s^{-1} (Figure 4.5.5). At higher rotation rates, Li^+-O_2^- is more likely to be coordinated by solvent molecules, explaining the increase in k_{solv} and decrease in $\sqrt{N}k_2^0$. To check that the two-parameter fits were physically meaningful, the quality of fit for adjusting one parameter was checked for each of these solvent alterations (Table A.2). The fits make clear that in all cases either k_{solv} or $\sqrt{N}k_2^0$ changed. Changes in $\sqrt{N}k_2^0$ were dominant in the salt concentration trend; changes in k_{sol} were dominant in the rotation rate trend. It was not possible to determine whether k_{solv} or $\sqrt{N}k_2^0$ changes were dominant for the water trend. Overall, there appears to be an inverse relation between k_{solv} or $\sqrt{N}k_2^0$ (Figure A.5). A promotion of solvating interactions between superoxide and solvent molecules will increase the solvation rate constant but also increase the solvent reorganization energy and suppress the superoxide reduction rate constant (Discussion A.2). The change in fitted values for solvation rate constant and superoxide reduction rate constant with water content, salt concentration, and rotation rate suggests that both the favorability of solvation and favorability of superoxide reduction are heavily dependent on solvent properties and how solvent molecules interact with Li^+-O_2^-.

4.6 Insights from the Model

a) Ring to Disk Ratio

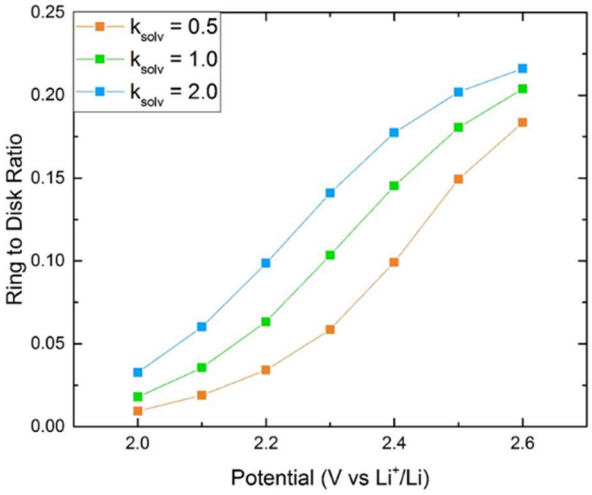

b) Disk Capacity

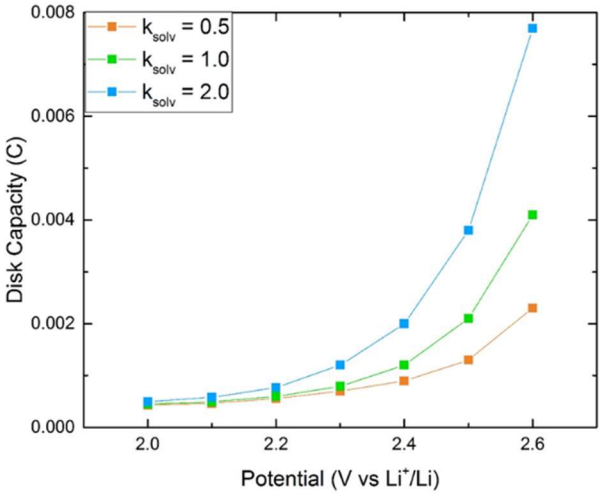

Figure 4.6.1: Modeled Cell Performance as Solvation Rate Constant Changes a) Ring to disk capacity ratio and b) disk capacity based on modeled results at $\sqrt{N}k_2^0$ = 30,000 s^{-1} and k_{solv} = 0.5, 1.0, and 2.0 in 0.1 M $LiClO_4$ DMSO at 1600 rpm.

The ability to fit the model to experimental RRDE data demonstrates that the modeling assumptions are physically reasonable and provides insight into what values of model parameters correspond to experimental properties. This enables modeling of the performance of a cell under physically reasonable values. The morphological composition can be modeled by predicting the ring-disk ratio (ring capacity/disk capacity) (Figure 4.6.1a). A ratio of 0 corresponds to the case of 100% film formation and a ratio of .23 corresponds to the case of 100% toroid formation (given that the ring collection efficiency is 23% and assuming parasitic reactions and disproportionation reactions are negligible). The modeled trend against disk potential qualitatively matches previous RRDE reports[6]. Increasing the solvation rate constant causes an increase in ring-disk ratio across all potentials. However, this change in morphology corresponds to a weak increase in capacity at high overpotential and a large increase in capacity at low overpotential (Figure 4.6.1b). This mirrors previous experimental observations of a discharge potential/rate dependence of the effect of water content[10,13].

a) Average Surface Li^+-O_2^- Concentration

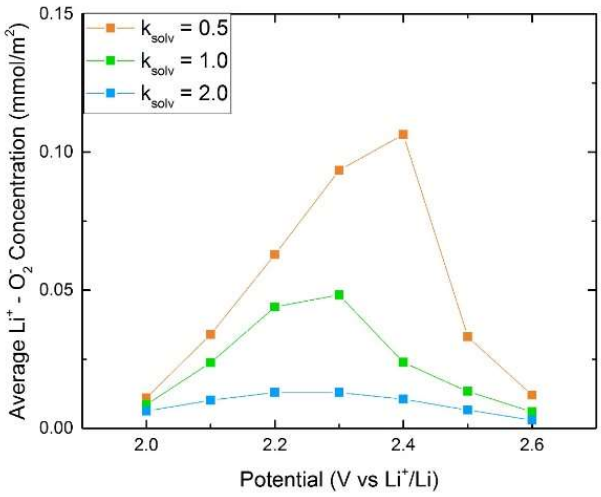

b) Discharge Cut-off Time

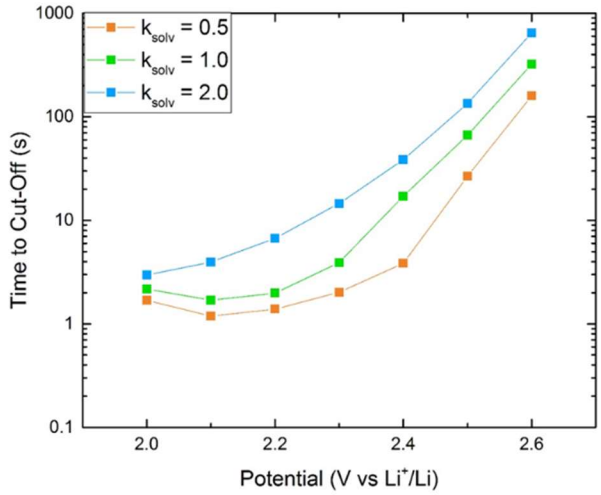

Figure 4.6.2 Effect of Solvation Rate Constant on Li^+-O_2^- Concentration a) Average surface Li^+-O_2^- concentration, and b) time to discharge cut-off (99% area coverage by Li_2O_2 film) based on modeled results at $\sqrt{N}k_2^0$ = 30,000 s^{-1} and k_{solv} = 0.5, 1.0, and 2.0 in 0.1 M $LiClO_4$ DMSO at 1600 rpm.

Physical intuition about these capacity increases and their potential dependence can be gained by considering the modeled prediction of surface Li^+-O_2^- concentration (Figure 4.6.2a) and the length of

time to electrode passivation (Figure 4.6.2b). Of particular interest is the prediction of the average value of surface Li^+-O_2^- concentration. This value is experimentally difficult to measure due to the instability of Li^+-O_2^- and limited technical means to characterize it *in situ* during discharge. The average value of the surface Li^+-O_2^- concentration passes through a maximum at intermediate potentials. Increasing the solvation rate constant causes a depletion of the surface Li^+-O_2^- concentration at all potentials and also flattens the potential dependence. Since the average radial growth rate of the film is proportional to the average surface Li^+-O_2^- concentration, the time to complete coverage of the electrode by Li_2O_2 increases inversely to this concentration. Under galvanostatic discharge conditions, the time of complete coverage by Li_2O_2 film is known as a "sudden death" time. At "sudden death", the potential rapidly decreases from a plateau potential that held for most of discharge to the cut-off potential. Under potentiostatic conditions, the current asymptotically approaches zero. The time of 99% area coverage by the Li_2O_2 film was chosen as a cut-off time, acting as an analog to "sudden death" time. Comparing Figure 4.6.2a and Figure 4.6.2b demonstrates that changes in the solvation rate constant and potential result in larger changes for the "sudden death" time than for the average surface Li^+-O_2^- concentration. The shape of the "sudden death" time potential dependence is similar to the shape of the capacity vs potential plot in Figure 4.6.1b. This suggests that increases in capacity are due to a slower surface pathway rate rather than a faster solvent pathway rate.

a) Average Solvent Pathway Rate vs k_{solv}

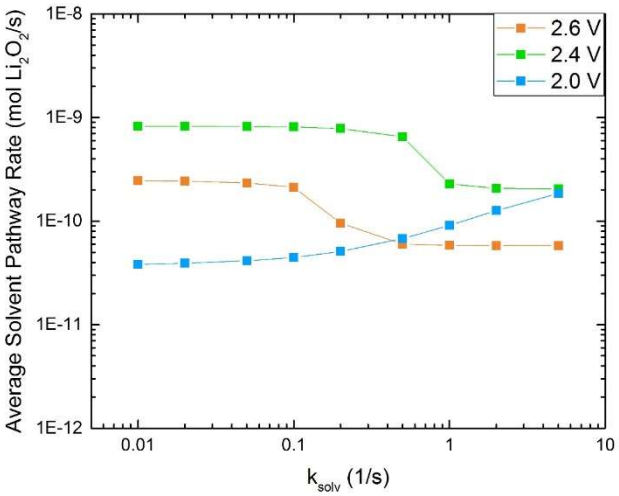

b) Average Surface Pathway Rate vs k_{solv}

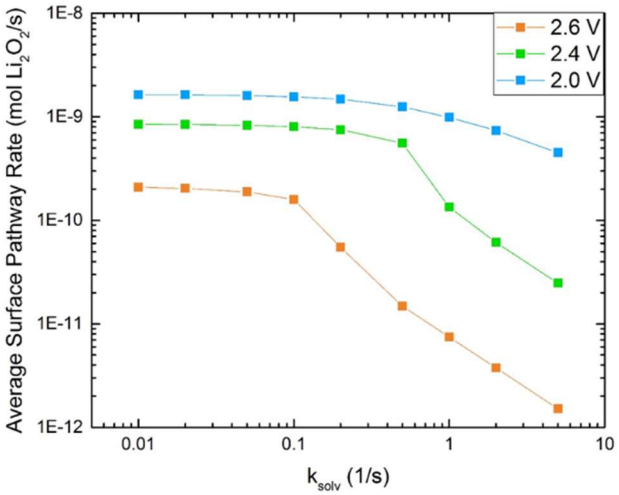

Figure 4.6.3: Modeled Effect of Solvation Rate Constant on Average Pathway Rates: a) Solvent pathway and b) surface pathway average rate at 2.0 V, 2.4 V, 2.6 V vs Li^+/Li in 0.1 M $LiClO_4$ DMSO at 1600 rpm and $\sqrt{N}k_2^0$ = 30,000 s^{-1}.

To help rationalize this observation, the average rate of both the solvent pathway and surface pathway were plotted as a function of k_{solv} (Figure 4.6.3a and 4.6.3b respectively). The average pathway rate is defined as the moles of Li_2O_2 that would form from a given pathway divided by the time to cut-off (Discussion A.4). At very low values of k_{solv} the effect of changing k_{solv} has limited effect on

the surface pathway rate at all potentials. However, as k_{solv} approaches larger values the average surface pathway rate begins to rapidly decline. The decline is sharper at lower overpotentials than at higher overpotentials. In contrast, the average solvent pathway rate is relatively independent of both potential and solvation rate constant. Higher solvation rate constants deplete the surface Li^+-O_2^- concentration (Figure 4.6.2a). Since the average solvent pathway rate is proportional to the average surface Li^+-O_2^- concentration and solvation rate constant by Equation 4.4, the rate changes little as one factor decreases and the other increases.

a) 2.0 V Average Pathway Rates

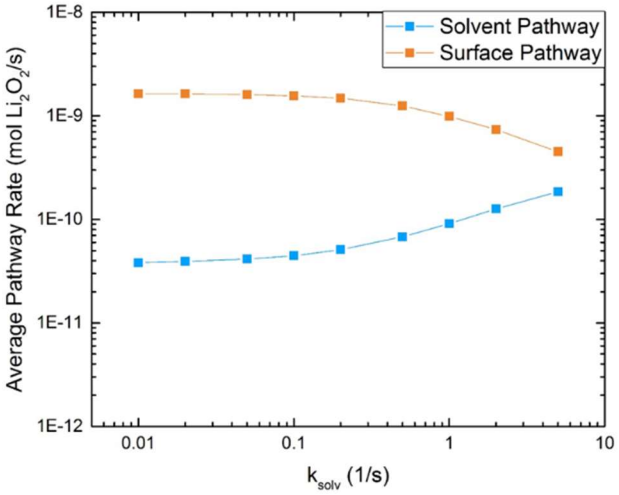

b) 2.6 V Average Pathway Rates

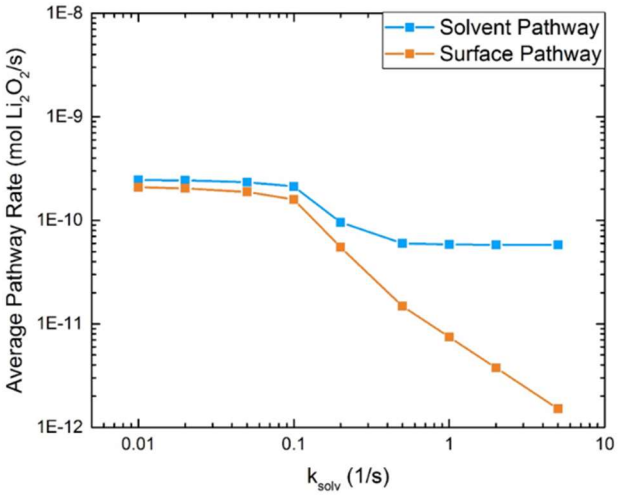

Figure 4.6.4: Modeled Effect of Potential on Average Pathway Rates a) The surface and solvent pathway average rate at 2.0 V vs Li^+/Li and b) at 2.6 V vs Li^+/Li in 0.1 M $LiClO_4$ DMSO at 1600 rpm and $\sqrt{N}k_2^0$ = 30,000 s^{-1}.

This insight can help explain the physical origin of the capacity dependence on both potential and solvation rate constant. Changing the solvation rate constant at high overpotential (Figure 4.6.4a) causes minimal change until the solvation rate constant is relatively high. Additionally, the size of the surface pathway average rate dominates relative to the solvation pathway average rate, which is nearly

constant. Therefore, the sudden death time and capacity increase little. The opposite occurs at low overpotential (Figure 4.6.4b). The solvent pathway rate is comparable to the surface pathway rate even at very low solvation rate constants. The surface pathway rate decreases rapidly at observed values of the solvation rate constant in experimental fits, causing a large increase in “sudden death” time and a longer time for the solvent pathway rate to occur over. This corresponds to a large promotion of toroids and capacity increases in a traditional cell.

a) Average Solvent Pathway Rate vs $\sqrt{N}k_2^0$

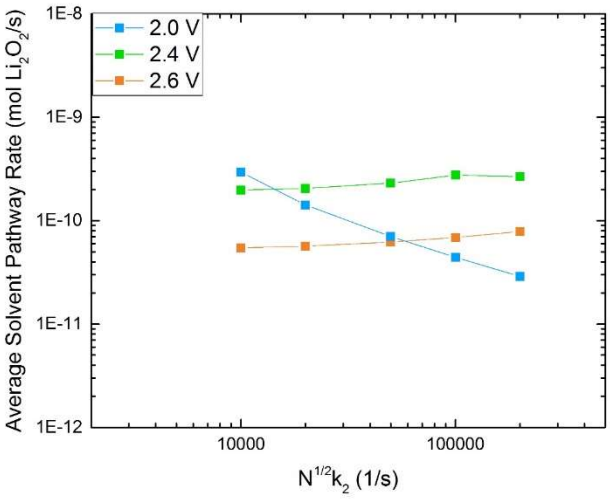

b) Average Surface Pathway Rate vs $\sqrt{N}k_2^0$

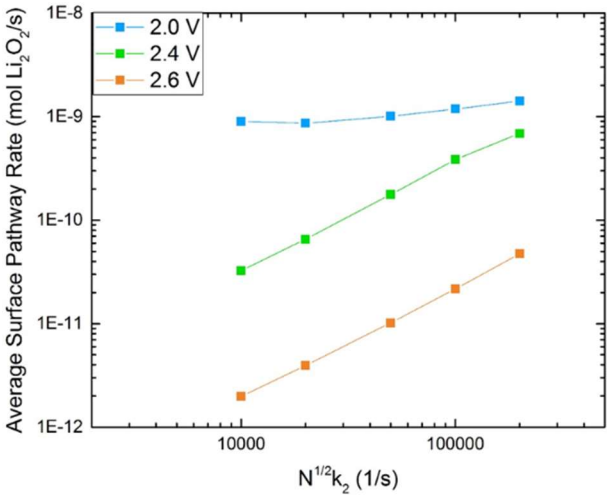

Figure 4.6.5 Modeled Effect of $\sqrt{N}k_2^0$ on Average Pathway Rates a) Solvent pathway average rate and b) surface pathway average rate at 2.0 V, 2.4 V, 2.6 V vs Li^+/Li in 0.1 M $LiClO_4$ DMSO at 1600 rpm and k_{solv} = 1.25 s^{-1}.

A similar trend with solvent pathway rate and surface pathway rate is observed with $\sqrt{N}k_2^0$ (Figures 4.6.5, A.6, and A.7). Increasing the favorability of Li^+-O_2^- reduction has a weak effect on the

average rate of solvation of Li^+-O_2^-, since the effect of this parameter on Li^+-O_2^- surface concentration is minimal (Figure 4.6.5a). However, increasing $\sqrt{N}k_2^0$ causes the surface pathway rate to increase, as the increase in $\sqrt{N}k_2^0$ is greater than the decrease in Li^+-O_2^- surface concentration (Figure 4.6.5b). Since increases in the solvation rate constant were found to correlate to lower values of $\sqrt{N}k_2^0$, it is expected that similar trends will be observed when both parameters are changing. Higher values of k_{solv} and lower values of $\sqrt{N}k_2^0$ both correspond to minimal changes in average solvent pathway rate and significant decreases in average surface pathway rate (Figure A.8).

Modeled and experimental results point toward inhibition of the surface pathway rate as the dominant factor in toroid promotion, rather than enhanced solvent pathway rate. This observation should be broadly applicable to any Li-O_2 cell where the Li_2O_2 film evolves by nucleation and growth and solvent properties determine the relevant solvation rate constant. The fits in Figure 4.5.3 suggest that modifying the solvent acceptor number by adding water is related to a change in the solvation rate constant and superoxide reduction rate constant. Connecting changes in acceptor and donor number to changes in the solvation rate constant is supported by linear free energy relationships for solvation. The logarithm of the solvation rate constant from a gas to a solvated state is linearly proportional to several variables including hydrogen bond acidity and hydrogen bond basicity[39]. Acceptor number correlates to hydrogen bond basicity and donor number correlates to hydrogen bond acidity in a broad array of solvents[40]. It is reasonable to assume that k_{solv} in the model is linearly proportional to both the acceptor number and donor number of a particular solvent. The relationship between water content and its effect on the acceptor number of the solvent mixture is non-linear and hard to predict. Small amounts of water produce large increases in acceptor number when the water content is low and the effect on acceptor number levels off as the water content becomes high[7,41]. Nevertheless, this model provides insight into the expected mechanism of surface pathway inhibition for capacity increases by any strategy that involves manipulation of the acceptor or donor number of the solvent. Since DMSO

and water have a high donor number and a high acceptor number respectively, it is likely that other solvents have lower solvation rate constants. The fit of k_{solv} for 0.1 M $LiClO_4$ DME at 1600 rpm was ~1/10 that of the fit of k_{solv} for 0.1 M $LiClO_4$ DMSO at 1600 rpm. Changes in k_{solv} with changing salt concentration and rotation rate suggest that reducing the solubility of Li^+-O_2^- in an electrolyte solvent broadly correlates with a reduced solvation rate constant. Decreasing the solvation rate constant is also correlated to a greater superoxide reduction rate constant, as the reorganization energy for the reduction reaction is decreased when solvation is weaker. The model makes a broad prediction about the effect of manipulating solvent superoxide solubility on the relative rates of the surface and solvent pathway.

There are some limits to the applicability of the study. The model assumes disproportionation and side reactions are slow enough to ignore. However, numerous studies have shown most battery solvents are not fully stable[42]. At slower discharge rates with longer time-scales for chemical decomposition, parasitic reactions might have an effect on either of the pathways[43]. Similarly, in a slow discharge in a traditional cell, Li_2O_2 toroids can precipitate onto electrode surfaces and might participate in electrode passivation.

Mechanistic insights from this study could provide broader lessons about what strategies are most likely to improve Li-O_2 performance. Adding oxygen reduction reaction redox mediators is a proposed strategy for promoting Li_2O_2 toroid formation by shuttling charge from the electrode surface to solvent species. For example, 2,5-di-*tert*-butyl-1,4-benzoquinone (DBBQ) has been shown to increase capacity by a factor of 100 in certain electrodes[44]. The effect of a redox mediator can be intuited with this model. In contrast to adjusting the acceptor or donor number of the solvent, which changes a potential-independent value of k_{solv}, the effect of a redox mediator could be modeled as a potential dependent component of k_{solv}. This suggests electrochemical additives such as redox mediators might outperform chemical additives such as water at high overpotential/high discharge rate conditions.

4.7 Conclusion

This study demonstrated that a model of nucleation and growth and tunneling accurately fits experimental RRDE data and can correctly predict the time evolution and relative size of both the surface and solvent pathway. The model suggests that the inhibition of the surface pathway is mechanically far more critical to the enhancement of capacity as solvent properties are changed than the rate of the solvent pathway. Knowledge of this mechanism and its relative dominance under an array of potentials and solvent Li^+-O_2^- solubilities can help guide optimal design of Li-O_2 batteries and provide insights into the most promising strategies for enhancing capacity.

References

1. Mitchell, R. R., Gallant, B. M., Thompson, C. V. & Shao-Horn, Y. All-carbon-nanofiber electrodes for high-energy rechargeable Li–O2 batteries. *Energy Environ. Sci.* **4,** 2952 (2011).
2. Viswanathan, V. *et al.* Electrical conductivity in Li2O2 and its role in determining capacity limitations in non-aqueous Li-O2 batteries. *J. Chem. Phys.* **135,** 214704 (2011).
3. Black, R., Adams, B. & Nazar, L. F. Non-aqueous and hybrid Li-O2 batteries. *Adv. Energy Mater.* **2,** 801–815 (2012).
4. Mitchell, R. R., Gallant, B. M., Shao-Horn, Y. & Thompson, C. V. Mechanisms of Morphological Evolution of Li2O2 Particles during Electrochemical Growth. *J. Phys. Chem. Lett.* **4,** 1060–1064 (2013).
5. Johnson, L. *et al.* The role of LiO2 solubility in O2 reduction in aprotic solvents and its consequences for Li-O2 batteries. *Nat. Chem.* **6,** 1091–1099 (2014).
6. Kwabi, D. G. *et al.* Controlling Solution-Mediated Reaction Mechanisms of Oxygen Reduction Using Potential and Solvent for Aprotic Lithium-Oxygen Batteries. *J. Phys. Chem. Lett.* **7,** 1204–1212 (2016).
7. Aetukuri, N. B. *et al.* Solvating additives drive solution-mediated electrochemistry and enhance toroid growth in non-aqueous Li-O2 batteries. *Nat. Chem.* **7,** 50–56 (2015).
8. Nazar, L. *et al.* Current Density Dependence of Peroxide Formation in the Li-O2 Battery and its Effect on Charge. *Energy Environ. Sci.* **6,** 1772–1778 (2013).
9. Laoire, C. O., Mukerjee, S., Abraham, K. M., Plichta, E. J. & Hendrickson, M. A. Influence of nonaqueous solvents on the electrochemistry of oxygen in the rechargeable lithium-air battery. *J. Phys. Chem. C* **114,** 9178–9186 (2010).

10. Schwenke, K. U., Metzger, M., Restle, T., Piana, M. & Gasteiger, H. A. The Influence of Water and Protons on Li2O2 Crystal Growth in Aprotic Li-O2 Cells. *J. Electrochem. Soc.* **162,** A573–A584 (2015).

11. Kwon, H.-M. *et al.* Effect of Anion in Glyme-based Electrolyte for Li-O2 Batteries: Stability/Solubility of Discharge Intermediate. *Chem. Lett.* **46,** 573–576 (2017).

12. Tatara, R. *et al.* Oxygen Reduction Reaction in Highly Concentrated Electrolyte Solutions of Lithium Bis(trifluoromethanesulfonyl)amide/Dimethyl Sulfoxide. *J. Phys. Chem. C* **121,** 9162–9172 (2017).

13. Kwabi, D. G. *et al.* The effect of water on discharge product growth and chemistry in Li–O_2 batteries. *Phys. Chem. Chem. Phys.* **18,** 24944–24953 (2016).

14. Lau, S. & Archer, L. A. Nucleation and Growth of Lithium Peroxide in the Li-O2 Battery. *Nano Lett.* **15,** 5995–6002 (2015).

15. Safari, M., Adams, B. D. & Nazar, L. F. Kinetics of oxygen reduction in aprotic Li-O2 cells: A model-based study. *J. Phys. Chem. Lett.* **5,** 3486–3491 (2014).

16. Rinaldi, A., Wijaya, O. & Hoster, H. Lithium-Oxygen Cells: An Analytical Model to Explain Key Features in the Discharge Voltage Profiles. *ChemElectroChem* **3,** 1944–1950 (2016).

17. Yin, Y., Torayev, A., Gaya, C., Mammeri, Y. & Franco, A. A. Linking the Performances of Li-O2Batteries to Discharge Rate and Electrode and Electrolyte Properties through the Nucleation Mechanism of Li2O2. *J. Phys. Chem. C* **121,** 19577–19585 (2017).

18. Ren, Y. X., Zhao, T. S., Tan, P., Wei, Z. H. & Zhou, X. L. Modeling of an aprotic Li-O2 battery incorporating multiple-step reactions. *Appl. Energy* **187,** 706–716 (2017).

19. Sankarasubramanian, S., Seo, J., Mizuno, F., Singh, N. & Prakash, J. Elucidating the Oxygen Reduction Reaction Kinetics and the Origins of the Anomalous Tafel Behavior at the Lithium-Oxygen Cell Cathode. *J. Phys. Chem. C* **121,** 4789–4798 (2017).

20. Herranz, J., Garsuch, A. & Gasteiger, H. A. Using rotating ring disc electrode voltammetry to quantify the superoxide radical stability of aprotic Li-air battery electrolytes. *J. Phys. Chem. C* **116,** 19084–19094 (2012).

21. Calvo, E. J. & Mozhzhukhina, N. A Rotating Ring Disc Electrode Study of the Oxygen Reduction Reaction in Lithium Containing Non Aqueous Electrolyte. *Electrochem. commun.* **31,** 56–58 (2013).

22. Torres, W., Mozhzhukhina, N., Tesio, A. Y. & Calvo, E. J. A Rotating Ring Disk Electrode Study of the Oxygen Reduction Reaction in Lithium Containing Dimethyl Sulfoxide Electrolyte: Role of Superoxide. *J. Electrochem. Soc.* **161,** A2204–A2209 (2014).

23. Kwabi, D. G. *et al.* Experimental and Computational Analysis of the Solvent-Dependent O2/Li+-O2− Redox Couple: Standard Potentials, Coupling Strength, and Implications for Lithium-Oxygen Batteries. *Angew. Chemie* **128,** 3181–3186 (2016).

24. Belova, A. I., Kwabi, D. G., Yashina, L. V., Shao-Horn, Y. & Itkis, D. M. Mechanism of Oxygen Reduction in Aprotic Li–Air Batteries: The Role of Carbon Electrode Surface Structure. *J. Phys. Chem. C* **121,** 1569–1577 (2017).

25. Sergeev, A. V, Itkis, D. M. & Chertovich, A. V. Applying the deconvolution approach in order to enhance RRDE time resolution : practical issues and limitations . *arXiv* (2018).

26. Lu, Y.-C., Gasteiger, H. A., Crumlin, E., McGuire, R. & Shao-Horn, Y. Electrocatalytic Activity Studies of Select Metal Surfaces and Implications in Li-Air Batteries. *J. Electrochem. Soc.* **157,** A1016 (2010).

27. Sharon, D. *et al.* Oxidation of Dimethyl Sulfoxide Solutions by Electrochemical Reduction of Oxygen. *J. Phys. Chem. Lett.* **4,** 3115–3119 (2013).

28. Bard, A. J. & Faulkner, L. R. *Electrochemical Methods: Fundamentals and Applications*. (2001).

29. Sawyer, D. T. & Roberts, J. L. Electrochemistry of oxygen and superoxide ion in dimethylsulfoxide at platinum, gold and mercury electrodes. *J. Electroanal. Chem.* **12,** 90–101 (1966).

30. Siver, Y. G. Non-stationary electrode processes in mixed environments. *Russ. J. Phys. Chem.* **33,** (1959).

31. Avrami, M. Kinetics of Phase Change. II Transformation-Time Relations for Random Distribution of Nuclei. *J. Chem. Phys.* **8,** 212 (1940).

32. Haynes, W. M. *'Physical Constants of Inorganic Compounds', CRC Handbook of Chemistry and Physics*. (2011).

33. Lu, Y.-C. *et al.* Lithium–oxygen batteries: bridging mechanistic understanding and battery performance. *Energy Environ. Sci.* **6,** 750 (2013).

34. Read, J. *et al.* Oxygen Transport Properties of Organic Electrolytes and Performance of Lithium/Oxygen Battery. *J. Electrochem. Soc.* **150,** A1351 (2003).

35. Lu, Y.-C. *et al.* The discharge rate capability of rechargeable Li–O2 batteries. *Energy Environ. Sci.* **4,** 2999 (2011).

36. Xu, D., Wang, Z., Xu, J., Zhang, L. & Zhang, X. Novel DMSO-based electrolyte for high performance rechargeable Li-O2 batteries. *Chem. Commun. (Camb).* **48,** 6948–50 (2012).

37. Kumar, G. *et al.* Conductivity and Viscosity of Lithium Perchlorate in Mixed Nonaqueous Solvents at Various Temperatures. *J. Chem. Eng. Data* **36,** 467–470 (1991).

38. Gallant, B. M. *et al.* Influence of Li2O2 morphology on oxygen reduction and evolution kinetics in Li–O2 batteries. *Energy Environ. Sci.* **6,** 2518 (2013).

39. Acree, Wlliam, E. & Abraham, M. H. The analysis of solvation in ionc liquids and organic solvents using the Abraham linear free energy relationship. *J. Chem. Technol. Biotechnol.* **81,** 1441–1446 (2006).

40. Taft, R. W., Pienta, N. J., Hamlet, M. J. & Arnett, E. M. Linear Solvation Energy Relationships. 7. Correlations between the Solvent-Donicity and Acceptor-Number Scales and the Solvatochromic Parameters π, α, and β. *J. Org. Chem.* **46,** 661–667 (1981).

41. Taha, A. & Mahmoud, M. M. Lewis acidity parameter for binary solvent mixtures and adduct formation studies using the solvatochromic dicyanobis(1,10-phenanthroline)iron(II) complex. *New J. Chem.* **26,** 953–957 (2002).

42. McCloskey, B. D., Bethune, D. S., Shelby, R. M., Girishkumar, G. & Luntz, A. C. Solvents' Critical

Role in Nonaqueous Lithium–Oxygen Battery Electrochemistry. *J. Phys. Chem. Lett.* **2,** 1161–1166 (2011).

43. Kwabi, D. G. *et al.* Chemical Instability of Dimethyl Sulfoxide in Lithium–Air Batteries. *J. Phys. Chem. Lett.* **5,** 2850–2856 (2014).

44. Gao, X., Chen, Y., Johnson, L. & Bruce, P. G. Promoting solution phase discharge in Li-O2 batteries containing weakly solvating electrolyte solutions. *Nat. Mater.* **15,** 882–888 (2016).

Chapter Five: Conclusions and Future Work

5.1 Summary and Conclusions

The work in this thesis has examined two intimately related issues in the development of Li-O_2 batteries: how to optimize capacity and how to achieve high stability of cell components and discharge product. Both of these goals are tied to solvent properties and the interactions between solvent molecules and discharge intermediates and products. High capacity can be achieved by enhancing the solubility of Li^+-O_2^- reaction intermediate to form larger toroidal deposits of Li_2O_2. However, solvents with high Li^+-O_2^- solubility or additives that improve it can be susceptible to side reactions.

In Chapter Two, the stability of dimethyl sulfoxide (DMSO) was examined. Due to its high Lewis basicity, DMSO stabilizes Li^+ and allows for high solubility of Li^+-O_2^- reaction intermediate. However, conflicting reports about its stability existed in the literature[1–3]. We tested the stability of electrochemically formed Li_2O_2 by aging electrodes discharged in DMSO and performing X-ray diffraction, electron microscopy, and Raman spectroscopy. These techniques showed that electrochemically formed Li_2O_2 converted to LiOH in the presence of DMSO over long periods of time. Mixtures of commercial ball-milled Li_2O_2 and DMSO were aged to check solvent stability. Fourier transform infrared spectroscopy and gas chromatography revealed the decomposition of DMSO to dimethyl sulfone. The decomposition reaction was promoted in the presence of superoxide. This study demonstrated that DMSO, while useful for fundamental experiments, is not suitable for commercial use. The study also showed the importance of performing aging studies of discharged electrodes when characterizing solvent stability.

In Chapter Three, the effect of adding water to the electrolyte solvent on capacity and stability was studied. X-ray diffraction demonstrated that Li_2O_2 formed in electrodes discharged with the electrolyte solvent dimethoxyethane (DME) regardless of water content. Scanning electron microscopy

showed that enhancing the water content caused the formation of larger Li_2O_2 toroids. In contrast, the same techniques showed that Li_2O_2 forms in anhydrous acetonitrile (MeCN) but LiOH forms when water is added. This was attributed to the greater favorability of deprotonation of water in acetonitrile compared to dimethoxyethane[4]. Discharges in carbon nanotube electrodes with high defect densities showed increases in toroid size but little impact on final capacity, indicating the dominance of the surface pathway. Potentiostatic discharges with and without water indicated that water likely affected the nucleation and growth kinetics of surface Li_2O_2 film evolution.

In Chapter Four, the relationship between discharge conditions and the surface pathway and solvent pathway of Li_2O_2 was studied. Experimental trends with potential, rotation rate, salt concentration, and water content were collected for potentiostatic discharges in a rotating ring-disk electrode setup. Using a rotating ring-disk electrode setup allowed for the separate measurement of the time evolution of the surface pathway rate creating thin film Li_2O_2 and of the solvent pathway rate creating solvated Li^+-O_2^-. A model was then constructed of the two discharge pathways and model assumptions were validated by fits to experimental trends. The model suggests that the favorability of the surface film evolution is affected by solvent properties. Additionally, due to the competition between the two pathways for surface Li^+-O_2^-, the rate of film evolution was heavily dependent on solvent properties in a physically reasonable regime of parameters. In contrast, the rate of solvation of Li^+-O_2^- was largely independent of solvent properties. As solvation of Li^+-O_2^- becomes more favorable, the concentration of surface Li^+-O_2^- tends to decrease. These mechanistic insights suggest that careful attention to the evolution of the Li_2O_2 surface film is critical to achieving high capacity Li-O_2 batteries.

All of these studies suggest that careful consideration of solvent molecule interactions is necessary to design high capacity and high stability Li-O_2 batteries. The strength of solvating interactions between Li^+-O_2^- and solvent molecules will determine the rate of formation of the Li_2O_2 surface film. The effect of the solvent molecules on deprotonation of water causes water additives to be stable in some

solvents and unstable in others. Reactions between Li_2O_2 and solvent molecules with aging could cause premature failure of Li-O_2 cells left in the discharged state. Any strategy that attempts to improve capacity or stability will need to consider these solvent molecule interactions.

5.2 Future Work

One strategy that could improve both the capacity and stability of Li-O_2 batteries is the use of redox mediators. Redox mediators carry charge between the electrode surface and a reactant. An oxygen reduction reaction redox mediator shown to facilitate Li-O_2 reactions is DBBQ (2,5-di-*tert*-butyl-1,2-benzoquinone).[5] DBBQ is reduced at the electrode surface to form LiDBBQ and competitively inhibits the formation of Li^+-O_2^-. LiDBBQ can then chemically react with O_2 in solution to form Li_2O_2 and DBBQ. Gao et al. demonstrated large increases in capacity by using DBBQ and avoiding the formation of reactive soluble Li^+-O_2^-, which should improve stability. Redox mediators for the charge process such as LiI[6] and TEMPO (2,2,6,6 tetramethylpiperidinyloxyl)[7] lower the charge overpotential and help to avoid decomposition reactions.

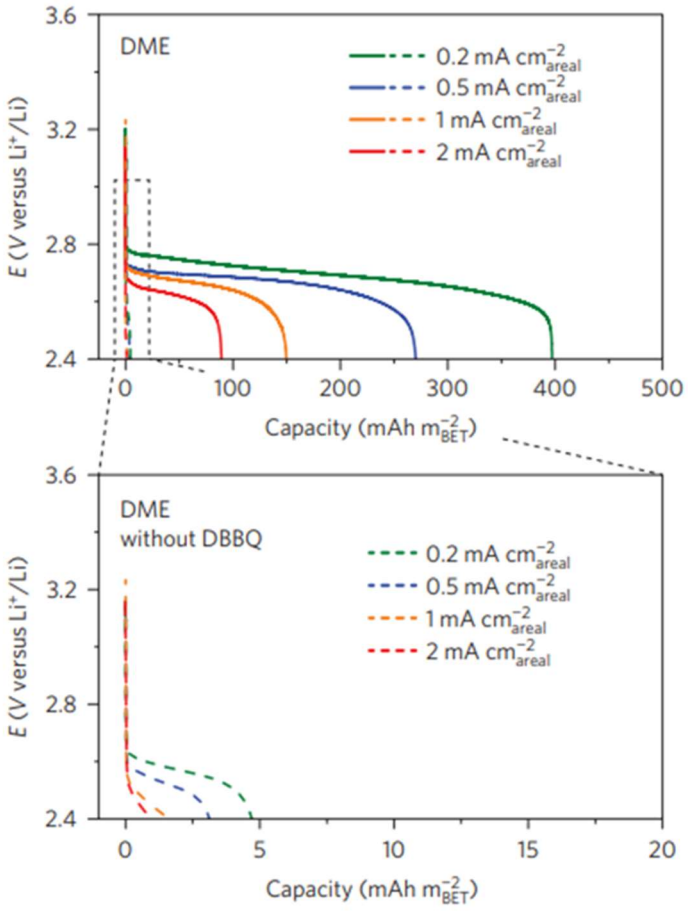

Figure 5.2.1 Effect on Capacity of DBBQ Redox Mediator Figure reproduced from Gao et al.[5] Discharges in 1 M LiTFSI DME on a gas diffusion layer carbon electrode with no added DBBQ (dashed lines) and with 10 mM added DBBQ (solid lines). The bottom plot is a magnification of the top plot at low depths of discharge. Reprinted from Springer Nature, Nature Materials, Ref. 5, "Promoting solution phase discharge in Li-O2 batteries containing weakly solvating electrolyte solutions," Gao et al., 2016.

ORR redox mediators are still in an early phase of development for Li-O_2 batteries. Extending the model used in Chapter Four could help to elucidate how redox mediators affect the surface film evolution and interact with other solvent properties. The model would rely on incorporating a potential dependent term for the solvation rate constant that reflects the properties of a given redox mediator. The model could then make predictions about how an ORR redox mediator such as DBBQ might behave

and affect toroid formation and surface film evolution under a variety of conditions. It is likely that the large gains in capacity observed by Gao et al. are due to suppression of the surface film evolution by inhibiting Li^+-O_2^- surface concentration through the reduction of the redox mediator.

Another application and extension of the model could be used to determine what stable electrodes contribute best to high capacity. While the vast majority of studies have used carbon electrodes, carbon is not completely stable[8,9]. Gold[3], titanium carbide[10], and molybdenum sulfide[11] have been reported to maintain high stability during Li-O_2 cycling. While gold is impractical for a commercial cell due to its weight and cost, titanium carbide and molybdenum sulfide could possibly offer attractive alternatives to carbon electrodes. An extension of the model in Chapter Four could fit discharge curves on different electrode surfaces for values of the surface reduction fitting parameter $\sqrt{N}k_2^0$ and determine how the kinetics of Li_2O_2 film evolution are altered by the electrode surface. Since the model has demonstrated that changes to both solvent and surface properties affect the surface film evolution rate, identifying which electrodes best suppress the growth of Li_2O_2 while still allowing for the production of solvated Li^+-O_2^- or reduction of a redox mediator is critical.

5.3 Perspective on Li-O_2 Batteries

This thesis suggests both caution and optimism for Li-O_2 batteries. Solvent stability continues to be the primary obstacle to achieving commercial batteries. However, while a fully stable solvent has yet to be discovered, the mechanisms of solvent decomposition are becoming better understood as discussed in Chapters Two and Three. While common battery solvents are not suitable, it may be possible to synthesize solvents with much higher stability based on these insights. Chapter Four demonstrated that controlling the solvent and surface properties can yield dramatic increases in capacity through inhibiting the rate of surface coverage of the electrode by Li_2O_2. Redox mediators are

still in an early stage of research and could dramatically improve both capacity and stability. Other strategies such as ionic liquid and solvent mixtures could possibly yield more stable cycling[11]. It is not possible to determine if Li-O_2 batteries will achieve wide-scale commercial adoption, but it is also not possible to determine if other "beyond lithium-ion" chemistries will achieve this either. Because they possess the largest upper bound in possible energy storage, Li-O_2 batteries require intense research and could help address the challenge of global climate change.

References

1. Mozhzhukhina, N., Méndez De Leo, L. P. & Calvo, E. J. Infrared spectroscopy studies on stability of dimethyl sulfoxide for application in a Li-air battery. *J. Phys. Chem. C* **117,** 18375–18380 (2013).
2. Sharon, D. *et al.* Oxidation of Dimethyl Sulfoxide Solutions by Electrochemical Reduction of Oxygen. *J. Phys. Chem. Lett.* **4,** 3115–3119 (2013).
3. Peng, Z., Freunberger, S. A., Chen, Y. & Bruce, P. G. A reversible and higher-rate Li-O2 battery. *Science* **337,** 563–6 (2012).
4. Kwabi, D. G. *et al.* The effect of water on discharge product growth and chemistry in Li–O_2 batteries. *Phys. Chem. Chem. Phys.* **18,** 24944–24953 (2016).
5. Gao, X., Chen, Y., Johnson, L. & Bruce, P. G. Promoting solution phase discharge in Li-O2 batteries containing weakly solvating electrolyte solutions. *Nat. Mater.* **15,** 882–888 (2016).
6. Liu, T. *et al.* Cycling Li-O2 batteries via LiOH formation and decomposition. *Science (80-.).* **350,** 530–533 (2015).
7. Bergner, B. J., Schuermann, A., Peppler, K., Garsuch, A. & Janek, J. TEMPO: A mobile catalyst for rechargeable Li-O2 batteries. *J. Am. Chem. Soc.* **136,** 15054–15064 (2014).
8. McCloskey, B. D. *et al.* Twin Problems of Interfacial Carbonate Formation in Nonaqueous Li–O 2 Batteries. *J. Phys. Chem. Lett.* **3,** 997–1001 (2012).
9. Gallant, B. M. *et al.* Chemical and Morphological Changes of Li–O 2 Battery Electrodes upon Cycling. *J. Phys. Chem. C* **116,** 20800–20805 (2012).
10. Ottakam Thotiyl, M. M. *et al.* A stable cathode for the aprotic Li-O2 battery. *Nat. Mater.* **12,** 1050–6 (2013).
11. Asadi, M. *et al.* A lithium–oxygen battery with a long cycle life in an air-like atmosphere. *Nature* **555,** 502–506 (2018).

Appendix A: Chapter Four Supplemental Information

a) 0.1 M $LiClO_4$ DMSO

b) 0.1 M $LiClO_4$ DME

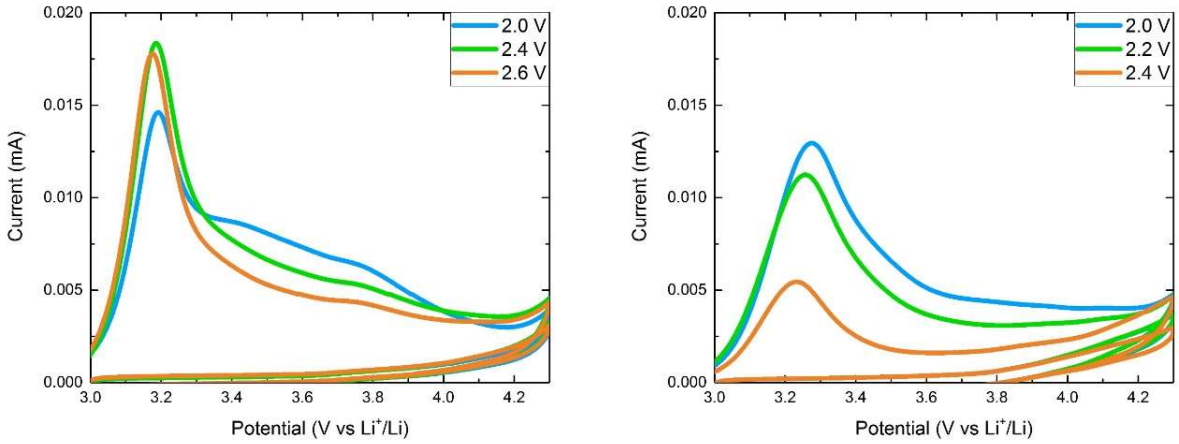

Figure A.1: Disk Oxidation Cyclic Voltammetry Potential Dependence a) Current vs potential for potential scans from 3 to 4.3 V vs Li^+/Li at 10 mV/s following 2 minute discharges at 2.0, 2.4, and 2.6 V vs Li^+/Li in 0.1 M $LiClO_4$ DMSO at 1600 rpm b) Current vs potential for potential scans from 3 to 4.3 V vs Li^+/Li at 10 mV/s following 2 minute discharges at 2.0, 2.2, and 2.4 V vs Li^+/Li in 0.1 M $LiClO_4$ DME at 1600 rpm.

The peak at ~3.2 V vs Li^+/Li corresponds to the oxidation of lithium superoxide or surface superoxide-like sites on lithium peroxide. Currents at ~3.8 V vs Li^+/Li correspond to the oxidation of bulk lithium peroxide. These curves support the assumption of superoxide reducing to lithium peroxide[1]. Final film capacity is comparable in both DMSO and DME. DME currents are lower in some cases because the film was not fully formed after 2 minutes.

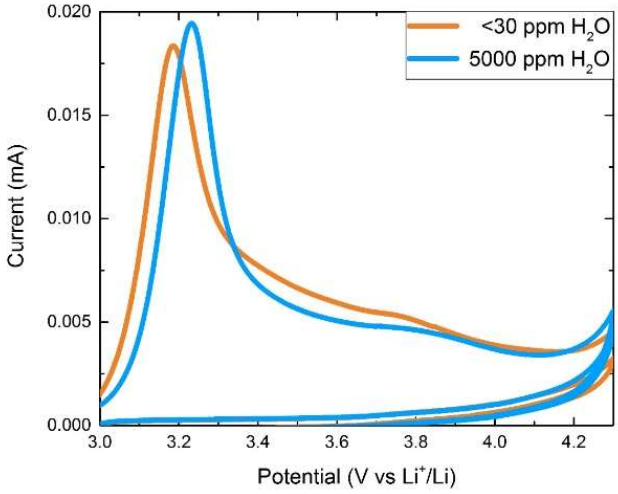

Figure A.2: Disk Oxidation Cyclic Voltammetry Water Content Effect Current vs potential for potential scans from 3 to 4.3 V vs Li^+/Li at 10 mV/s following 2 minute discharges at 2.4 V vs Li^+/Li in 0.1 M $LiClO_4$ DMSO at 1600 rpm with <30 ppm H_2O and ~5000 ppm H_2O.

Similar disk oxidation potential scans for the anhydrous case and the case with ~5000 ppm H_2O suggest both discharges formed lithium superoxide and lithium peroxide.

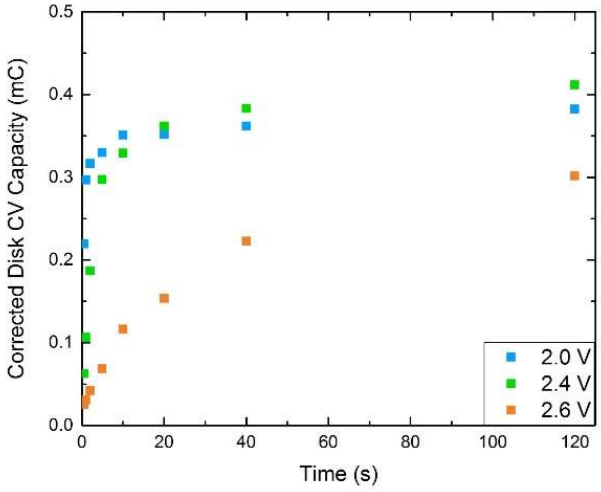

Figure A.3: Time Progression of Corrected Capacity from Oxidative Potential Scan A time progression of corrected capacity from disk oxidation is shown for 2 minute discharges at 2.0 V, 2.4 V, and 2.6 V vs Li^+/Li with a rotation rate of 1600 rpm in 0.1 M $LiClO_4$ DMSO anhydrous. Capacity was based on a potential sweep from 3 to 4 V vs Li^+/Li as values above 4 V are associated with solvent decomposition. The capacity was corrected by subtracting the second cycle capacity from the first cycle capacity to eliminate non-faradaic effects such as double layer charging.

The initial rapid increase to ~.3 mC at high overpotentials is attributed to nucleation and growth of a Li_2O_2 thin film. The long slow increase at long time is attributed to tunneling through the film. For this reason, the height of the initial film prior to tunneling is calculated from a capacity of .3 mC, giving a value of ~1.6 nm.

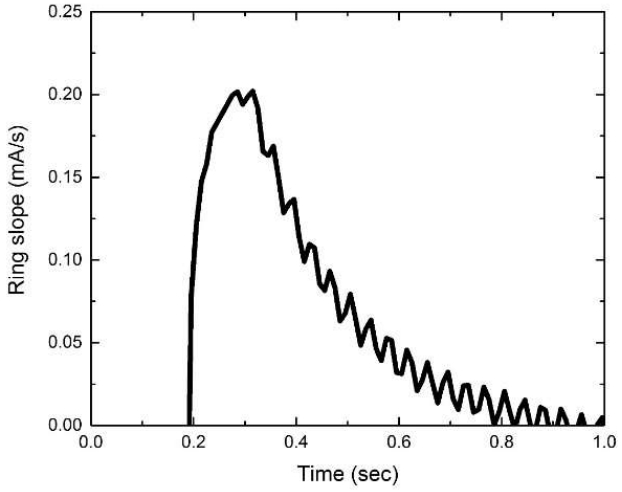

Figure A.4: First Derivative of Ring Current Slope of ring current collected at 2.4 V vs Li^+/Li in 0.1 M $LiClO_4$ DMSO anhydrous at 1600 rpm with ring potential at 3.5 vs Li^+/Li. Slope was calculated for each time t_i as $\frac{I_{i+1}-I_{i-1}}{t_{i+1}+t_{i-1}}$ where I_i is the ring current at t_i. The curve was smoothed by averaging from $i+4$ to $i-4$ to give the slope at each time t_i. The first derivative of the ring current with time gives the shape of the distribution for arrival times at the ring for soluble species simultaneously produced at the disk[2]. Since the build-up time was on the order of ~1 sec and the transit time distribution was on the order of ~100 msec, the transit time distribution for arrival of soluble species from the disk to the ring was approximated as an instantaneous step function.

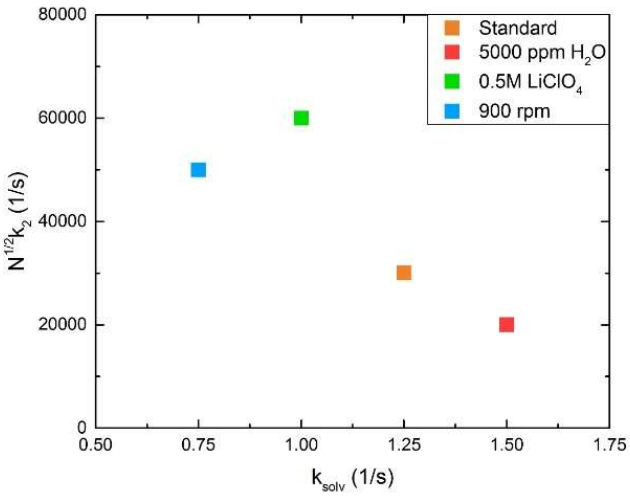

Figure A.5: Trend in Fit Parameters for Experimental Fits A plot of the fit parameters $\sqrt{N}k_2^0$ and k_{solv} for the modeled fits of experimental discharges at the standard condition of 2.4 V vs Li^+/Li in 0.1 M $LiClO_4$ DMSO anhydrous at 1600 rpm (orange), with an increase in water content to ~5000 ppm H_2O (red), with an increase in salt concentration to 0.5 M $LiClO_4$ (green), and a change in rotation rate to 900 rpm (blue).

a) Ring to Disk Ratio

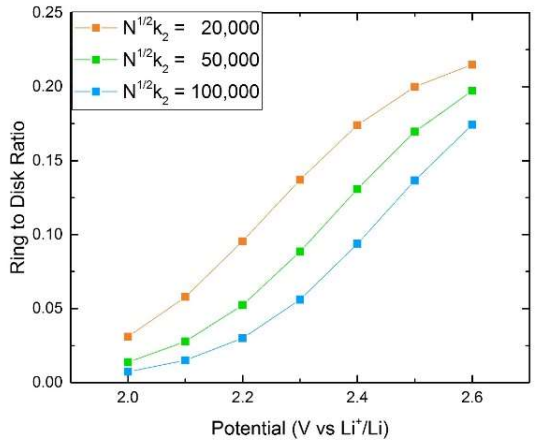

b) Disk Capacity

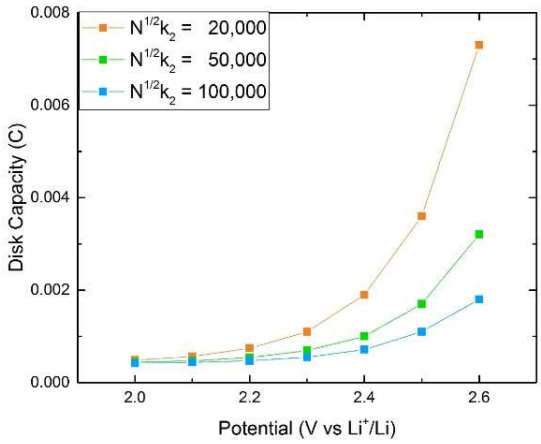

c) Average Li^+-O_2^- Concentration

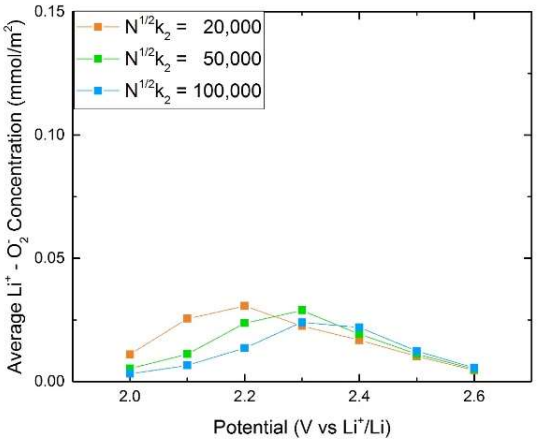

d) Cut-off Time

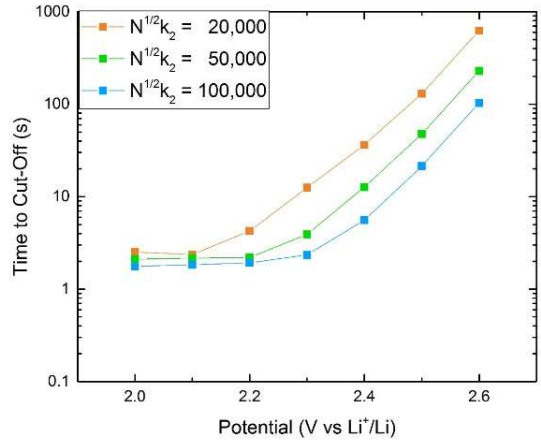

Figure A.6: Cell Performance Dependence on $\sqrt{N}k_2^0$ Surface Factor Modeled values for 0.1 M $LiClO_4$ DMSO anhydrous at 1600 rpm with k_{solv} = 1.25 s^{-1} and $\sqrt{N}k_2^0$ = 20000, 50000, and 100,000 s^{-1} of a) ring capacity to disk capacity ratio, b) disk capacity, c) average Li^+-O_2^- concentration, d) and cut-off time when area coverage by Li_2O_2 film is 99%.

a) 2.0 V Average Pathway Rates

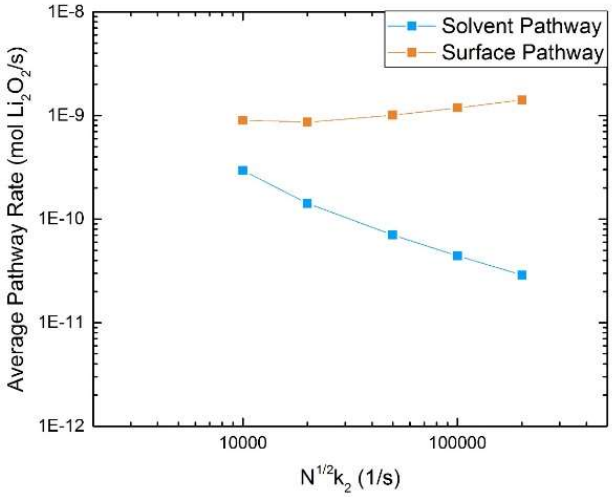

b) 2.6 V Average Pathway Rates

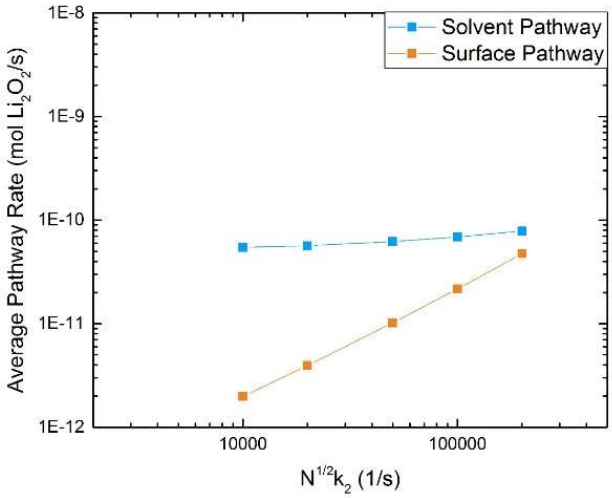

Figure A.7: Solvent vs Surface Pathway Competition Dependence on $\sqrt{N}k_2^0$ Surface Factor Average solvent pathway rate (blue) and average surface pathway rate (orange) for modeled fits of 0.1 M $LiClO_4$ DMSO anhydrous discharges at 1600 rpm to 99% area coverage cut-off at a) 2.0 V and b) 2.6 V vs Li^+/Li.

a) Solvent Pathway

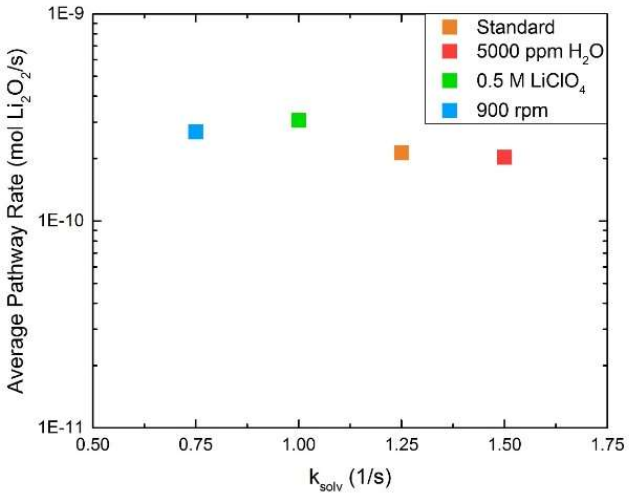

b) Surface Pathway

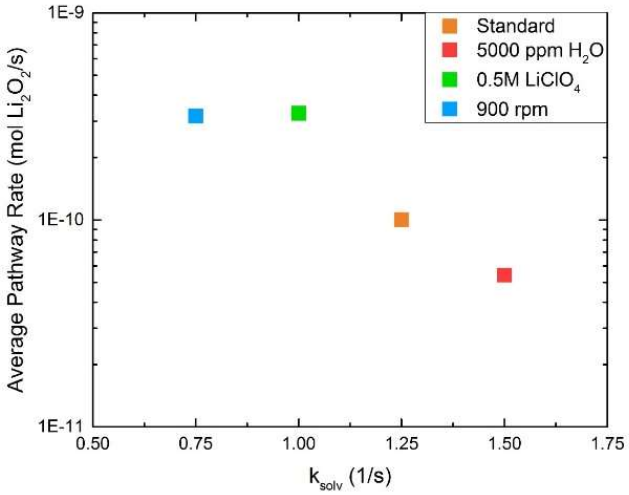

Figure A.8: Solvent and Surface Average Pathway Rates for Experimental Fits a) Average solvent pathway rate and b) average surface pathway rate for the modeled fits of experimental discharges at the standard condition of 2.4 V vs Li^+/Li in 0.1 M $LiClO_4$ DMSO anhydrous at 1600 rpm (orange), with an increase in water content to ~5000 ppm H_2O (red), with an increase in salt concentration to 0.5 M $LiClO_4$ (green), and a change in rotation rate to 900 rpm (blue).

Discussion A.1: Equation Derivations

Equation 4.3 is a straight-forward application of the Koutecky-Levich equation for a single electron transfer to a single species[4].

The pre-factor accounts for the non-steady state change in surface oxygen concentration from open circuit potential to a reduction potential. The pre-factor is based on a model of current transients due to a change in surface reactant concentration from an initial value prior to a potential step and the steady state surface concentration. The model is designed for the case when the steady state current is at the mass transfer limiting condition, but the factor is used as an approximation for all conditions in this model[3,4].

The current from first electron transfers to reduce oxygen is:

$$I_{disk}^{1st\ e^-} = FA_e * \left[1 + \exp(-.386 * \pi^2 \omega (\frac{D_{O_2}}{\nu_{kin}})^{\frac{1}{3}} t) + \exp(-1.54 * \pi^2 \omega (\frac{D_{O_2}}{\nu_{kin}})^{\frac{1}{3}} t)\right] *$$

$$(\frac{1}{k_1^0 \exp(\frac{-\alpha_1 F}{RT}\eta)} + \frac{1}{.62({D_{O_2}}^{2/3} \omega^{1/2} \upsilon_{kin}^{-1/6})})^{-1} * C_{O_2}^{bulk}$$

Equation 4.4 follows from considering solvation to be a first order reaction with Li^+-O_2^-. The rate of solvation is converted to a modeled ring current by assuming rapid transit from disk to ring and considering the collection efficiency of the ring (~23%).

$$I_{ring}(t) = .23 * F * A_e * r_{solv}(t)$$

In practice, there will be a time distribution for the arrival at the ring for soluble species formed at the disk, based on area distribution and varying convection currents. However, at high rotation rates this spread should be ~100 ms (Figure A.4) and can be reasonably ignored for the time scales involved in this study. For a full treatment of disk to ring time distribution models, see Sergeev et al.[2]

Equation 4.5 is derived from the Butler-Volmer equation and charge conservation. The current reducing lithium superoxide is proportional to the volume change of the Li_2O_2 film for a single island:

$$\frac{dV_{Li2O}}{dt} = \frac{I(t)M}{F\rho}$$

The current is based on the Butler-Volmer equation applied to the edge of the film. $r(t)$ is the radius of the Li_2O_2 island.

$$I(t) = 2\pi F h_0 r(t) C_{LiO2}^{surf} k_2^0 \, exp\left(\frac{-\alpha_2 F}{RT}\eta\right)$$

The volume change can be expressed as a function of the radial growth rate v:

$$\frac{dV_{Li2O2}}{dt} = \frac{d}{dt}(\pi h_0 r(t)^2) = 2\pi h_0 r(t)\frac{dr}{dt} = 2\pi h_0 r(t) v$$

Substituting the expressions for $I(t)$ and $\frac{dV_{Li2O2}}{dt}$ into the first equation yields Equation 4.5:

$$v = \frac{M}{\rho} C_{LiO2}^{surf} k_2^0 \, exp\left(\frac{-\alpha_2 F}{RT}\eta\right)$$

Equation 4.6 is derived from the Johnson-Mehl-Avrami Kolmogorov equation[6]. The area coverage of the film without impingement by growing islands, referred to as the extended area, can be related to the true area coverage when impingement is considered.

$$a_{film} = 1 - exp(-a_{extended})$$

In this case, the extended area fraction is calculated from determining the area of one island with a given radius and multiplying by the number of nuclei:

$$Fractional\ Area_{extended} = \frac{Total\ island\ area}{Electrode\ area} = \frac{N\pi r^2}{A_e}$$

The radius can be related to the average radial growth rate:

$$r(t) = \sum_i \nu_i \Delta t$$

Substitution gives Equation 4.6:

$$a_{film} = 1 - \exp(-\pi \frac{N}{A_e} (\sum_i (\nu_i \Delta t))^2)$$

Equation 4.8 assumes a competition between the rate of oxygen reduction and rate of superoxide reduction from a limited amount of tunneled electrons. The oxygen reduction rate is assumed to be the same at the film and electrode:

$$r_{1,tunn} = r_1$$

The superoxide reduction rate is assumed to be governed by a Butler-Volmer relation:

$$r_{2,tunn} = k_2^{tunn} * C_{LiO_2}^{surf} * exp\left(\frac{-\alpha_2 F}{RT}\eta\right)$$

The fraction of electrons reducing superoxide,γ, is calculated from the fraction of the rate of superoxide reduction to the total reduction rate.

$$\gamma = \frac{r_{2,tunn}}{r_{2,tunn} + r_{1,tunn}}$$

Equation 4.9 applies an assumption of charge conservation to the reduction of superoxide to increase the thickness of the film. First the superoxide reduction rate is calculated using the fraction γ:

$$r_{2,tunn} = \gamma * r_1 * \exp(-\beta * (h - h^0))$$

Based on the rate of peroxide formation, the amount of height increase in the Li_2O_2 film is derived:

$$\Delta h = \Delta t * \gamma * \frac{M}{\rho} * r_1 * \exp(-\beta * (h - h^0))$$

Equation 4.10 is the sum of different contributions to the surface Li^+-O_2^- concentration:

$$Electrode\ Oxygen\ Reduction: \Delta C_{LiO_2}^{surf} = \Delta t * \left((1 - a_{film}) * r_1\right)$$

$$Electrode\ Superoxide\ Reduction: \Delta C_{LiO_2}^{surf} = -\Delta a_{film} * \frac{h\rho}{M}$$

$$Film\ Oxygen\ Reduction: \Delta C_{LiO_2}^{surf} = \Delta t * \left(a_{film} * r_{1,tunn} \right)$$

$$Film\ Superoxide\ Reduction: \Delta C_{LiO_2}^{surf} = \Delta t * \left(-a_{film} * r_{2,tunn}\right)$$

$$Superoxide\ Solvation: \Delta C_{LiO_2}^{surf} = \Delta t * r_{solv}$$

Summing these terms yields the net change in surface Li^+-O_2^- concentration during a time increment of Δt:

$$\Delta C_{LiO_2}^{surf} = \Delta t * \left((1 - a_{film}) * r_1 + a_{film} * (r_{1,tunn} - r_{2,tunn}) - r_{solv}\right) - \Delta a_{film} * \frac{h\rho}{M}$$

Discussion A.2: Marcus Theory Application to Transfer Coefficients and Reduction Rate Constants

Marcus theory provides a model of electron transfer that considers the effects of molecular interactions[4,7]. The energy barrier for reduction is modeled by treating the free energy of both the reactant and the product as parabolic against a reaction coordinate. Electron transfer can only occur at the intersection of the quadratic free energy curves for reactant and product, as the Franck-Condon principle states that electronic changes occur more rapidly than changes in positions of nuclei in molecules. These assumptions yield an equation for the activation energy barrier.

$$\Delta G_{barrier} = \frac{\lambda}{4}(1 + \frac{F\eta}{\lambda})^2$$

$\Delta G_{barrier}$ is the activation energy barrier, F is the Faraday constant, and η is the overpotential. The solvent reorganization energy, λ, reflects the energy required for the reactant and surrounding solvent

molecules to rearrange as the product is formed. From this expression, the transfer coefficient, α, can be derived by taking the derivative with overpotential.

$$\alpha = \frac{1}{2} + \frac{F\eta}{2\lambda}$$

The second term is generally small enough that the standard approximation of $\alpha \approx 0.5$ used in the Butler-Volmer equation is reasonable. However, Sankarasubramanian et al. provided estimates of the reorganization energy for oxygen reduction in DME and DMSO for Li-O_2 that are in a regime in which $\alpha < 0.5$ beyond low overpotentials[8]. This explains reports of higher than expected Tafel slopes in Li-O_2 studies[9,10]. Based on values reported in these studies, estimates of $\alpha \approx 0.3$ and $\alpha \approx 0.2$ for the reduction of oxygen in DMSO and DME respectively were used in our study. Laoire et al. suggest that the Tafel slope for superoxide reduction is ~100 mV greater than for oxygen reduction[9], providing estimates of $\alpha \approx 0.2$ and $\alpha \approx 0.1$ for the reduction of superoxide in DMSO and DME respectively in our study. These are inherently approximate average values of α, as Marcus theory is considered to be more useful for qualitative results, and precise quantitative modeling of reorganization energy and α potential dependence is difficult.

Marcus theory can also explain the changes in the model parameter $\sqrt{N}k_2^0$ as changes are made in solvent properties. Assuming that N is a function of the active site density of the electrode and holds constant as the solvent changes, changes in k_2^0 can be ascribed to changes in reorganization energy. Reorganization energy is known to correlate with the strength of solvation of solvent molecules with the reactant molecule and the polarity of the solvent. Bondue et al. have reported correlations of superoxide reduction rates with solvent acceptor number and polarity[11]. Large differences in oxygen and superoxide reduction rate constants in DMSO and DME can be attributed to the significant differences in viscosity, donor number, acceptor number, and polarity between the two solvents. Smaller differences in solvent properties such as the water content, salt concentration, and rotation rate explain the trend

in DMSO for $\sqrt{N}k_2^0$. Adding water causes stronger solvating interactions between surface Li^+-O_2^- and solvent molecules, which increases reorganization energy and decreases k_2^0. Increasing the salt concentration both promotes the forward reaction by increasing Li^+ concentration and suppressing the amount of free solvent available for solvation, causing an increase in k_2^0. This is consistent with the observations of Johnson et al[12]. Higher rotation rates ensure sufficient solvent molecules are provided to the surface by convection to coordinate any surface Li^+-O_2^-, which increases the reorganization energy and decreases k_2^0. In general, greater solvation effects, modeled by k_{solv}, increase the reorganization energy and decrease the favorability of surface Li^+-O_2^- reduction, modeled by $\sqrt{N}k_2^0$. This explains the inverse correlation in Figure A.5.

Discussion A.3: Calculation of Correction for Rotation, Salt Concentrations, Donor Number, and Acceptor Number

The effect of Li^+ concentration, c_{Li^+}, on overpotential is given simply by the Nernst equation:

$$\Delta\eta = \frac{RT}{F} ln(\frac{c_{Li^+\,2}}{c_{Li^+\,1}})$$

For a change from 0.5 M to 0.1 M $LiClO_4$:

$$\Delta\eta = \frac{RT}{F} \ln\left(\frac{.5}{.1}\right) = 42\ mV$$

The effect of altering the acceptor number on overpotential is linear[13,14]. Taha et al. show that adding 10% water raises the acceptor number of the solvent mixture from 19.3 to 26.4[15]. Aetukuri et al. show that the O_2/O_2^- potential has a slope of ~.012 with acceptor number[14]. The addition of 10% water would then represent a shift of ~85 mV. Since the water addition is <1% in this study, the effect should be small.

As the transfer coefficient can only be reported to one significant digit, changes in the second significant digit of the overpotential (ie. on the order ~10 mV) can be reasonably ignored.

Discussion A.4: Definition of Average Pathway Rate

Electron transfers are assumed to completely stop at the cut-off time, for simplicity. The surface concentration of Li^+-O_2^- at the end of discharge is counted toward the solvent pathway since all superoxide will eventually solvate if electron transfers cease. The average pathway rate is the amount of Li_2O_2 that forms (or would form by disproportionation) divided by the cut-off time.

For the surface pathway this is simply calculated from the amount of charge for second electron transfers.

$$\overline{r_{surf}} = \frac{Q_{2n\ \ e^-}}{F\tau_{cut-off}}$$

The solvent pathway is calculated from the difference in charge passed between first and second electron transfers:

$$\overline{r_{solv}} = \frac{Q_{1st\ e^-} - Q_{2nd\ e^-}}{F\tau_{cut-off}}$$

$\overline{r_{solv}}$ and $\overline{r_{surf}}$ are the average solvent and surface pathway rates in mol Li_2O_2/s, F is the Faraday constant in C/mol, $Q_{1st\ e^-}$ is the amount of charge that reduced oxygen in C, $Q_{2nd\ e^-}$ is the amount of charge that reduced superoxide in C, and $\tau_{cut-off}$ is the discharge cut-off time (99% area coverage by Li_2O_2 film) in s.

Table A.1: $k_2^{tunn} \approx 1$ s^{-1} Estimate

k_2^{tunn}	Disk R^2	Ring R^2	R^2 Sum
0.1	0.97	0.97	1.94
0.5	0.98	0.98	1.96
1	0.98	0.98	1.96
2	0.98	0.98	1.96
10	0.98	0.98	1.96

R-square values for fits of 2.4 V vs Li^+/Li at 1600 rpm in 0.1 M $LiClO_4$ DMSO anhydrous at k_{solv} = 1.25 s^{-1} and $\sqrt{N}k_2^0$ = 30,000 s^{-1} with varying values of k_2^{tunn}. The estimate of k_2^{tunn} does not greatly affect the quality of the fit provided that an appropriate order of magnitude is chosen.

Table A.2: Strength of Fits for Water Content, Salt Concentration, and Rotation Rate

0.1 M to 0.5 M $LiClO_4$	k_{solv}	$\sqrt{N}k_2^0$	Disk R^2	Ring R^2	R^2 Sum
Two Free	1	60000	0.93	0.93	1.86
Fixed k_{solv}	1.25	70000	0.94	0.92	1.86
Fixed $\sqrt{N}k_2^0$	0.5	30000	0.85	0.78	1.63

30 to 5000 ppm H_2O	k_{solv}	$\sqrt{N}k_2^0$	Disk R^2	Ring R^2	R^2 Sum
Two Free	1.5	20000	0.97	0.91	1.89
Fixed k_{solv}	1.25	20000	0.95	0.92	1.87
Fixed $\sqrt{N}k_2^0$	2.25	30000	0.98	0.88	1.85

1600 rpm to 900 rpm	k_{solv}	$\sqrt{N}k_2^0$	Disk R^2	Ring R^2	R^2 Sum
Two Free	0.75	50000	0.98	0.94	1.92
Fixed k_{solv}	1.25	60000	0.98	0.78	1.77
Fixed $\sqrt{N}k_2^0$	0.5	30000	0.97	0.90	1.87

The table summarizes the best fit if both parameters are kept free or if one is constrained as the experimental condition is varied from the standard case of 2.4 V vs Li^+/Li in 0.1 M $LiClO_4$ DMSO anhydrous at 1600 rpm. Reasonable fits can be produced of the increased water content discharge by altering either k_{solv} or $\sqrt{N}k_2^0$ alone. Since either can be physically justified, it is likely that changes are due to a combination of changes in both parameters. Increased salt content could be fit by increasing $\sqrt{N}k_2^0$ but not by toggling k_{solv} alone. The effect of reducing rotation is only fit by assuming both k_{solv} and $\sqrt{N}k_2^0$ are changed. Comparing all of these results suggests that $\sqrt{N}k_2^0$ and k_{solv} are inversely related, as seen in Figure A.5.

References

1. Belova, A. I., Kwabi, D. G., Yashina, L. V., Shao-Horn, Y. & Itkis, D. M. Mechanism of Oxygen Reduction in Aprotic Li–Air Batteries: The Role of Carbon Electrode Surface Structure. *J. Phys. Chem. C* **121,** 1569–1577 (2017).

2. Sergeev, A. V, Itkis, D. M. & Chertovich, A. V. Applying the deconvolution approach in order to enhance RRDE time resolution : practical issues and limitations . *arXiv* (2018).

3. Siver, Y. G. Non-stationary electrode processes in mixed environments. *Russ. J. Phys. Chem.* **33,** (1959).

4. Bard, A. J. & Faulkner, L. R. *Electrochemical Methods: Fundamentals and Applications*. (2001).

5. Bruckenstein, S. & Feldman, G. A. Radial transport times at rotating ring-disk electrodes. *J. Electroanal. Chem.* **9,** 395–399 (1965).

6. Avrami, M. Kinetics of phase change. II Transformation-time relations for random distribution of nuclei. *J. Chem. Phys.* **8,** 212–224 (1940).

7. Marcus, R. A. On the Theory of Electron-Transfer Reactions. VI. Unified Treatment for Homogeneous and Electrode Reactions. *J. Chem. Phys.* **43,** 679–701 (1965).

8. Sankarasubramanian, S., Seo, J., Mizuno, F., Singh, N. & Prakash, J. Elucidating the Oxygen Reduction Reaction Kinetics and the Origins of the Anomalous Tafel Behavior at the Lithium-Oxygen Cell Cathode. *J. Phys. Chem. C* **121,** 4789–4798 (2017).

9. Laoire, C. O., Mukerjee, S., Abraham, K. M., Plichta, E. J. & Hendrickson, M. A. Influence of nonaqueous solvents on the electrochemistry of oxygen in the rechargeable lithium-air battery. *J. Phys. Chem. C* **114,** 9178–9186 (2010).

10. Gallant, B. M. *et al.* Influence of Li2O2 morphology on oxygen reduction and evolution kinetics in Li–O2 batteries. *Energy Environ. Sci.* **6,** 2518 (2013).

11. Bondue, C. J., Bawol, P. P., Abd-El-Latif, A. A., Reinsberg, P. & Baltruschat, H. Gaining Control over the Mechanism of Oxygen Reduction in Organic Electrolytes: The Effect of Solvent Properties. *J. Phys. Chem. C* **121,** 8864–8872 (2017).

12. Johnson, L. *et al.* The role of LiO2 solubility in O2 reduction in aprotic solvents and its consequences for Li-O2 batteries. *Nat. Chem.* **6,** 1091–1099 (2014).

13. Sawyer, D. T., Chiericato, G., Angelis, C. T., Nanni, E. J. & Tsuchiya, T. Effects of media and electrode materials on the electrochemical reduction of dioxygen. *Anal. Chem.* **54,** 1720–1724 (1982).

14. Aetukuri, N. B. *et al.* Solvating additives drive solution-mediated electrochemistry and enhance toroid growth in non-aqueous Li-O2 batteries. *Nat. Chem.* **7,** 50–56 (2015).

15. Taha, A. & Mahmoud, M. M. Lewis acidity parameter for binary solvent mixtures and adduct formation studies using the solvatochromic dicyanobis(1,10-phenanthroline)iron(II) complex. *New J. Chem.* **26,** 953–957 (2002).

Appendix B: Discharge Pathway Model Code

Written in Matlab R2016b, The Mathworks, Inc.

Variables set to sample values.

```
%Rate constants
ksolv = 1.25; %solvation rate constant
k1 = 4*10^-6; %1st electron transfer rate constant
rootNk2 = 30000; %2nd electron transfer and nucleation density
tunnk2 = 1; %superoxide reduction rate constant
Qf = .00015; %capacity of 2nd e- transfers in C
alpha1 = .3; %oxygen reduction symmetry factor
alpha2 = .2; %superoxide reduction symmetry factor
nu = .4; %overpotential in V

%Literature value constants and various standard constants
D = 3.23*10^-9; %diffusivity m^2/s
vkin = 1.77*10^-6; %kinetic viscosity m^2/s
omega = 1600*2*3.14/60; %rotation rate rad/s
F = 96485; %Faraday constant C/mol
R = 8.314; %gas constant J/(mol*K)
T = 300; %temperature K
Ae = 3.14*.0025^2; %electrode area m^2
CO2 = 2.1; %O2 bulk concentration mol/m^3
CO2surf = 0; %surface O2 concentration in mol/m^3
M = 45.881; %molar mass of Li2O2 in g/mol
rho = 2.31*10^6; %density of Li2O2 in g/m^3
B = 2.303*3*10^9; %exponential factor for height decay
lambdaO2 = 1.61*D^(1/3)*omega^(-1/2)*vkin^(1/6); %diffusion layer thickness
in m

%Calculation of Dependent Variables

%Initial oxygen current calculation
CO2surf = (D*CO2)/(D+lambdaO2*(k1*exp(alpha1*F*nu/(R*T))));
Iinitial_lio2 = Ae*F*k1*CO2surf*exp(alpha1*F*nu/(R*T));

hinitial = Qf*M/(rho*F*Ae); %initial height in m based on film capacity

%Variables for time progression loop
t=0; %time in s
deltaT = .01; %time increment in s
molLio2=0; %mol of Lio2 on top of electrode
molSolv =0; %mol of lio2 solvated during a time increment
Clio2 = 0; %concentration of LiO2 in mol/m^2 on top of electrode
ratio = 0; %ratio of tunneled electrons that reduce superoxide
ratio2nd =0; %ratio of tunneled electrons that reduce superoxide
ratio1st = 0; %ratio of tunneled electrons that reduce oxygen
extR = 0; %radius of islands for external volume calculation * rootN
deltaR = 0; %increment increase of radius in a time loop *rootN
extVel = 0; %growth rate of islands for external volume calculation * rootN
```

```
%Data storage matrices
Clio2Data = []; % [mol/m^2] array of electrode concentration data
timeData = []; %[s] array of time data
hData = []; %[m] array of height data
Ifirste = []; %[A] 1st electron current
Iseconde = []; %[A] 2nd electron current
Itunn = []; % [A] tunneling current
ITunnDist = []; % [A] array of tunneling current for various area increments
ratio1stData= []; %fraction of tunneled e- reducing oxygen
ratio2ndData = []; %fraction of tunneled e- reducing superoxide
ItotalData = []; %[A] disk current
AreaDist = []; %fraction of total area covered during time increment
ringCurrentData = []; %[A] prediction of current read at ring
areaUnnoc = 1; %fraction of the area not covered by Li2o2
areaUnnocData = []; %array of area coverage data

%Time evolution model
for i=1:1:120000
    t= i*deltaT;
    timeData(1,i)=t;


    %Avrami Time Evolution
    Ifirste(1,i) = Iinitial_lio2*(1+2*exp(-
(3.14/1.61)^2*omega*(D/vkin)^(1/3)*t)+2*exp(-
4*(3.14/1.61)^2*omega*(D/vkin)^(1/3)*t))*areaUnnoc;
    extVel = M/rho*Clio2*rootNk2*exp(alpha2*F*nu/(R*T));
    deltaR = extVel *deltaT;
    AreaDist(1,i) = exp(-3.14*(extR)^2/Ae)-exp(-3.14*(extR+deltaR)^2/Ae);
% fraction area increment at time increment
    Iseconde(1,i) = (Qf/deltaT)*(exp(-3.14*(extR)^2/Ae)-exp(-
3.14*(extR+deltaR)^2/Ae));

    %Tunneling Time Progression
    hData(1,i)= hinitial;
    ITunnDist = (AreaDist.*Iinitial_lio2 .* exp(-B.*(hData-hinitial)));
    hData = hData + ratio2nd*Iinitial_lio2.*exp(-B.*(hData-
hinitial))*deltaT*1/(Ae*F)*(M/rho);
    Itunn(1,i)=sum(ITunnDist);
    ratio2nd
=(tunnk2*Clio2*exp(alpha2*F*nu/(R*T)))/(tunnk2*Clio2*exp(alpha2*F*nu/(R*T))+k
1*CO2surf*exp(alpha1*F*nu/(R*T)));
    ratio1st =
(k1*CO2surf*exp(alpha1*F*nu/(R*T)))/(tunnk2*Clio2*exp(alpha2*F*nu/(R*T))+k1*C
O2surf*exp(alpha1*F*nu/(R*T)));
    ratio2ndData(1,i)=ratio2nd; %ratio 2nd electron data
    ratio1stData(1,i)=ratio1st; %ratio 1st electron data

    %Surface LiO2 concentration calculation
    molLio2 = molLio2 + Itunn(1,i)/F*deltaT*(ratio1st-
ratio2nd)+Ifirste(1,i)/F*deltaT - Iseconde(1,i)/F*deltaT -
ksolv*Clio2*deltaT*Ae;
    molSolv = ksolv*Clio2*deltaT*Ae;
%mol of Lio2 solvated during time increment
    areaUnnoc = exp(-3.14*(extR+deltaR)^2/Ae);
```

```
    Clio2 = molLio2/(Ae);
    if Clio2 < 0
      Clio2 = 0;
    end
    if areaUnnoc ==0
       Clio2 = 0;
    end
   Clio2Data(1,i) = Clio2;
   extR = extR + deltaR;
   areaUnnocData(1,i) = areaUnnoc;

   ringCurrentData(1,i)= .23*F* molSolv/deltaT; % 23% collection efficiency

    if areaUnnoc < .01
       break;
   end

end

ItotalData= Ifirste+Iseconde+Itunn;

plot(timeData,ItotalData); %Disk Current in A
figure;
plot(timeData,ringCurrentData); %Ring Current in A
figure;
```